UNIVERSITÉ DE MONTRÉAL

MODEL ANALYSIS AND NONLINEAR CONTROL OF AIR COMPRESSORS

GHOLAM-REZA SARI

DÉPARTEMENT DE GÉNIE ÉLECTRIQUE

ÉCOLE POLYTECHNIQUE DE MONTRÉAL

THÈSE PRÉSENTÉE EN VUE DE L'OBTENTION

DU DIPLÔME DE PHILOSOPHIAE DOCTOR

(GÉNIE ÉLECTRIQUE)

AOÛT 2014

UNIVERSITÉ DE MONTRÉAL

ÉCOLE POLYTECHNIQUE DE MONTRÉAL

Cette thèse intitulée:

MODEL ANALYSIS AND NONLINEAR CONTROL OF AIR COMPRESSORS

présentée par : SARI Gholam-Reza

en vue de l'obtention du diplôme de : Philosophiae Doctor

a été dûment acceptée par le jury d'examen constitué de :

M. GOURDEAU Richard, Ph. D., président

M. SAYDY Lahcen, Ph. D., membre et directeur de recherche

Mme AKHRIF Ouassima, Ph. D., membre et codirectrice de recherche

M. ZHU Guchuan, Ph. D., membre

M. DOEDEL Eusebius J., Ph. D., membre

DEDICATIONS

To my lovely wife Nazanin

ACKNOWLEDGMENT

I wish to thank all those who supported me in the completion of this study. I would like to express my sincere gratitude to my doctoral advisors Prof. Lahcen Saydy and Prof. Ouassima Akhrif for their patience, guidance and valuable support throughout the realization of this research. My sincere appreciation goes to Prof. Eusebious J. Doedel, Prof. Richard Gourdeau, and Prof. Guchuan Zhu for taking part in my dissertation committee. This project has been made possible by precious support from Fonds québécois de la recherche sur la nature et les technologies FQRNT.

Finally, and most importantly, I would like to thank my family, especially my lovely wife.

RÉSUMÉ

Pendant des décennies, les turbines à gaz ont été des dispositifs importants et fiables dans les domaines de la production d'énergie, de l'industrie pétrochimique, et de l'aéronautique. Ces machines utilisent les compresseurs centrifuges et axiaux qui se dégradent en présence d'instabilités aérodynamiques telles que le pompage et le décrochage tournant. Ces dernières limitent la performance et peuvent causer des sollicitations mécaniques importantes, une réduction de la durée de vie, du bruit et des vibrations. De plus, dans les compresseurs axiaux à vitesse variable (CAVV), les variations de vitesse affectent la stabilité des systèmes et peuvent entraîner le pompage et le décrochage tournant. Cela limite le taux de variation de vitesse et pénalise la performance.

Le travail présenté dans cette thèse dresse premièrement l'analyse de bifurcation du modèle des CAVVs afin d'étudier l'impact de la dynamique de la vitesse sur la stabilité de points de fonctionnement efficaces. Ici, le taux de variation de vitesse (accélération) est défini comme un nouveau paramètre du modèle et une analyse détaillée de bifurcation numérique est fournie. Les résultats des simulations dans le domaine temporel valident non seulement l'analyse de bifurcation, mais élargissent aussi nos connaissances sur la réponse transitoire du modèle, qui est d'une importance majeure. L'analyse réalisée révèle que les variations de vitesse peuvent mener à un décrochage tournant entièrement développé ainsi qu'au décrochage temporaire mentionné précédemment. Les résultats montrent que les instabilités développées dépendent fortement du taux d'accélération. L'impact des autres paramètres du modèle, les vitesses initiale et finale, et la contribution des modes du décrochage sont également étudiés.

Au niveau du contrôle, malgré toutes les réalisations présentées, la conception d'une commande robuste même pour des systèmes de compression axiaux à vitesse constante demeure encore un problème difficile. Ici, deux méthodes de commande non linéaires: le contrôle par modes glissants et le contrôle par passivité sont proposées pour résoudre ce problème de stabilité. Ces deux approches traitent de tous les aspects difficiles du sujet qui apparaissent dans la littérature : l'impact des perturbations externes, le manque de connaissance précise des paramètres du modèle, et l'absence d'un retour d'état complet. Enfin, cette étude propose une méthode de contrôle robuste qui peut contrôler simultanément la vitesse et les instabilités des

CAVVs. Cela a été jusqu'à date un problème ouvert et la solution apportée permet d'augmenter la performance des turbines à gaz.

ABSTRACT

For decades, gas turbines have been important, widespread, and reliable devices in the field of power generation, petrochemical industry, and aeronautics. They employ centrifugal and axial compressors which suffer from aerodynamic instabilities, namely, surge and rotating stall. These performance limiting instabilities can cause component stress, lifespan reduction, noise, and vibration. Furthermore, in variable speed axial compressors (VSACs), speed variations affect the system stability and can lead to surge and rotating stall. This limits the rate of speed variations and results in important performance penalties.

The present work firstly addresses the bifurcation analysis of VSACs' model to investigate the impact of speed dynamics on the stability of efficient operating points. Here, the rate of speed variations (acceleration rate) is defined as a new parameter of the model and a detailed numerical bifurcation analysis is provided. The results of time-domain simulations not only validate the results of bifurcation analysis, but also broaden our knowledge about the transient response of the model, which is a matter of importance as well. The analysis reveals that speed variations can lead to a fully developed rotating stall as well as the previously reported temporary stall developments. The results show that the developed instabilities depend to a great extent on the acceleration rate. The impact of other key issues such as throttle gain, viscosity factor, initial speed, final speed, and the contribution of stall modes are also explored.

From the control point of view, despite reported achievements, robust control design for compression systems remains a challenging problem. In this work, at first, two nonlinear approaches are proposed to tackle the stability problem of constant-speed axial compressors (CSACs). The first approach is a robust passivity-based control and the second one is a second order sliding mode control. The approaches tackle the challenging problems being addressed in the literature such as: the impact of external perturbations, the lack of detailed parameters knowledge, and the absence of full-state feedback. They drive the control from pressure and mass flow measurements and use throttle and close-coupled valve actuations. Finally, this study reports that these methods can be used in the case of VSACs by applying the required modifications to simultaneously control speed and instabilities. This simultaneous control design has been an open problem and the proposed method can improve the performance of VSACs.

TABLE OF CONTENT

LIST OF TABLES

LIST OF FIGURES

LIST OF APPENDICES

LIST OF ABREVIATIONS

CCV	Close-coupled Valve
CSAC	Constant-speed Axial Compressor
FOSMC	First Order Sliding Mode Control
IFT	Implicit Function Theorem
MG3	Three-state form of lumped parameter Moore and Greitzer model for CSACs
OP	Operating Point
PBC	Passivity-based Control
SMC	Sliding Mode Control
SOSMC	Second Order Sliding Mode Control
VSAC	Variable Speed Axial Compressor

CHAPTER 1

INTRODUCTION AND MOTIVATION

The development of the first gas turbine dates back to 1791 when John Barber patented a machine which looks structurally similar to the modern gas turbines. In 1899, Charles Gordon Curtis filed the first patent application for a gas turbine "Apparatus for generating mechanical power" [1] in the United State . The decade of the 30's was a turning point for the applications of gas turbines. At first in 1937, the Brown Boveri Company of Switzerland used gas turbines for power generation. Then the first aircraft to fly purely on turbojet power was designed and tested in 1939 [2]. Today, gas turbines are widely used in industries and aeronautics. Petroleum industries rely on turbo compressor stations in the transportation of natural gas and chemical industries require turbo machines to pressurize chemical products. The current generation of aircraft habitually uses gas turbines to produce mechanical and electrical power.

However, gas turbines have always suffered from important aerodynamic instabilities. Among these, rotating stall and surge occur in the compressor stage and badly affect the performance of the system. They possibly result in engine failures and severe mechanical damages due to high blade vibrations, pressure oscillations, and flow reversal. To understand the origin of these instabilities, we briefly describe next the operation of air compressors in gas turbines.

1.1 Air Compressors in Gas Turbines

Figure 1.1 shows the schematic of a gas turbine including the compressor, the combustor, and the power turbine.

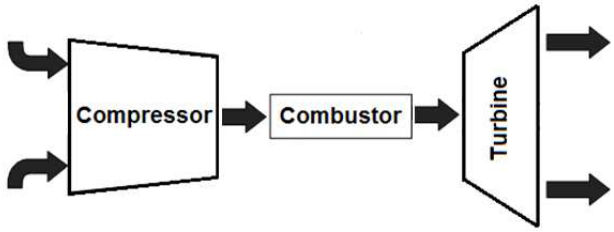

Figure 1.1: Schematic of a gas turbine

As an integrated part of the gas turbine, the compressor delivers the compressed air to the combustion chamber where fuel is added. The combustor then burns the mix and feeds the hot and high pressure exhaust into the power turbine components. The expanded gas drives the power turbine producing the needed energy for turning the compressor and other mechanical parts.

There are two basic types of compressors; axial flow and centrifugal flow. The difference between them is the way that the air flows through the compressor. Depending on the application, gas turbines utilize either or both axial or centrifugal compressors.

1.2 Principal Operation of Compressors

1.2.1 Centrifugal Compressors

Figure 1.2 shows impellers (the rotary section) of a centrifugal compressor's stage in a gas turbine. The continuous flow of centrifugal compressors receives energy from the shaft's impellers. The impellers and the diffusers contribute to transform the energy to the flow in different ways. The impellers add kinetic energy to the fluid which is proportional to the tangential velocity of the impellers according to Euler's fluid dynamics equation. On the other hand, outside of the rotary parts, there is no transfer of mechanical work and the total energy of the fluid does not change in traversing the stationary components. During the diffusion process, the fluid's velocity decreases, and according to Bernoulli's law, the pressure of the fluid therefore increases and the added kinetic energy changes to a potential form (static pressure rise, see [3-5] for more details). In centrifugal compressors, the flow leaves the compressor in a direction perpendicular to the axis of the rotor.

Centrifugal compressors are popular throughout industry because they achieve high efficiency, high reliability, and high flow rates with a few moving parts. Furthermore, their seals allow them to operate nearly oil-free. The main drawback of centrifugal compressors is that they cannot provide high compression ratios without multiple stages.

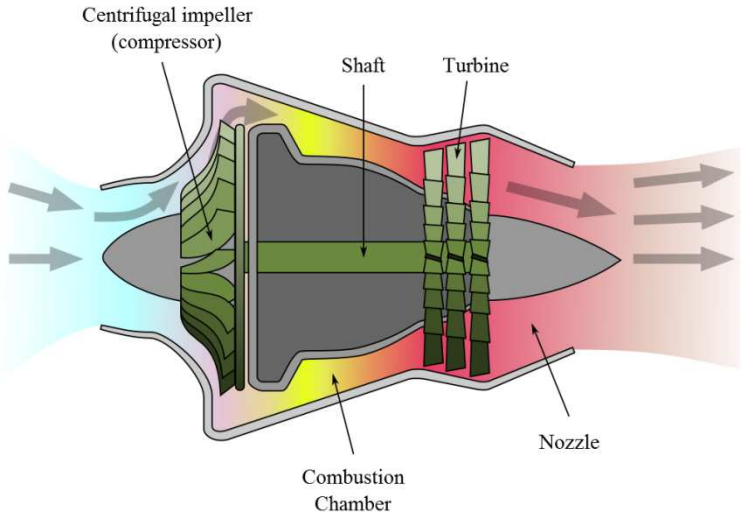

Figure 1.2: Centrifugal Compressor (image courtesy of Wikipedia)

1.2.2 Axial Compressors

An axial compressor consists of rotary and stationary blades; Figure 1.3 shows the rotor and the stator of an axial-flow compressor. In this type of compressors, the flow of the fluids is parallel to the rotational axis. Axial compressors normally comprise different stages to achieve the required pressure rise. Each stage is configured by a combination of a rotor which accelerates the fluid, followed by a diffusing stator which obtains a pressure increase.

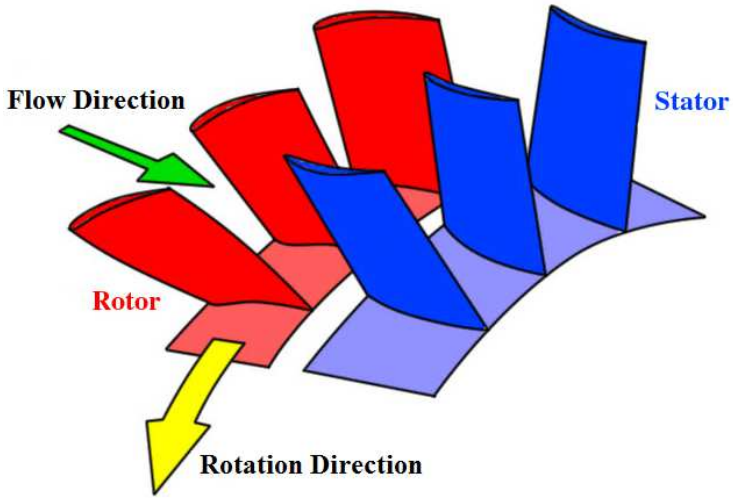

Figure 1.3: Axial compressor's rotor and stator (image courtesy of Wikipedia)

In a multi-stage axial compressor, by producing low pressure increases in the stages on the order of 1.1:1 to 1.4:1, very high efficiencies can be obtained. This multi-stage configuration permits an overall pressure increase of up to 40:1 in some aerospace applications and a pressure ratio of 30:1 in industrial applications.

1.3 Compressors' Instabilities

As already mentioned, compressors suffer from two kinds of instabilities limiting their efficiency and performance: rotating stall and surge. These instabilities arise in the unsteady fluid and structural dynamics and can lead to catastrophic failure of the system due to large mechanical or thermal loads on the different parts of compressors. These unsteady aerodynamic nonlinearities are difficult to predict accurately. Over the years, sensing, preventing, or controlling such instabilities have been posing complex problems to researchers.

1.3.1 Rotating Stall

Emmon's et al. [6] model for the formation of rotating stall provides a simple explanation about its propagation. As a likely consequence of a closing throttle or a perturbation in the incoming flow, the angle of attack in one of the rotor blades excessively increases which causes the flow separation from the blade. This creates a blockage or a vacuum area that prevents air from entering the blade and then redirects the flow toward the lower and the upper blades.

Consequently, the angle of attack decreases in the lower blade and reduces the risk of the flow separation in this area. Otherwise, for the upper blade, the angle of attack increases to a point where the flow separates from the next blade. The stall development in the upper blade in turn decreases the angle of attack in the initial blade and forces it to go out of the stall condition. Therefore, the stall cell starts to propagate from one blade to the next; in other words rotates around the annulus of the compressor.

Figure 1.4 demonstrates a simple schematic of a compression system in which the rotating stall is formed as a perturbation in the axisymmetric mean flow in the first stage of the compressor. One can imagine the rotating stall as a mass flow perturbation that consists of different harmonics.

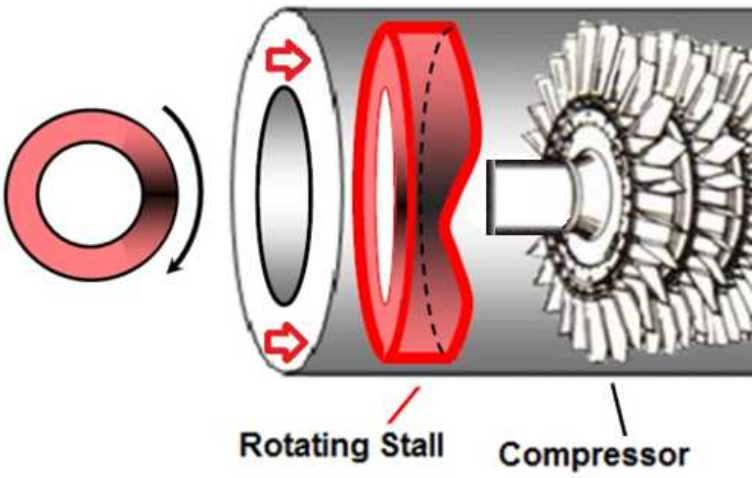

Figure 1.4: Rotating stall as a perturbation of the axisymmetric mean flow

1.3.2 Surge

Compression systems also suffer from deep surge which is a violent instability represented by a large axial oscillation of the flow. As a result, the direction of the flow changes and the pressure rise capability of the system dramatically decreases. This instability causes component stress (i.e. the backflow including the hot gas of the combustor can damage the blades of the compressor in few cycles), lifespan reduction, noise and vibration, and large penalties in performance. As explained in [7], surge is caused by alternating the storage and the release of compressed air in the downstream ducting of the compressor. The compressibility of the air acts as a spring system, and the nonlinear compressor performance characteristic provides a negative damping to this spring under some operating conditions and leads to surge. At least two different types of surge exist: 1- Mild/Classical surge in which flow reversal does not occur and a small pressure fluctuation can be seen, 2- Deep surge in which flow reversal is possible (Figure 1.5). This is an axisymmetric limit cycle of flow.

The main difference between deep surge and rotating stall is that the average mass flow in deep surge is circumferentially uniform but axially unstable, but rotating stall has a circumferentially nonuniform mass flow with a steady average value. Experimental results show that rotating stall has little effect on the performance of centrifugal compressors; however, in the case of axial compressors, rotating stall seems more important at low shaft speeds and surge

occurs more frequently at high speeds [8, 9]. Furthermore, in variable speed axial compressors, the speed dynamics can deeply affect these nonlinearities [10].

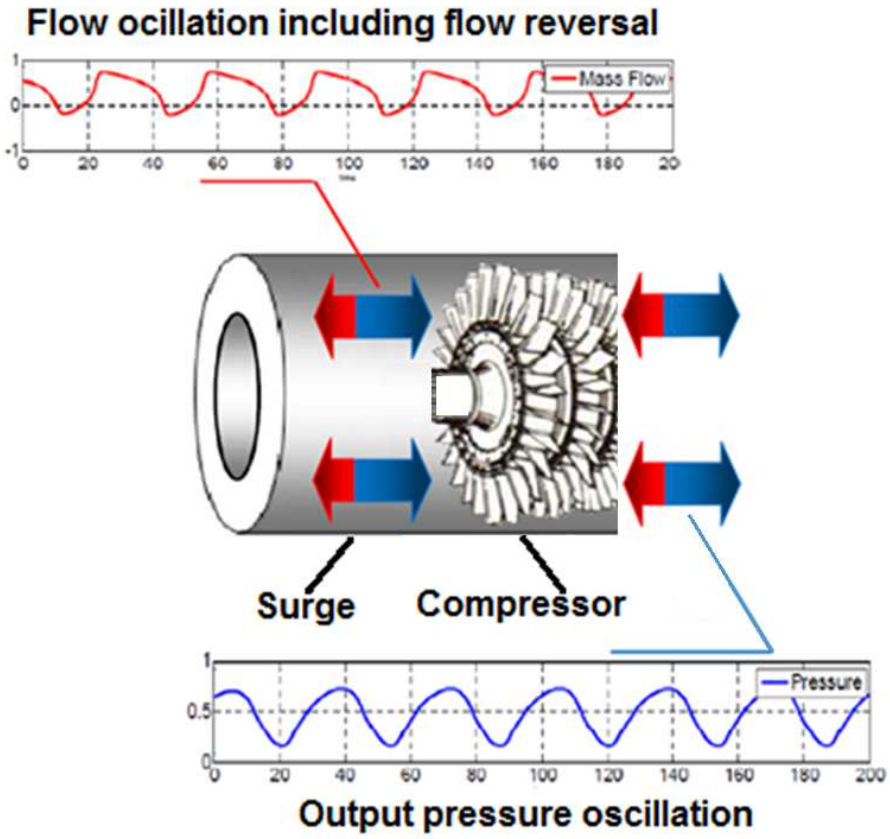

Figure 1.5: Pressure variation and flow oscillations including a flow reversal during deep surge

1.4 Research Questions

Previous sections highlighted the importance of compression systems in industries and briefly explained the instabilities which limit the performance of compressors. These instabilities will be addressed in detail later in Chapter 3. In this section, a set of questions addressing the key issues and open problems in the literature is formulated to direct the research efforts. The current research is centered around the following questions:

- Is there an association between the characteristics of speed variations (e.g. the rate and the range of variations) and the instabilities in variable speed axial compressors?
- How does a speed variation affect compressor behavior? Can it lead to fully developed stall on top of the already observed temporary rotating stall?
- What role, if any, do model parameters (such as throttle gain and viscosity) play in the multi-mode rotating stall developments?
- What robust strategies can one employ to overcome the challenging problems of control design in constant-speed compressors?
- How can one simultaneously and robustly control speed and surge/stall instabilities in variable speed compressors?
- How do the saturation and the dynamics of actuators affect the performance of the controllers?

1.5 Research Objectives

In light of these questions, three main objectives of the present work are stated as follows:

I. Investigation of the Qualitative Behavior of VSACs' Model

In the present work, the first objective is to carry out a bifurcation analysis to determine how model dynamics depend upon the choice of model's parameters. It is important to explore the qualitative properties of nonlinear instabilities: surge and rotating stall, and determine the impact of speed variations on the nonlinearities as well. The impact of the transient response of the model on the nonlinear stationary behavior is also addressed. A better knowledge of the qualitative behavior of variable speed axial compressors will shed lights into methods to suppress

the exclusive instabilities of these widely used machines, and may also lead to the refinements of the existing models.

II. Robust Control of Constant-speed Axial Compressors

The second objective is to develop a robust control approach to stabilize compressors when the rotor speed is constant. This approach should tackle all challenging problems such as the impact of external perturbations, the lack of detailed parameter knowledge, and the absence of full-state feedback.

III. Simultaneous Speed and Surge/Stall Robust Control of VSAC

In variable speed axial compressors, the temporary stall during the speed variations leads to temporary pressure drops at the output and spells serious operational problems. Consequently, satisfying the procedural speed variation requirements and achieving the required pressure rise, at the same time, reflect a need for simultaneous speed and surge/stall control in these machines.

The third and final objective of the present research is thus to develop an effective control approach which not only guarantees surge-free and stall-free speed variations, but also takes on all the challenges of the second objective.

1.6 Contributions of Current Work

The contributions of the thesis can be summarized as follows:

a- Broaden our knowledge of bifurcations in variable speed axial compressor model and the effect of parameter variations

This work firstly serves to provide a better understanding of the qualitative behavior of variable speed axial compressors. Here, the impact of speed variations on the temporarily developed rotating stall is investigated in detail. The rate of speed variation (acceleration rate) is defined as a new parameter of the model and a detailed numerical bifurcation analysis is provided for this parameter. This study reveals that speed variations not only cause temporary rotating stall developments and pressure drops but can also lead to a fully developed rotating stall or deep surge. It is demonstrated that the compressor's instabilities depend to a great extent on the

acceleration rate as a new bifurcation parameter. The impact of other key issues such as throttle gain, viscosity factor, initial speed, final speed is investigated as well.

b- Contribution of higher order harmonics of rotating stall during speed variations

In addition to stationary solutions and instabilities that develop, the transient response of the compression systems deserves close attention. As discussed before, the speed transitions result in temporary stall developments, which cannot be studied by a bifurcation analysis. Time-domain simulations reveal that higher order harmonics of rotating stall are deeply affected by the acceleration rate. It is shown here that the higher order harmonics dominate the first harmonic for high acceleration rates. This underlines the need for a multi-mode robust control approach to effectively damp out rotating stall and surge in variable speed compressors. The results report that the viscosity factor affects also the contribution of higher harmonics in VSACs.

c- Robust stabilization of constant speed compressors comprising CCV

Despite all achievements in stabilizing CSACs, a control design, which takes on all previously mentioned challenges, is still an open problem. In this work, two nonlinear approaches are proposed to tackle the problem. The first approach is a robust passivity-based control (RPBC). The simple form of the developed controller is the first advantage of the applied method. It is not based on full-state feedback and does not require the knowledge of model parameters. Furthermore, the new developed RPBC greatly relaxes the assumptions on perturbations, which are usually supposed to be vanishing [11, 12], by introducing bounded non-vanishing disturbances. The controller then achieves the global ultimate boundedness of state variables of the system.

The second proposed approach is a second order sliding mode control (SOSMC). The proposed chattering-free SOSMC combined with feedback linearization robustly stabilizes both surge and rotating stall by throttle and CCV actuations in the presence of external disturbances and model uncertainties. Full state feedback including rotating stall amplitude is not assumed and the control is only driven from pressure and mass flow measurements. Furthermore, the control scheme does not require the accurate knowledge of the compression system parameters. The global asymptotic stabilization of the closed-loop system is achieved in a finite time by adjusting

only a small number of control parameters. The reasonable computation load and the fairly straightforward implementation of SOSMC make it an excellent choice for this application. The impact of actuator dynamics is also addressed.

d- Simultaneous robust control of speed and surge/stall in VSACs

In the present research, it is shown that the developed robust control designs for CSAC (e.g RPBC) can be applied with appropriate modifications to VSACs. It is demonstrated that the controller can damp out temporary rotating stall during speed variations and stabilize the compressor at an efficient operating point in the vicinity of unstable zone. The impact of actuator saturation is investigated as well.

1.7 Outline of the Thesis

The main body of this thesis is organized as follows. Chapter 2 provides a brief literature review on the three aspects of modeling, sensors/actuators, and control of compression systems. Chapter 3 recalls two of the most important models used in the literature: the one developed by Moore and Greitzer for CSACs, the so-called MG3, and the one developed by Gravdahl for VSACs, and defines different characteristics of these two models. It then reviews the time-domain simulation results of surge and rotating stall and the bifurcation analysis of MG3 to describe the issues to be addressed for VSACs and to serve as a background to the next chapters. Chapters 4 and 5 extensively investigate the qualitative behavior of variable speed axial compressors by performing numerical bifurcation analysis based on continuation method and by carrying out time-domain simulations. In these chapters both the stationary and the transient response of Gravdahl's model are explored. Chapters 6 and 7 report on the results of two submitted manuscripts which tackle the robust control of MG3 by CCV and throttle actuations. These chapters propose two different approaches based on RPBC and SOSMC. Both of these methods, at first, partially decouple the original system by applying a preliminary feedback and then robustly stabilize the nominal system. Here, the control is driven from pressure and mass flow measurements. In these chapters, the impact of actuators' dynamics is also studied. Chapter 8 consists of the content of a manuscript which successfully overcomes the problems of stall developments during speed variations in VSACs. In this chapter, the impact of actuator saturation is also studied.

Finally, the conclusions about this work are drawn in Chapter 9 and references and appendices are given at the end.

CHAPTER 2

LITERATURE REVIEW

The literature on compressors is vast. A basic introduction is given by e.g. Ferguson [13], Cohen et al. [14], and more advanced topics are covered by Cumpsty [5], Aungier [15], and Giampaolo [3]. In the 1950s and 1960s, it was found that rotating stall and surge appear in compressors in a region of working points. This led to a series of theoretical and experimental studies on rotating stall and surge [16-26]. A lot of research was then conducted to develop anti stall/surge systems for compressors [27-29]. Although these instabilities are often considered as separate phenomena, there is a coupling between them and rotating stall is a precursor to the onset of surge in many compressors [30, 31]. The prediction of the onset of rotating stall or surge has also been addressed by many investigators [32-35].

To situate the present study and its contribution in relation to previous research and to obtain the required background, a brief literature review is provided on three aspects: modeling, sensors/actuators, and control.

2.1 Modeling

Due to the diversity of compressor applications, a wide variety of models exists for compressor dynamics simulations and control design, each model with its own strengths and limitations. Generally, the models can be divided into three categories: 1- 1D models being only capable of predicting surge, 2- 2D models describing both surge and rotating stall, and 3- 3D models describing the spatial non-linear aspects of the flow in multi-stage transonic compressors including compressibility.

Modeling the nonlinear behavior of rotating stall and surge in compression systems has been pursued for decades. Greitzer is clearly a pioneer in this area [18]. Although there are many models for rotating stall and surge, from a control point of view, a nonlinear 2D model developed by Moore and Greitzer [36] dominates the recent studies on rotating stall and surge [37]. This basic model has been successfully applied to a wide variety of stability and control problems. The initial formulation of the model is based on a two-dimensional incompressible

flow assumption in the duct and the compressor. The model was converted to a suitable form for system analysis and control design by Paduano [38, 39] and Mansoux [40]. The Moore-Greitzer model and its extensions have the following advantages: they are low order, they can capture most of nonlinearities and operational effects, and they are physical rather than computational. A shortcoming of these models is that they do not describe multistage effects and gas compressibility. This limitation becomes important when the level of required fidelity increases, but in control studies, it has not been debilitating [41].

The three-state lumped parameter Moore and Greitzer model or MG3 is based on a first harmonic approximation of rotating stall. This model was developed by using a Galerkin procedure applied to the original PDE form of the model. Great efforts have been made to augment this model in various ways, to increase its accuracy, and to model the force of actuators for active control. The main shortcoming of MG3 is the one mode approximation of rotating stall (see chapter 3 for more information). Mansoux et al. [40] found that during the stall inception, higher order modes interact with and dominate the first harmonic. The relaxation of the one mode approximation was derived by Adomaitis and Abed [42], Mansoux et al. [40] and Leonessa et al. [43].

Another shortcoming of the original work of Moore and Greitzer lies in its constant compressor speed assumption. In 1997, Fink et al. [44] presented a model for variable speed centrifugal compressors. In the same year, Gravdahl and Egeland [45] derived a similar variable speed model and investigated surge and speed control. However, these models were both developed for centrifugal machines, and do not include rotating stall as a state variable. For the first time, the model developed by Gravdahl [46, 47] considered the speed of the rotor as a state variable and included higher harmonics (modes) of rotating stall. This is an extension to MG3 where the effect of gas viscosity is also taken into account. The gas viscosity was first introduced in the Moore-Greitzer model by Adomaitis and Abed [42] and its effects were investigated by Gu et al. [37] and Hendrickson and Sparks [48]. Researchers have also focused their efforts on exploring the qualitative behavior and bifurcation analysis of MG3 to determine the impact of model parameters on the developed instabilities [48-53]. Most of these studies have addressed the effects of the throttle gain as a bifurcation parameter of MG3. The bifurcation analysis of MG3 is briefly reviewed in chapter 3.

Gravdahl's model for variable speed axial compressors is explored in this work to investigate the qualitative of the model including surge and rotating stall, which has been an open problem since 1998. This model is explored to firstly broaden our knowledge about the impact of speed variations on model nonlinearities, and finally, to develop a simultaneous speed and stall/surge control. The model is reviewed in chapter 3. Table 2.1 briefly summarizes the different types of models developed by various researchers. These models consider axial or centrifugal compressor dynamics and can be used for either modeling or control purposes.

Table 2.1: Compression system modeling techniques

CC: Centrifugal compressor, AC: Axial compressor, C: Control, M: Modeling, S: Variable speed

Reference	**Dim.**	**Compressible**	**States**	**Compressor**	**Application**
Greitzer [18]	1	Incompressible	ϕ, Ψ	AC	M
Hansen[54]	1	Incompressible	ϕ, Ψ	CC	M
Fink et al.[44]	1	Incompressible	ϕ, Ψ, B	CC	MS
Gravdahl-Egeland	1	Incompressible	ϕ, Ψ, B	CC	MCS
Eveker-Nett [55]	2	Incompressible	ϕ, Ψ, B	CC	MCS
Moore-Greitzer	**2**	**Incompressible**	$\boldsymbol{\phi, \Psi, J}$	**AC**	**MC**
Adomaitis [56]	2	Incompressible	ϕ, Ψ, J	AC	MC
Hynes [57]	2	Incompressible	ϕ, Ψ, J	AC	MC
Wang et al.[58]	2	Incompressible	ϕ, Ψ, J	AC	MC
Mansoux [40]	2	Incompressible	ϕ, Ψ, J_n	AC	M
Hendrickson[48]	2	Incompressible	ϕ, Ψ, J_n	AC	C
Humbert-Krener	2	Incompressible	ϕ, Ψ, J_n	AC	C
Adomaitis[42]	2	Incompressible	ϕ, Ψ, J_n	AC	C
Paduano [38]	2	Incompressible	ϕ, Ψ, J_n	A	MC
Gravdahl [47]	**2**	**Incompressible**	$\boldsymbol{\phi, \Psi, J_n, B}$	**AC**	**MS**
Hendricks et	2	Comp./Multi.	spatial	AC	M
Fulner et al.[61]	2	Comp./Multi.	spatial	AC	MC
Gong et al.[62]	3	Comp./Multi.	spatial	AC	M
Weigl et al.[63]	3	Comp./Multi.	spatial	AC	MC

In the table, the models specified by "J_n" include higher order harmonics of rotating stall. The non-constant speed compressor models, which involve the speed of the rotor B as a state, are also pointed out in the table.

2.2 Sensors and Actuators

Several studies have been done on different types of sensors and actuators for measuring surge and rotating stall. The number of sensors or actuators being needed is another key issue, which has been addressed. Contrary to 1D surge sensing and actuating, the control of rotating stall requires information about the non-uniformity of the flow, so an array of sensors placed around the circumference of the compressor should be used (2D sensor). Badmus et al. [64] found that the linearized compressor dynamics around an unstable equilibrium point are uncontrollable and unobservable if 1D actuation and annulus-averaged sensing is applied. They then concluded that 2D sensors and 2D actuators are required for linear feedback stabilization [65]. A common realization of the 2D sensor is a circular array of pressure transducers [64, 66, 67] or hot wire anemometers [39, 54, 68]. As seen from the quantitative analysis in [69], the effect of position, number, and type of sensors and actuators seems worthy of further research. The important drawbacks of 2D sensors and actuators are: complexity, overall weight and cost due to the large number of required sensors and actuators, which reduces reliability as well.

Among the several actuators used for stabilizing compression systems, the most promising are air injection [70] and close-coupled valves (CCV) [71] (see Table 2.2). Other examples include bleed valves[72], throttle valves [73], variable inlet guide vanes [74], loudspeakers [75], tailored structures [8], recirculation [76], movable plenum walls [77], synthetic jets [78], tip clearance [79] and plasma actuator [80]. The impacts of actuators' and sensors' dynamics, their noise levels, and their saturation limits on the effectiveness of the compression control systems have also been investigated [81, 82].

In this work, throttle and CCV actuations are applied to tackle the stabilization problems of compression systems. The impact of actuators' dynamics is also addressed.

Table 2.2: Sensors and actuators for measuring and controlling rotating stall and surge

A: axial, C: centrifugal, L: low speed, H: high speed, S: single-stage, M: multi-stage V: variable speed

Reference	Sensor	Actuator	Compressor	Surge/Stall control
Badmus et al. [83]	Plenum pressure	Throttle	AS	Surge
Badmus et al. [84]	Inlet pressure	Throttle	AL	Surge
Williams et al.[75]	Diffuser pressure	Loudspeaker	C	Surge
Gysling et al.[8]	Plenum pressure	Movable wall	C	Surge
Jungowski [85]	Duct Pressure	Loudspeaker	C	Surge
Nakagawa [86]	Plenum pressure	Suction-side valve	C	Surge
Pinsley [87]	Plenum pressure	Throttle	C	Surge
Badmus [64]	Inlet pressure	Throttle	ALS	Stall
Behnken [66]	Inlet pressure	Air-injection	AL	Stall
Gysling et al. [88]	Inlet pressure	Air-injection	ALS	Stall
Haynes et al. [89]	Hot wires	Movable IGVs	ALM	Stall
Paduano et al. [39]	Hot wires	Movable IGVs	ALS	Stall
Simon Yeung [90]	Inlet pressure	Air-injection/Bleed	ALS	Stall
Gravdahl et al. [91]	**Pressure/speed**	**CCV**	**AV**	**Surge/speed**
Song et al. [92]	**Flow/pressure**	**CCV**	**AV**	**Surge/speed**
Day [68]	Hot wires	Air-injection	ALM	Surge/Stall
Der-Chreng et al. [93]	**Pressure/flow**	**CCV**	**AL**	**Surge**
Gravdahl[47]	**Pressure**	**CCV**	**AL**	**Surge/Stall**
Bartolini [94]	**Pressure/Flow**	**CCV/Throttle**	**ACL**	**Surge**
Liaw[95]	**Pressure/flow/stall**	**CCV/Throttle**	**AL**	**Stall/Surge**
Williams et al.[67]	Diffuser pressure	Air-injection	C	Surge/Stall
Feulner [96]	Static Press. array	Air-injection	AMH	Surge/Stall
Berndt et al.[97]	3D flow measure	Air-injection	AMH	Surge/Stall
Weigl [63]	Static Press. array	Air-injection	ASH	Surge/Stall

2.3 Control

The prevention and control of surge and rotating stall in compression systems has been the subject of many studies during the last decades. First methods are based on maintaining stable operation with a sufficient margin from the instabilities [98-102]. This stability margin is considered by including uncertainties in the location of the stall point, typical disturbances, load variations, inlet distortions, combustion noises, and a consideration of the sensors' and actuators' limitations. These methods as standard and simple industrial solutions achieve stability at the expense of performance [103]. Contrary to conventional methods which work far from the unstable zone, the aim of recent active methods is to push the stable domain farther away from the operating point. However, the dynamic equations of compressors' models, which are highly nonlinear, represent a complex problem both for system analysis and control design. Furthermore, uncertain terms comprising external disturbances and parametric uncertainties stress a need for robust control approaches.

From a control point of view, the active control of centrifugal compressors is almost restricted to surge consideration because it is believed that rotating stall has little effect on centrifugal compressor performance [6, 104]. However, in axial compressors, both rotating stall and surge control are addressed in the literature. Most control-oriented studies published during the last decades employed Moore and Greitzer model or its extensions, because they are well suited for control applications.

Active surge control was first introduced in the literature by Epstein et al. [77] in 1989 by using a linear method. The main drawback of the method was the limited operating region. The next efforts were mostly based on nonlinear control approaches. The simultaneous control of speed and surge in centrifugal compressors has been widely investigated as well (see [91-93, 105] e.g.). In comparison with surge control design in centrifugal compressors, rotating stall and surge control in axial flow compressors poses a challenging problem due to several reasons. The first key issue is that the precise estimation of axial compressor's model parameters, especially in the unstable zone, is difficult. Therefore, control approaches that require the knowledge of model parameters and set some constraints on them cannot be robustly implemented (see [106-110] where the knowledge of model parameters is essential to form the control laws). Another issue is

that the rotating stall, as a state of axial compressor model, is experimentally difficult to measure; and control methods that need full-state feedback cannot practically overcome this problem (see [95, 110-112] where the amplitude of rotating stall is used to form feedback laws). Although, the measurement of mass flow, as the second state of compressors' model, is a challenge, it is surmountable [113]. Mass flow is frequently used in the literature to develop control design methodologies [114, 115], and there exist some implemented controllers that use this measurement [116]. Furthermore, nonlinear observers are proposed to estimate mass flow [112, 117-122]. The last, but not least, problem is the effect of external disturbances that can drive axial compressors toward instabilities (see [109, 121, 123] where external perturbations are not included). Pressure and mass flow disturbances were first taken into account in a compressor model by Simon and Valavani [124]. As demonstrated by Haddad et al., a feedback controller that does not consider model uncertainties and external perturbations can have adverse effects on compression system performance by driving the compression system to a stalled equilibrium or a surge limit cycle [125].

Table 2.3-1 shows the most significant efforts in the active control design of rotating stall and surge during the last two decades. In this table, the used model, control approach, and actuation method are mentioned for each work. Furthermore, Table 2.3-2 highlights the limitation of each work. This table reports that despite great achievements in the control of compression systems, even in the case of CSACs, a robust control design, which includes external perturbation and model uncertainties and does not rely on full-state feedback, is still a challenging problem. In spite of devoted efforts to control surge and speed in centrifugal compressors, the simultaneous control of instabilities (rotating stall and surge) and speed in variable speed axial compressors is still an open problem.

The early work of Gravdahl [47] briefly reported some exclusive behavior of variable-speed axial compressors, which cannot be captured by constant-speed models (see chapter 3 for details). He performed limited time-domain simulations and showed that rotating stall can temporarily develop during speed transitions even far from the unstable zone where MG3 does not imply any stall developments. Gravdahl's work stressed the need for detailed model analysis to assess the impact of parameters' variations on the qualitative behavior of the system. The

problem of variable speed compressors' control design is also pointed out among topics for further research in Moore and Greitzer work [36] and Gravdahl's thesis [47].

Table 2.3-1: Some of the most significant efforts in active control of compressors

SMC: Sliding Mode Control, EKF: Extended Kalman Filter, UDE: Uncertainty and Disturbance Estimator

No	Year	Author	Control method	Actuator	Type	Model
1	2013	Chen [126]	Nonlinear	Throttle	A	MG3
2	2013	Lin [127]	Fuzzy	Throttle+Speed	C	Gravdahl
3	2012	Ananth [128]	Nonlinear	Throttle	C	Ext. MG3
4	2012	Xiao [129]	UDE	CCV	C	MG
5	2011	Javadi [130]	NFuzzy+SMC	Throttle	A	MG3
6	2010	Vepa [103]	Nonlinear	Pressure	A	Ext. MG3
7	2009	Song [92]	FOSMC	Pressure (throttle)	C	MG
8	2009	Shehata [131]	FOSMC(CCV)	CCV+Throttle	A	MG3
9	2009	Ahn [132]	LQR+EKF	Thrust magnetic	C	MG
10	2008	Liaw [123]	Feedback linearisation	CCV or Throttle	C	MG
11	2008	Bartolini [133]	SOSMC	CCV+Throttle	C	Ext. MG
12	2007	Murrey [134]	Bifurcation	Throttle	A	MG3
13	2005	Sanadgol [135]	Backstepping	Magnetic Thrust	C	Ext. MG
14	2005	Bohagen [136]	Backstepping	Drive torque	C	Gravdal
15	2004	Sanadgol [137]	FOSMC	Magnetic Thrust	C	Ext. MG
16	2004	Liaw [138]	Backstepping	backstepping	C	Fink
17	2003	Ananthkrish [139]	Bifurcation	Throttle	A	MG3
18	2002	Liaw [140]	Lyapunov	Throttle+CCV	A	MG3
19	2001	Liaw [141]	FOSMC	CCV	A	MG3
20	2000	Leonessa [105]	FOSMC	Throttle/Tourque	C	Ext. MG
21	1999	Gravdahl [47]	Passivty-Based	CCV	A	Ext. MG3
22	1998	Krstic [50]	Backstepping	Throttle	A	MG3

Table 2.3-2: Limitations of the work being mentioned in Table 2.3-1

No	Year	Author	Surge/Stall	Limitations
1	2013	Chen [126]	Surge/Stall	Needs the knowledge of model parameters
2	2013	Lin [127]	Surge	Only can be used for surge control
3	2012	Ananth [128]	Surge	Only can be used for surge control
4	2012	Xiao [129]	Surge	Only can be used for surge control
5	2011	Javadi [130]	Surge/Stall	Knowledge of model parameters by NFuzzy
6	2010	Vepa [103]	Rotating stall	Needs the knowledge of model parameters
7	2009	Song [92]	Surge/Speed	Needs the knowledge of model parameters
8	2009	Shehata [131]	Surge	Needs the knowledge of model parameters
9	2009	Ahn [132]	Surge	Needs the knowledge of model parameters
10	2008	Liaw [123]	Surge	Does not include uncertainties and perturbations
11	2008	Bartolini [133]	Surge	Only can be used for surge control
12	2007	Murrey [134]	Stall/Surge	Needs the knowledge of model parameters
13	2005	Sanadgol [135]	Surge	Only can be used for surge control
14	2005	Bohagen [136]	Surge	Needs the knowledge of model parameters
15	2004	Sanadgol [137]	Surge	Only can be used for surge control
16	2004	Liaw [138]	Surge	Only can be used for surge control
17	2003	Ananthkrish [139]	Surge/Stall	Needs the knowledge of model parameters
18	2002	Liaw [140]	Surge	Only surge and add delay (washout)?
19	2001	Liaw [141]	Surge/Stall	Full state Feedback, some knowledge of pars
20	2000	Leonessa [105]	Surge	Only can be used for surge control
21	1999	Gravdahl [47]	Surge/stall	Model parameter information and (ϕ_0, ψ_0)
22	1998	Krstic [50]	Surge/Stall	Model parameters without perturbations

2.4 Conclusion

This tailored literature review not only supports the choice of the model and the actuation method but also reveals the remaining questions in model analysis and control design of constant-speed and variable-speed axial compressors. The review has direct links to the research questions and objectives stated in Chapter 1.

CHAPTER 3

MODELING AND ANALYSIS

In what follows, MG3 for CSACs and Gravdahl's model for VSACs are recalled, surge and stall time-domain simulations are presented and bifurcation curves of MG3 are reviewed. This chapter provides the needed background for the more detailed analysis given later.

3.1 MG3 for CSACs

MG3 is a low order state space model capturing rotating stall and surge phenomena in CSACs. A basic compression system is shown in Figure 3.1 [36]. P_T is the total upstream pressure of the compressor and P_S is the static pressure in the plenum. The flow is assumed to be incompressible in the compressor and compressible in the plenum. It is also assumed that the speed of compressor is constant (see [36] for more details and typical numerical parameters).

By applying a Galerkin approximation [36], the original model in PDE form is changed to three ordinary differential equations given by equations (3.1)-(3.3).

$$\dot{\Phi} = \frac{1}{l_c}\left(-\Psi + \Psi_C(\Phi) - \frac{3JH}{4}\left(\frac{\Phi}{W} - 1\right)\right) \tag{3.1}$$

$$\dot{\Psi} = \frac{1}{4B^2 l_c}(\Phi - \Phi_T(\Psi)) \tag{3.2}$$

$$\dot{J} = J\left(1 - \left(\frac{\Phi}{W} - 1\right)^2 - \frac{J}{4}\right)\varrho \tag{3.3}$$

where Φ is the annulus averaged mass flow coefficient, Ψ is the non-dimensional plenum pressure and J is the squared amplitude of rotating stall.

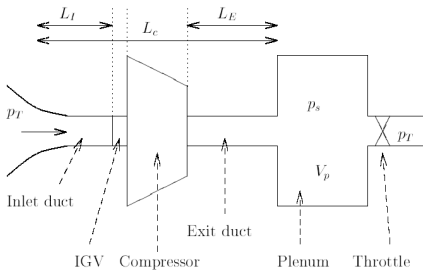

Figure 3.1: Schematic of a compressor showing non-dimensional lengths

$l_c = \frac{L_c}{R}$ is the effective flow-passage non-dimensional length with respect to R the mean compressor radius, and ϱ is a positive constant. B (Greitzer B-parameter) is another model parameter which is related to the constant tangential speed of the compressor $U = bB$, where b is also a positive constant. $\Psi_C(\Phi)$ is known as the steady state compressor characteristic (compressor map) which represents nonlinear relationship between the pressure rise at the output of the compressor and the mass flow. Typically this map is presented by a polynomial:

$$\Psi_C(\Phi) = \psi_{c0} + H\left(1 + \frac{3}{2}\left(\frac{\Phi}{W} - 1\right) - \frac{1}{2}\left(\frac{\Phi}{W} - 1\right)^3\right) \tag{3.4}$$

Here, H is the compressor characteristic height factor, W is the compressor characteristic width factor, and ψ_{c0} is shut-off head (see Figure 3.2). Note that in this figure, the compressor map is plotted using typical numerical values of model parameters. In experiments, compressors should operate in the negative slope area since in region with positive slope rotating stall or surge occurs. $\Phi_T(\Psi)$ is the throttle mass flow coefficient. The throttle can be thought of as a simplified model of the power turbine and its characteristic can be given by:

$$\Phi_T(\Psi) = \gamma_T\sqrt{\Psi} \tag{3.5}$$

where γ_T is the throttle gain. The physical amount of throttle opening is determined by the value of γ_T; large γ_T implies an open throttle and small γ_T means a closed throttle.

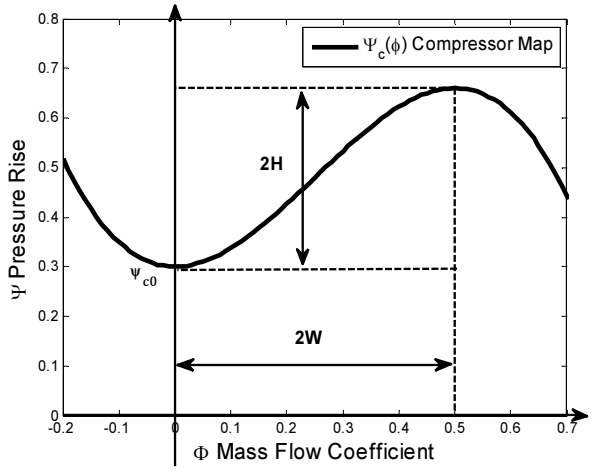

Figure 3.2: Compressor map, H, W, and ψ_{c0}

At equilibrium, we have:

$$\dot{\Phi} = \dot{\Psi} = 0 \tag{3.6}$$

$$\dot{J} = J\left(1 - \left(\frac{\Phi}{W} - 1\right)^2 - \frac{J}{4}\right) = 0 \tag{3.7}$$

which lead to two equilibria. The first one, $J_{e1} = 0$ **,** corresponds to the compressor being in its active operating point (OP). The second one, $J_{e2} = 4\left(1 - \left(\frac{\Phi}{W} - 1\right)^2\right) > 0$, corresponds to the system being in a fully developed rotating stall. For the second J_{e2}, one can obtain the stall characteristic $\Psi_s(\phi)$ of the compressor by considering (3.6), (3.2) and (3.3). Indeed:

$$\begin{cases} \frac{1}{l_c}\left(-\Psi + \Psi_c(\Phi) - \frac{3JH}{4}\left(\frac{\Phi}{W} - 1\right)\right) = 0 \\ \frac{1}{4l_cB^2}(\Phi - \Phi_T) = 0 \\ J_e = J_{e2} = 4\left(1 - \left(\frac{\Phi}{W} - 1\right)^2\right) \end{cases} \rightarrow \Psi_s(\Phi) = \psi_{c0} + H\left(1 - \frac{3}{2}\left(\frac{\Phi}{W} - 1\right) + \frac{5}{2}\left(\frac{\Phi}{W} - 1\right)^3\right) \tag{3.8}$$

Figure 3.3 shows the characteristic map of the compressor (3.1), throttle characteristic (3.5) and the stall characteristic of the compressor (3.8) in the same coordinate system. The operating point (OP) of the compressor is the intersection of compressor map and throttle characteristic.

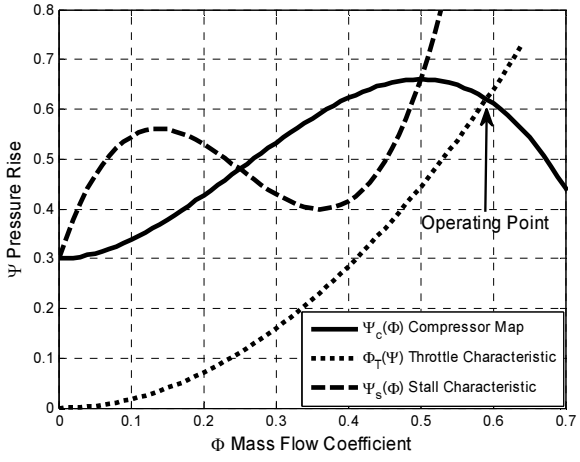

Figure 3.3: $\Psi_c(\Phi)$, $\Phi_T(\Psi)$, and $\Psi_s(\Phi)$

The Jacobian matrix at an equilibrium point where $J = 0$ can be calculated as below:

$$Jacobian|_{J=0} = \begin{bmatrix} \varrho - \varrho\left(\frac{\Phi}{W} - 1\right)^2 & 0 & 0 \\ -\frac{3H}{4l_c}\left(\frac{\Phi}{W} - 1\right) & \frac{3H}{2Wl_c}\left(1 - \left(\frac{\Phi}{W} - 1\right)^2\right) & -\frac{1}{l_c} \\ 0 & \frac{1}{4B^2 l_c} & -\frac{\gamma}{8B^2 l_c\sqrt{\Psi}} \end{bmatrix} \tag{3.9}$$

The first eigenvalue of the matrix given by:

$$\lambda_1 = \varrho\left(1 - \left(\frac{\Phi}{W} - 1\right)^2\right) = \varrho\frac{\Phi}{W}\left(2 - \frac{\Phi}{W}\right)$$

It can be seen that $\lambda_1 < 0$ for all $\Phi > 2W$ and when $\Phi = 2W$, the OP is at the peak of compressor map (Φ_0, Ψ_0). With the typical numerical values of model parameters in Table 3.1, (Φ_0, Ψ_0)=$(0.5, 0.66)$ for a throttle gain $\gamma_T = 0.615$.

Other eigenvalues can be found from the following equation:

$$\left(\lambda - \frac{3H}{2Wl_c}\left(1 - \left(\frac{\Phi}{W} - 1\right)^2\right)\right)\left(\lambda + \frac{\gamma_T}{8B^2 l_c\sqrt{\Psi}}\right) + \frac{1}{4B^2 l_c^2} = 0$$

$$\lambda^2 + \lambda\left(\frac{\gamma_T}{8B^2 l_c\sqrt{\Psi}} - \frac{3H}{2Wl_c}\left(1 - \left(\frac{\Phi}{W} - 1\right)^2\right)\right) + \frac{1}{4B^2 l_c^2}\left(1 - \frac{3H}{4W}\left(1 - \left(\frac{\Phi}{W} - 1\right)^2\right)\frac{\gamma_T}{\sqrt{\Psi}}\right) = 0$$

Here, if $\left(1 - \left(\frac{\Phi}{W} - 1\right)^2\right) < 0 \rightarrow Re(\lambda_2), Re(\lambda_3) < 0$ which means that all of OPs on the negative slope portion of compressor map (i.e. $\Phi > 2W$) are stable. It is obvious that the position of λ_2, λ_3 depend on many factors among them γ_T and B. One can use the numerical bifurcation packages to trace the variation of eigenvalues due to the variations of parameters. The locus of λ_2 and λ_3, which is affected by the choice of parameters, determines the type of bifurcations and the developed instabilities (e.g. Hopf bifurcation in deep surge, when γ_T is small and B is high enough). Figure 3.4 shows how the number of OPs and the their stability vary when one closes the throttle (i.e. γ_T decreases, further information is provided later).

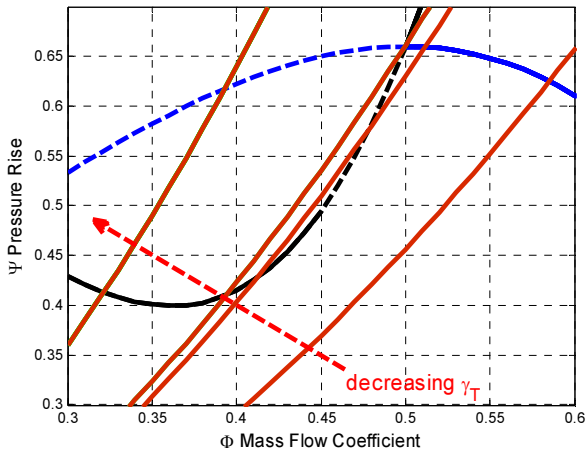

Figure 3.4: Stable OPs: Bold curves, Unstable OPs: Dashed curves

3.2 Surge and Rotating Stall Simulation

Figure 3.5 explains the development of rotating stall. Suppose that the system is initially at a stable OP (1) where $J = 0$. A disturbance can force the system to move toward the unstable area (OP (2)) where rotating stall initiates and the system jumps to fully developed stall OP (3) where $J > 0$. At this working point the pressure rise is dramatically reduced. By opening the throttle, the flow increases but the system cannot immediately return to OP (1) until OP (4) where the throttle characteristic is tangent to the stall characteristic and the system then jumps back to OP (1).

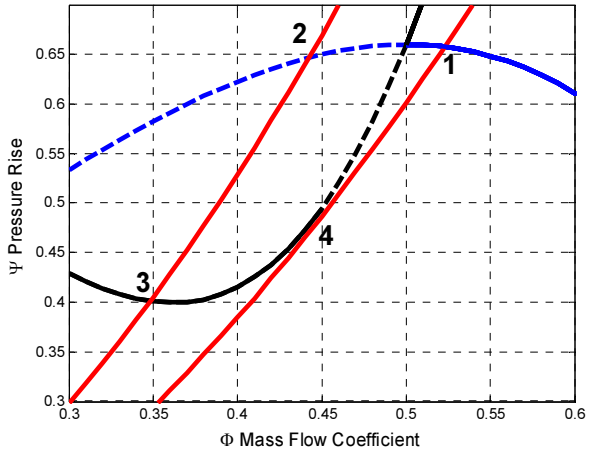

Figure 3.5: Rotating Stall Formation

There exists a severe hysteresis between the steady axisymmetric flow and the fully developed rotating stall OPs. The hysteresis can prevent systems from returning to the stable area when one tries to clear rotating stall by opening the throttle. This hysteresis is recalled again in greater detail in the bifurcation analysis of MG3.

Figure 3.6 shows an example of deep surge: at OP (1) the flow becomes unstable and cycle starts and the compression system jumps to OP (2) where the flow is negative. Then, the system descends until OP (3) where the flow is negligible. At this OP the system jumps very fast to OP (4) with a positive flow and then moves again toward OP (1) and the cycle continues.

Time domain simulations of MG3 clarify its behavior which depends on the choice of parameters. If $\gamma_T < 0.615$, by setting $B = 0.1$, which corresponds to a low rotor speed, the compressor goes into fully developed rotating stall, but by setting $B = 1$, which corresponds to a high rotor speed, the compressor initiates surge. Figures 3.7 and 3.8 show simulation results for fully developed rotating stall and deep surge respectively. As Figure 3.7 shows, in the case of rotating stall, J grows and the output pressure dramatically decreases. This pressure drop spells operational problems for the compressor. In Figure 3.8, the direction of the flow periodically changes and consequently causes the pressure fluctuation at the output of the compressor. During flow reversal, hot gases return to the compressor and damage the mechanical parts.

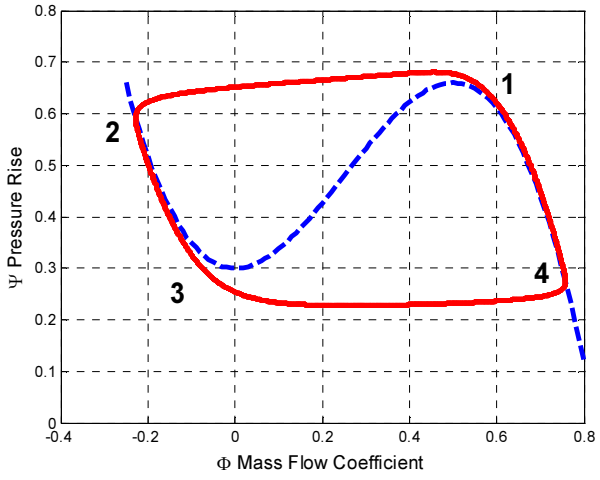

Figure 3.6: Deep surge cycle

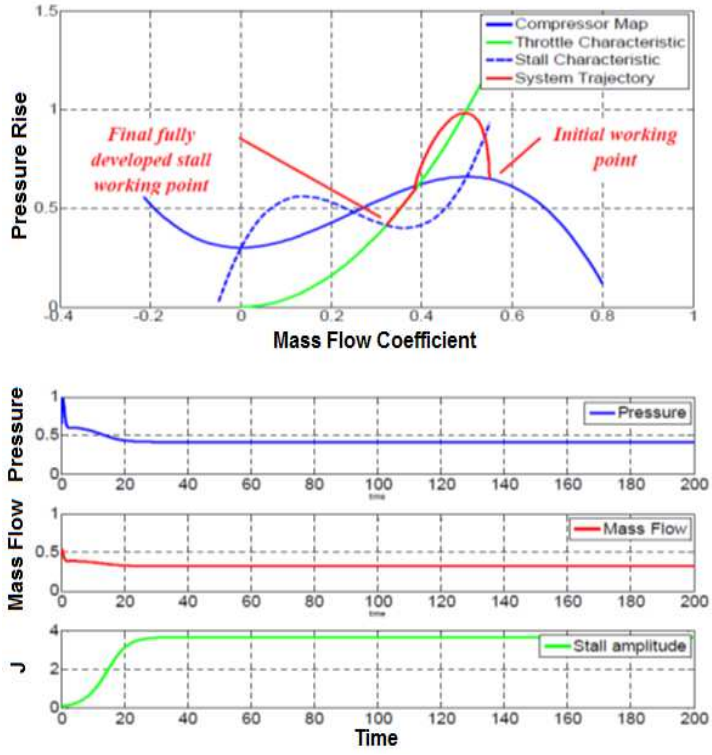

Figure 3.7 Fully developed rotating stall B=0.1

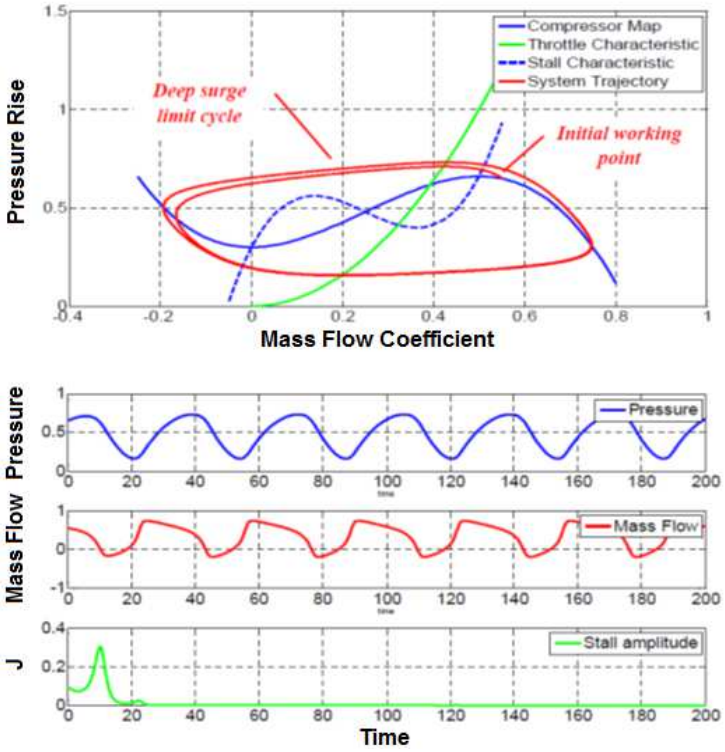

Figure 3.8 Deep surge B=1

3.3 Bifurcation Analysis of MG3

Most studies on the bifurcation analysis of the Moore-Greitzer model [48-51] in open-loop and closed-loop systems point out the effects of the throttle gain as a bifurcation parameter. Here, the bifurcation diagram of the squared amplitude of rotating stall J is reviewed. Figure 3.9 shows the stable and unstable solutions for low B-parameter values (e.g. $B = 0.1$). The attracting and repealing zones of manifolds are also emphasized by arrows in the figure. The bifurcation point (BP) in this figure is a subcritical pitchfork bifurcation implying a severe hysteresis in the behavior of the system. The system behavior in the interval between the limit point (LP) and the bifurcation point (BP), which takes on a considerable importance, is explored below.

For all throttle gains greater than LP, starting from every initial stall value (e.g. an external perturbation) ends up with fully damped out rotating stall. By decreasing the throttle gain to a value between LP and BP, stall may be generated or damped out depending on its initial value. Here, OP (A) is an effective OP but OP (C) is a fully developed rotating stall. OP (B) is an unstable OP. Figure 3.9b shows how the throttle characteristic intersects with the compressor map and the stall characteristic in three points (A, B and C). If the throttle gain is less than BP, stall is generated for all initial stall values.

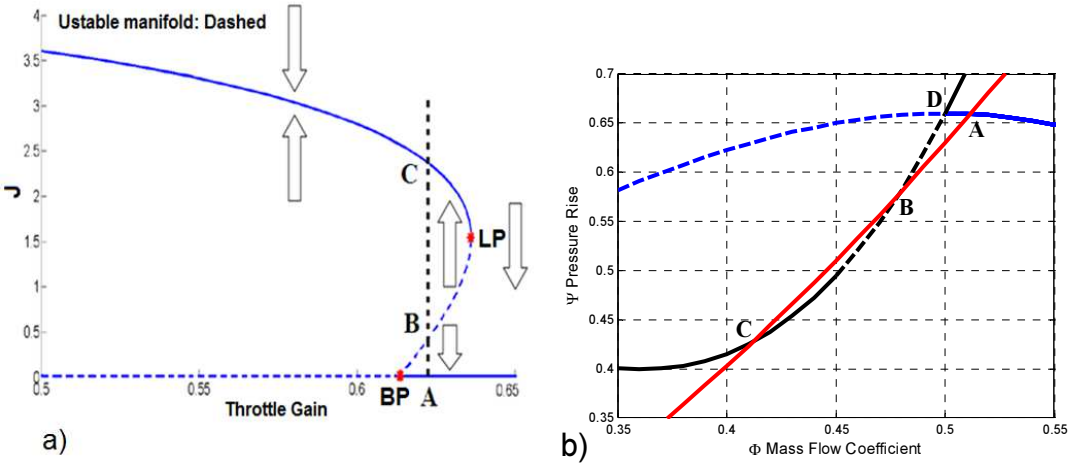

Figure 3.9 Bifurcation diagram of MG3 for low B-parameter values

(Bold lines: Stable manifolds, Dashed lines: Unstable manifolds)

The LP in the bifurcation curve corresponds to a throttle gain where the throttle characteristic is tangent to the stall characteristic. BP in the bifurcation curve is a throttle gain in

which throttle characteristic intersects with the compressor map and stall characteristic at two points including OP (D).

The hysteresis can also be seen in the bifurcation curve. Again suppose that the system has gone into a fully develop stall condition at OP (C) on the upper solution where $J > 0$. One may want to remove the stall by opening the throttle. The flow increases but the system cannot immediately return to the active area until when the throttle curve is tangent to stall characteristic (LP in bifurcation curve) where the OP jumps to a fully damped out stall manifold corresponding to OP (A).

Another important phenomenon is the presence of a Hopf bifurcation point. This mainly depends on the value of B-parameter. The Hopf bifurcation point can only be seen for higher values of B (e.g. $B = 2$) where points H appears in the bifurcation diagrams and shows the inception of surge (see for more details [37, 139, 142]).

In Figure 3.10, all trajectories starting from an initial point in zone A converge to the fully developed stall manifold and all trajectories starting from an initial condition in zone C converge to fully damped stall conditions. In zone B, all trajectories starting from this area converge to a limit cycle reporting deep surge.

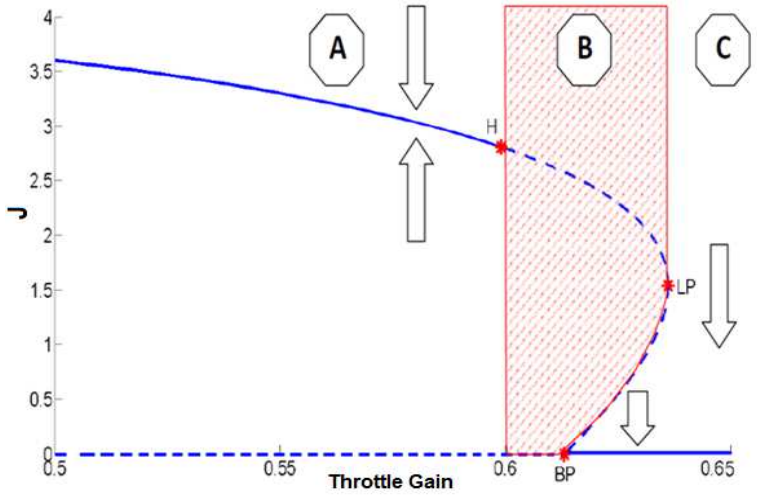

Figure 3.10: Bifurcation diagram for MG3 (high values of B-parameter)

3.4 Impact of Rotating Stall High Order Harmonics

As mentioned earlier, MG3 as a lumped parameter model considers only the first mode of rotating stall dynamics, but rotating stall can be thought of as a perturbation consisting of different harmonics. In 1994, Mansoux et al.[40] found that higher order harmonics of rotating stall can dominate and temporarily become larger than the first harmonic during the stall inception. Leonessa et al. [143] then emphasized the particular importance of higher order harmonics in a realistic control law design. They showed that using a stabilizing recursive backstepping controller based on the one mode Moore-Greitzer model cannot guarantee the global stability of the multi-mode case and drives the system to a fully developed stall.

Furthermore, the Moore–Greitzer model does not consider the time lag between flow perturbation across the compressor and the development of the perturbation in pressure rise. This problem was investigated further in [89]. An interesting fact is that such time lag stabilizes the high-order spatial modes to a greater extent than the lower ones. Consequently, only a small number of spatial modes require control action to be suppressed. Another key issue which affects the higher order harmonics is the gas viscosity. The gas viscosity was first introduced in the Moore-Greitzer model by Adomatis and Abed [42] and its effects were investigated by Gu et al. [37] and Hendrickson and Sparks [48]. Adomatis and Abed [42] demonstrated that the large velocity gradients associated with higher modes will be damped out by viscous effects. They also studied the important effects of viscosity on the bifurcation behavior of the modified model. Roughly speaking the number of stall modes is determined by the gas viscosity. Without viscosity, all the modes would have the same amplitude in fully developed rotating stall. The impact of viscosity on the qualitative behavior of VSACs will be discussed in detail later in the next chapter.

Figure 3.11 demonstrates the growth of higher order harmonics during the fully developed stall inception. It is also shown that the second, third, and forth harmonic temporarily dominate the first one. This outcome is generated by a simulation of a multi-mode Moore-Greitzer model where although the effect of higher harmonics is included, the speed is constant.

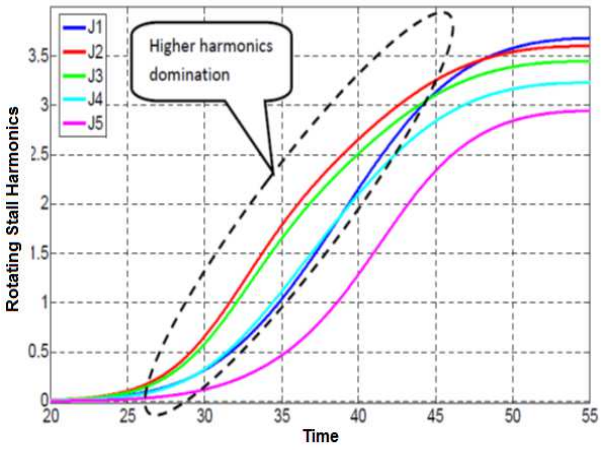

Figure 3.11: Contribution of higher harmonics of rotating stall up to 5th during the stall inception

3.5 Gravdahl's Model for VSACs

In this section, Gravdahl's model for VSACs is recalled. As discussed before, the stability of compressors and the influence of speed transitions on the compression dynamics are of great importance especially in aeronautics. In the original MG3 model and its higher order harmonics extensions, although B-parameter is proportional to the compressor speed, it is constant. The model developed by Gravdahl [46, 47] considers the speed of the rotor as a state variable. The model also includes the higher order harmonics of rotating stall and the gas viscosity as a model parameter. The compression system consists of an inlet duct, inlet guide vanes IGV, variable speed axial compressor, exit duct, plenum volume and a throttle (as shown in Figure 3.1). Gravdahl developed the model in the form of: $\dot{z} = f(z, \Gamma_t)$ where $z = (\Phi, \Psi, B, J_1 \ldots J_N)^T$ and Γ_t is the non-dimensional drive torque used as an input to change the speed. The variables Φ, Ψ represent, as in MG3, the annulus averaged mass flow coefficient and the non-dimensional plenum pressure respectively. $J_1 \ldots J_N$ are the squared amplitudes of rotating stall's harmonics and B, the new added state, is the speed of the rotor.

The following equations (3.10)-(3-13) introduce the model (See [46, 47] for further details).

$$\dot{\Phi} = \frac{H}{l_c(B)}\left(-\frac{\Psi-\psi_{c0}}{H} + 1 + \frac{3}{2}\left(\frac{\Phi}{W}-1\right)\left(1-\frac{J}{2}\right) - \frac{1}{2}\left(\frac{\Phi}{W}-1\right)^3 - \frac{l_E U_d \Gamma \Lambda_1}{bH}\Phi\right) \tag{3.10}$$

$$\dot{\Psi} = \frac{\Lambda_2}{B}(\Phi - \Phi_T) - 2\Gamma\Lambda_1 B\Psi \tag{3.11}$$

$$\dot{B} = \Lambda_1 B^2(\Gamma_t - \Gamma_c) \tag{3.12}$$

$$\dot{J}_n = J_n\left(1 - \left(\frac{\Phi}{W} - 1\right)^2 - \frac{J_n}{4} - \frac{\mu n^2 W}{3aH} - \frac{2U_d \Gamma \Lambda_1 (m-1)W}{3bHn}\right)\frac{3aHn}{(n - m_B(B)a)W} \tag{3.13}$$

$n = 1,2,\dots,N$

J_n is defined as the squared amplitude of the n[th] harmonic of rotating stall and

$$J = \frac{1}{N}\sum_{n=1}^{N} J_n \tag{3.14}$$

Here, all derivatives are calculated with respect to a normalized time $\xi := {Ut}/{R}$ where t is the actual time, R is the mean compressor radius, and U is the constant compressor tangential speed.

Γ_c the non-dimentional compressor torque is given by:

$$\Gamma_c = -\phi^2(tan\beta_{1b} - tan\beta_{2b}) \tag{3.15}$$

where β_{1b} and β_{2b} are constant blade angles at the rotor entrance and exit respectively [14].

In the model Λ_1, Λ_2, a, W, and H are constant.

In order to study the effects of speed variations on the system behavior, a simple proportional speed controller of the form $\Gamma_t = C_s(U_d - U)$ is used in Gravdahl's model to increase the speed of the rotor. In this equation U_d is the desired velocity of the wheel and C_s is a gain defining the rate of the acceleration. Higher (lower) C_s leads to faster (slower) rates of speed variations. The difference between rotor speed U and desired speed U_d drives the system toward the final steady speed. As before the compressor speed U and B are related (i.e. $U = bB$ where b is a constant).

Here, l_c and m_B depend on the speed of the rotor as follows:

$$m_B(B) = (1 - m)\frac{U_d}{bB} - 1 \tag{3.16}$$

$$l_c(B) = l_I + l_E\frac{U_d}{bB} + \frac{1}{a} \tag{3.17}$$

where m is the compressor duct flow parameter ($m = 1$ for a very short exit duct, and $m = 2$ otherwise). All distances are nondimensionalized with respect to R (the mean compressor radius) and $l_I = \frac{L_I}{R}$, $l_E = \frac{L_E}{R}$ (see L_I and L_E in Figure 3.1).

In this model, the effect of viscosity is taken into account by including the μ parameter. The compressor map and the throttle characteristic are considered as (3.1) and (3.5) respectively.

3.6 Speed Variations and Temporary Stall Developments in VSACs

Gravdahl's model not only captures the previous behavior of MG3 such as surge and rotating stall developments but also introduces some novel phenomena such temporary stall development during speed variations.

Gravdahl briefly studied the temporary stall development as an exclusive qualitative behavior of the model by preforming limited time-domain simulations [47]. The simulation showed that during speed transitions, amplitudes of rotating stall harmonics increase temporarily. Note that for the selected OP and the final speed (e.g. $\gamma_T = 0.65$ and $B = 2.2$), MG3 does not imply any rotating stall development since the OP is situated in the safe area by an adequate margin to the unstablilities. This temporary growth of stall harmonics causes a pressure drop at the output of the compressor and disturbs the normal operation of the gas turbine.

In Figure 3.12 two different acceleration rates are studied. In both cases, although the initial OP is located in the safe area far from unstable zone, the amplitude of rotating stall is temporarily increased due to speed variations. During these speed variations, the output pressure decreases. For the higher acceleration rates, the pressure drop is higher. Simulations show that this stalling can be avoided by accelerating the compressor at a lower rate or in other words by using a smaller C_s , but this may not satisfy the speed variation requirements.

Table 3.1: Numerical values used in simulations and bifurcation analysis

Symbol	Value	Symbol	Value	Symbol	Value
R	0.1	l_c	3	μ	0.01
V_p	1.5	l_E	8	ψ_{c0}	0.3
a	0.3	l_I	2	W	0.25
a_s	340	m	1.75	H	0.18
ϱ	1.15	I	0.03	$tan\beta_{1b} - tan\beta_{2b}$	0.7
A_c	0.01	B	0.1, 2.2		
Λ_1	2.168e-4	Λ_2	0.0189		

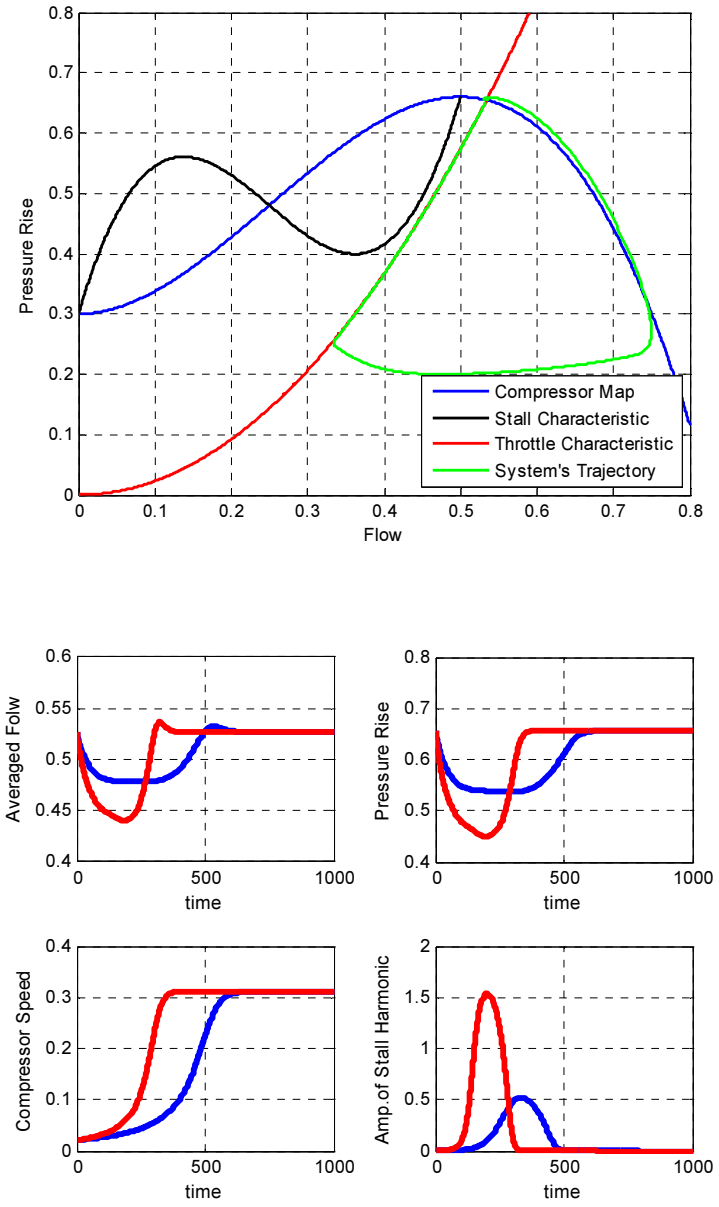

Figure 3.12: Temporary stall growth and pressure drop during speed transitions for two different acceleration rates C_s even far from unstable zone (Red: high acceleration, Blue: low acceleration)

In two next chapters, we provide a detail bifurcation analysis of Gravdahl's model for VSAC. Results reveal the impact of parameter variations on the model instabilities. Time-domain simulations not only corroborate the bifurcation analysis but also shows novel transient behavior of the model which is not explored before.

CHAPTER 4

QUALITATIVE BEHAVIOR OF VARIABLE SPEED AXIAL COMPRESSORS

4.1 Introduction

Despite the great importance of variable speed axial compressors (VSACs), detailed model analysis and stabilizing control design have remained a challenging problem. In this chapter, we focus on the qualitative analysis of the Gravdahl model for VSACs. To this end, we first investigate the developed nonlinearities by exploring the stationary and periodic solutions of the model. Next, we analyze the impact of parameters such as the throttle gain and the acceleration rate on both the transient and steady–state response of the compressor. The effect of initial and desired (final) speed on developed instabilities is studied as well. This detailed model analysis leads to a better understanding of feasible control approaches in next chapters.

4.2 Methodology

Here, our main objective is to carry out a detailed bifurcation analysis to determine how model dynamics depend upon the choice of parameters. In order to study the structural stability of the model, we employ numerical bifurcation analysis method as a standard approach by using MATCONT [144] and AUTO [145], two packages based on continuation method. The outcome of the bifurcation analysis is also corroborated through a set of time-domain simulations. This multi-method approach allows us to validate our results.

Bifurcation refers to the appearance of a topologically nonequivalent phase portrait under the variation of parameters. The parametric portrait together with phase portrait for each state constitutes a bifurcation diagram [146] (See Appendix A and B for more details). In Chapter 3.3, we briefly presented the bifurcation diagrams of MG3 and described the stationary and periodic solutions corresponding to stall and surge respectively. In most studies on bifurcation analysis of the Moore-Greitzer model [48-51], the effects of the throttle gain as a bifurcation parameter on stall dynamics are addressed. Gu [147] and Ananthkrishnan [139] demonstrated the presence of a Hopf bifurcation point (H in Figure 3.10) which indicates the onset of surge for high B-parameter

values (see also [142]). Gu [37] also developed the bifurcation diagram of deep surge dynamics and demonstrated the dependence of the Hopf bifurcation point on the *B*-parameter value.

For bifurcation analysis of VSAC's model, we consider Gravdahl's Model recalled in the Chapter 3.5 by (3-10)-(3-13) and consider only the first harmonic of the rotating stall. The investigation of the stationary and periodic solutions of the model reveals that the acceleration rate significantly affects the steady state behavior in addition to the transient response. For this reason, the acceleration rate is viewed as a novel bifurcation parameter. Furthermore, the continuation of critical points such as Hopf bifurcation points demonstrates that the desired speed deeply affects the qualitative properties of the model. In addition to these new findings, time-domain simulations indicate that the initial speed is yet another key factor having considerable influence on the developed nonlinearities. This shows that incorporating spool dynamics in the model leads to a far richer dynamical behavior than that of MG3. All of numerical values, which are used in this study, are provided in Table 3.1.

4.3 Stationary and Periodic Solutions

The specific objective of this section is the study of stationary and periodic solutions of the model by depicting the bifurcation diagrams. This is mainly performed by AUTO and verified by Matcont. Operational considerations lead us to treat the throttle gain as a natural bifurcation parameter. Other model's parameters such as viscosity and the acceleration rate can modify the qualitative behavior of the system as well. The location of manifolds and the diversity of bifurcation points highly depend on the acceleration rate and the desired speed value which define the speed dynamics. Another key factor affecting the system responses is the initial speed.

Figure 4.1 shows the bifurcation diagrams of the model including the stationary and periodic solutions for three different values of the desired speed U_d while the acceleration rate C_s and the initial speed U_i are kept constant (the impacts of these parameters are explored in sequel). In this figure, stable and unstable solutions are respectively depicted by bold lines and dashed lines. A reasonable range of the throttle gain as the main bifurcation parameter is covered. Figure 4.1a shows the bifurcation diagram of the first harmonic of stall when $U_d = 10$. In this case, no periodic solution exists. Stable stationary solutions include the fully developed rotating stall and no stall manifolds. When the throttle gain is more than 0.64, there is only one stable no stall

manifold (black-bold). This corresponds to the active operation of the compressor. When the throttle gain is between 0.615 and 0.64, the convergence toward fully develop stall or no stall stable manifold depends on the initial condition. If the system initially starts from the shaded area, it converges to no stall manifold; otherwise it leads to a rotating stall. Finally, when the throttle gain is less than 0.615, the only stable manifold is fully developed stall (green-bold). Therefore, starting from every initial value of stall amplitude, the system converges to fully developed stall which leads to a reduction in output pressure. In Figure 4.1b, the bifurcation diagram of the first harmonic of stall is depicted for $U_d = 65$. A periodic solution (red manifold) starts at the first Hopf bifurcation point HB1 where $\gamma_T = 0.613$. At this point, the equilibrium point loses its stability as a pair of complex conjugate eigenvalues of the linearization cross the imaginary axis of the complex plane. The stable part of this periodic solution approaches a homoclinic orbit when the throttle gain increases. Around this homoclinic orbit, the period becomes very large and continuation fails to converge.

The corresponding time-domain simulation result depicted in Figure 4.2 corroborates the presence of this periodic solution. The trajectory of the system in flow and pressure rise plane is depicted in Figure 4.2a and the oscillations of flow, pressure rise, and the first harmonic of stall are shown in Figure 4.2b, Figure 4.2d, and Figure 4.2e respectively. In contrast with other limit cycles which will be discussed later, the period of oscillation is large in this case (about 600). The final value of speed $U_d = 65$ corresponds to $B = 0.67$ which is shown in Figure 4.2c.

Higher desired speed values (e.g. $U_d = 100$) drastically change the qualitative behavior of the model. The presence of new periodic families (red and blue) corresponding to deep and mild surge is among these changes. These periodic solutions starting at the second Hopf bifurcation point (HB2) are depicted in Figure 4.1c. They can be categorized into two families. The first one (bold-blue manifold) shows a stable limit cycle of mass flow and the pressure rise where the amplitude of stall is zero. This manifold corresponds to surge. The other family (red manifold) is a periodic solution of rotating stall which is partially unstable (dashed). This manifold finally changes to a stable periodic solution where the amplitude of stall is not zero. Further details are given in Figure 4.1f where the stable periodic orbits of surge are clearly indicated on the bifurcation diagram of flow. The corresponding manifolds with Figure 4.1c are depicted with the same color and style in Figure 4.1f. These manifolds show the maximum amplitude of flow oscillations (which is obviously not zero).

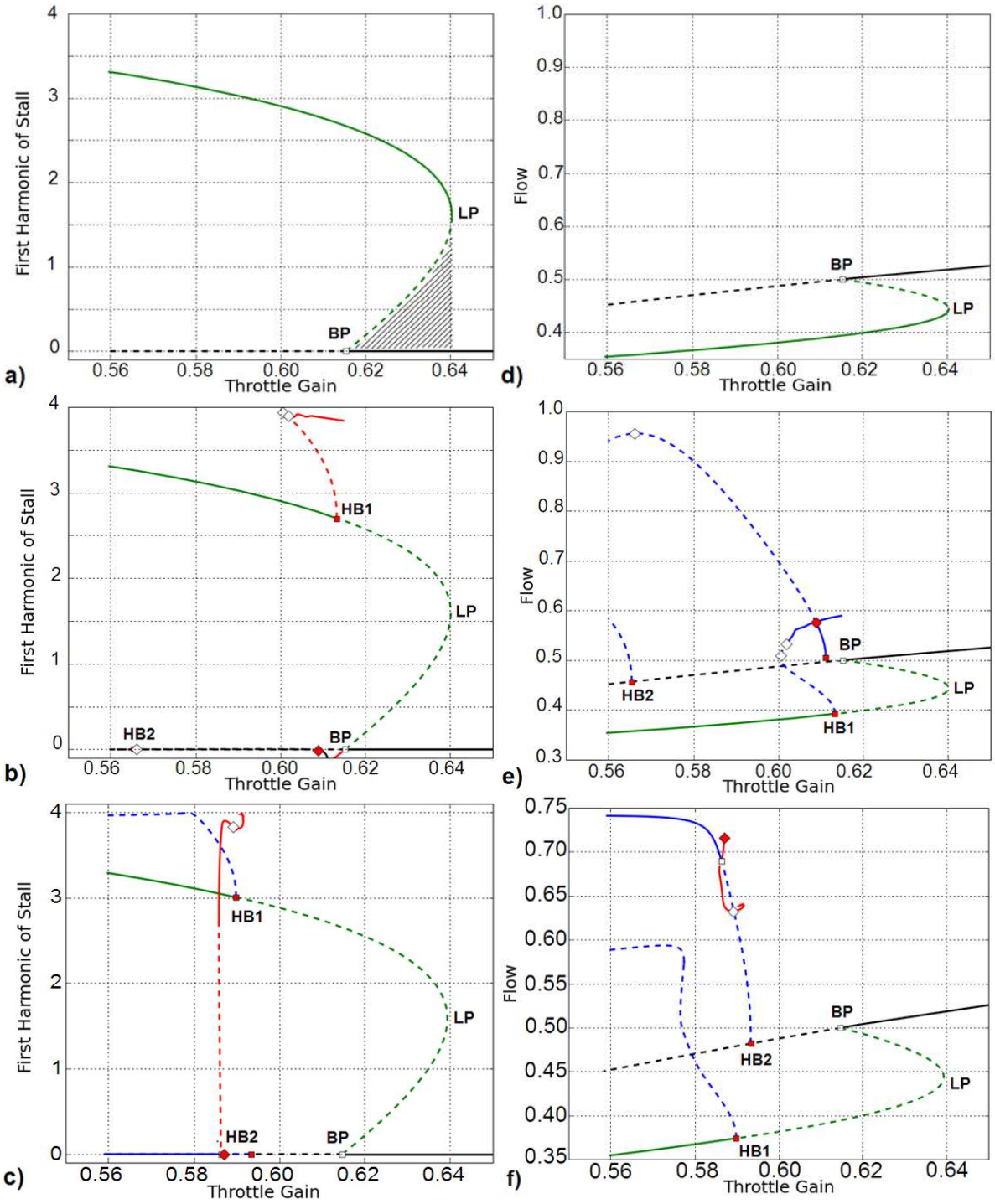

Figure 4.1: Periodic orbits (blue and red) and stationary solutions (black and green) of the model for $C_s = 1$, Bolds show stable and dashed lines show unstable manifolds.

$U_d = 10$ in a), d), $U_d = 65$ in b) and e), and $U_d = 100$ in c) and f)

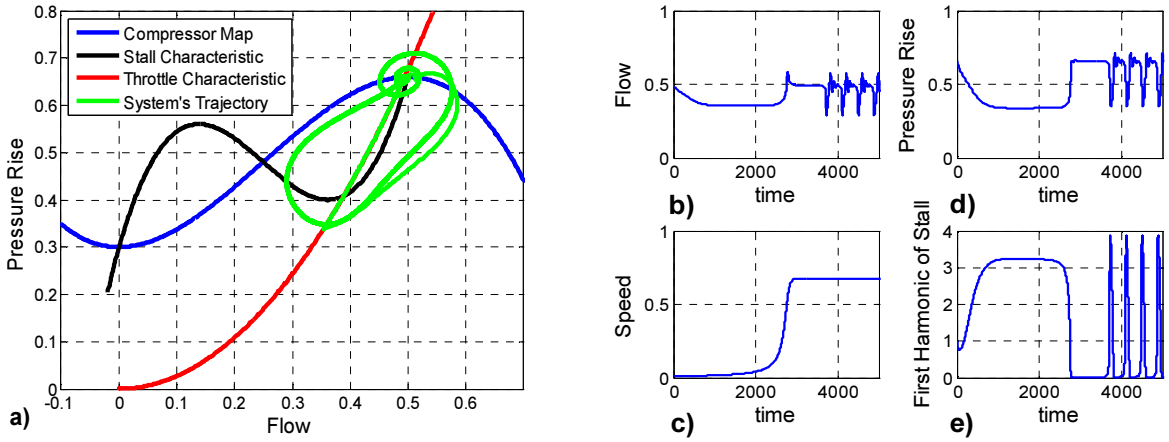

Figure 4.2: Limit cycle of first harmonic of stall $U_d = 65, C_s = 1$ and $\gamma_T = 0.61$

Figure 4.3a is added to clearly identify three different oscillations pertaining to Figure 4.1f. The first one is deep surge leading to flow reversal (pointed out as a part of bold-blue manifold). The second one is mild surge where the oscillation does not imply flow reversal and the amplitude of rotating stall is zero (indicated as mild surge1). Finally, the third periodic family (indicated by mild surge2) does not cause flow reversal as well but it results in the rotating stall oscillation. The period of the oscillations in this case is higher than the two previous cases. Figure 4.3b shows the period of deep and mild surges. The time-domain simulations of deep surge and two different mild surges are shown in Figure 4.4, Figure 4.5, and Figure 4.6 respectively.

It is worth noting that the bifurcation diagrams of Gravdahl's model are significantly different than the bifurcations of MG3. The differences naturally arise from the dimension of the parameter space. Bifurcation diagrams of Gravdahl's model should be depicted in a multi-parameter space including the acceleration rate and the throttle gain, whereas the bifurcation analysis of MG3 is performed when only the throttle gain varies [139, 148]. Therefore the depicted diagrams here are only a slice of the multi-parameter bifurcation space.

In the next section, to avoid practical difficulties of the bifurcation analysis in a multi-parameter space, we carry out the analysis of the model in different two-parameter spaces.

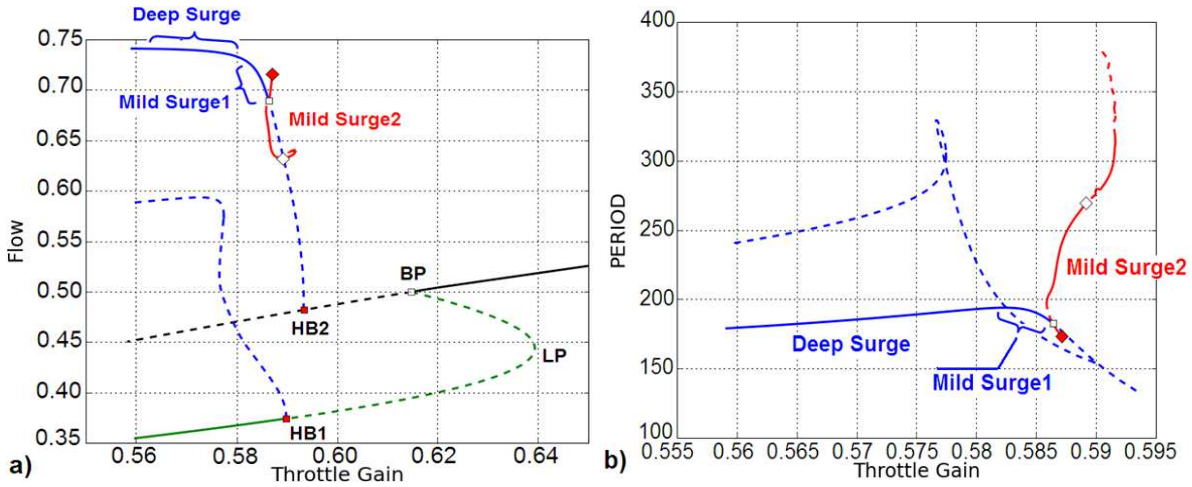

Figure 4.3: Mild surge and deep surge periodic solutions $U_d = 100$ and $C_s = 1$

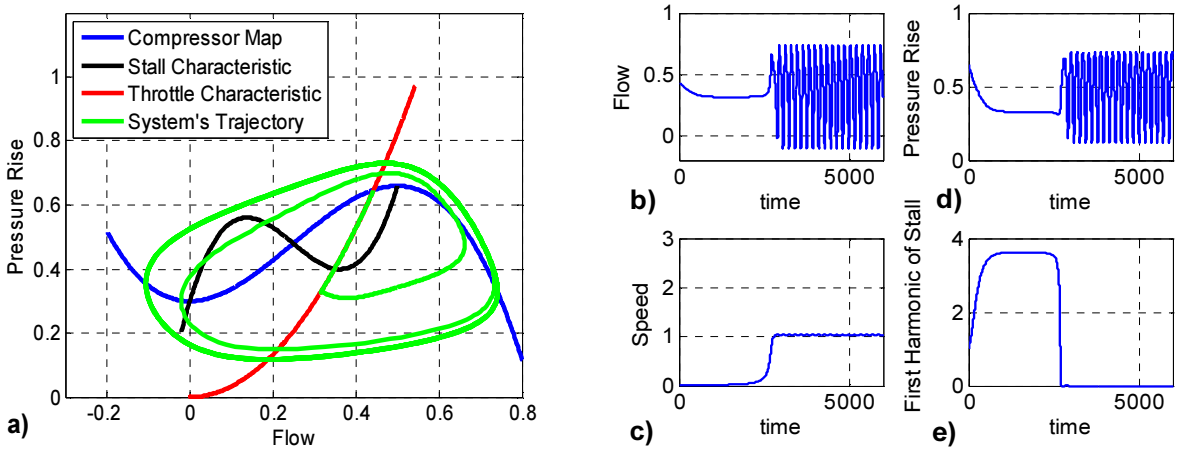

Figure 4.4: Deep surge including flow reversal $U_d = 100, C_s = 1$ and $\gamma_T = 0.56$

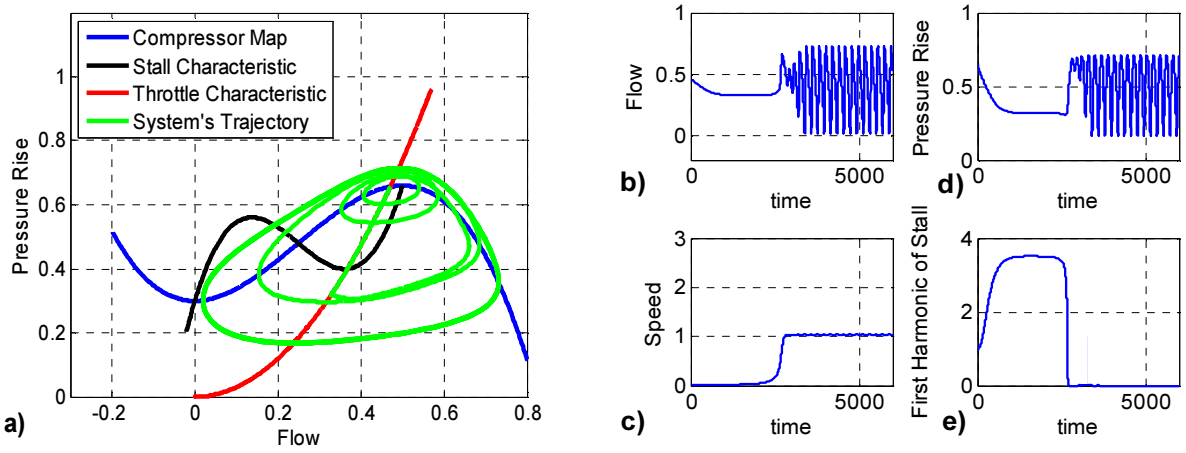

Figure 4.5: Mild surge without flow reversal and stall oscillation $U_d = 100, C_s = 1$ and $\gamma_T = 0.58$

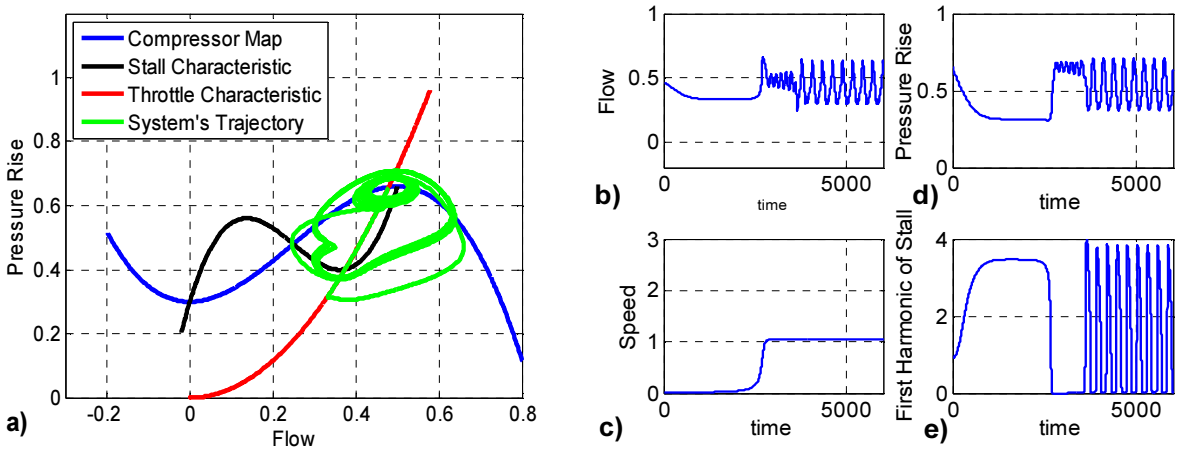

Figure 4.6: Mild surge without flow reversal including stall oscillation $U_d = 100, C_s = 1$ and $\gamma_T = 0.58$

4.4 Bifurcation Analysis in 2-parameter Space

In the previous section, we provided the bifurcation diagrams of the model for the different desired speeds. Here, we study the persistence of critical points of the bifurcation diagrams due to the variation of a second parameter.

Normally, when a parameter passes a fold (limit point) the behavior of the system can change drastically. Thus it is useful to determine how the location of a fold changes when a second parameter varies [149]. Another point presenting a change in the nature of the solution is a Hopf bifurcation point where an equilibrium loses its stability. The persistence of a Hopf bifurcation due to the variation of a second parameter is also of great importance in system analysis and control design. In this section, we compute critical stability curves or the loci of fold and Hopf bifurcation points in 2-parameter space. Two accepted methods are employed here to present the effect of a second bifurcation parameter. Firstly, we trace the solution families for different values of the second parameter and show the qualitative changes. Secondly, we compute the continuation of critical points due to the variation of the second parameter and point out the qualitative changes. Along the way, time-domain simulation is again used to validate the bifurcation analysis results.

4.4.1 Impact of the Acceleration Rate

The proportional controller gain, which initially introduced by Gravdahl [47] to increase the speed of the compressor, is considered as a model parameter in this study. This parameter is

referred to as acceleration rate C_s and defines the rise time of the speed transitions and deeply affects the speed dynamics. The main objective of this section is to show that the acceleration rate can modify the bifurcation diagrams and changes the qualitative behavior of the system.

Obviously, this is a case-dependent parameter meaning that a new speed control method can completely change the parameter definition. However in the case of other speed controllers, the speed dynamics behaves in the same way and makes it possible to follow the same approach as applied here to study the effect of the controller on the qualitative behavior of the system.

Figure 4.7, which is depicted for two different acceleration rates and desired speeds, shows that the variation of the acceleration rate changes the bifurcation points and also modifies the form of the manifolds. These can change the behavior of the system in different ways, including the type and the range of instabilities and the relevant domain of attractions as well. The deformation also indicates that the amplitude of fully developed stall and the amplitude of the limit cycles corresponding to surges vary due the acceleration rate variations. A set of time-domain simulations also emphasizes the impact of speed dynamics and the acceleration rate.

Figure 4.8 presents time-domain simulations for the specific values of the acceleration rate and initial speed U_i. This figure demonstrates that initial speed U_i also has considerable influence on the behavior of the system. The throttle gain is kept constant during these simulations. The desired speed is $U_d = 60$ for simulations a, b, and c, and $U_d = 165$ for simulations d, e, and f. As Figure 4.8a shows, the system initially goes into fully developed rotating stall when $C_s = 1$ and $U_i = 2$. By increasing the acceleration rate to $C_s = 15$ while keeping U_i constant, the system goes into deep surge as demonstrated in Figure 4.8b. This phenomenon shows a qualitative change in the model characteristics depending on the rate of the rotor acceleration. To describe the importance of the initial speed, we only modify the initial speed U_i in the third simulation (Figure 4.8c). The developed deep surge in Figure 4.8b has disappeared in Figure 4.8c where the initial speed is higher $U_i = 30$.

Similarly, Figure 4.8d and 4.8e show that a deep surge condition changes into fully developed rotating stall because of a slow acceleration rate. In Figure 4.8d, the system is driven to a deep surge condition due to the selected values of the desired speed $U_d = 165$, initial speed $U_i = 2$, and the throttle gain $\gamma_T = 0.45$. In Figure 4.8e, we decrease the acceleration rate while keeping the other parameters constant. Although the desired speed is the same as before, the

system goes into fully developed rotating stall due to the slow acceleration. Again, an increase in the initial speed ($U_i = 75$) causes that fully developed rotating stall in Figure 4.8e to change to deep surge in Figure 4.8f.

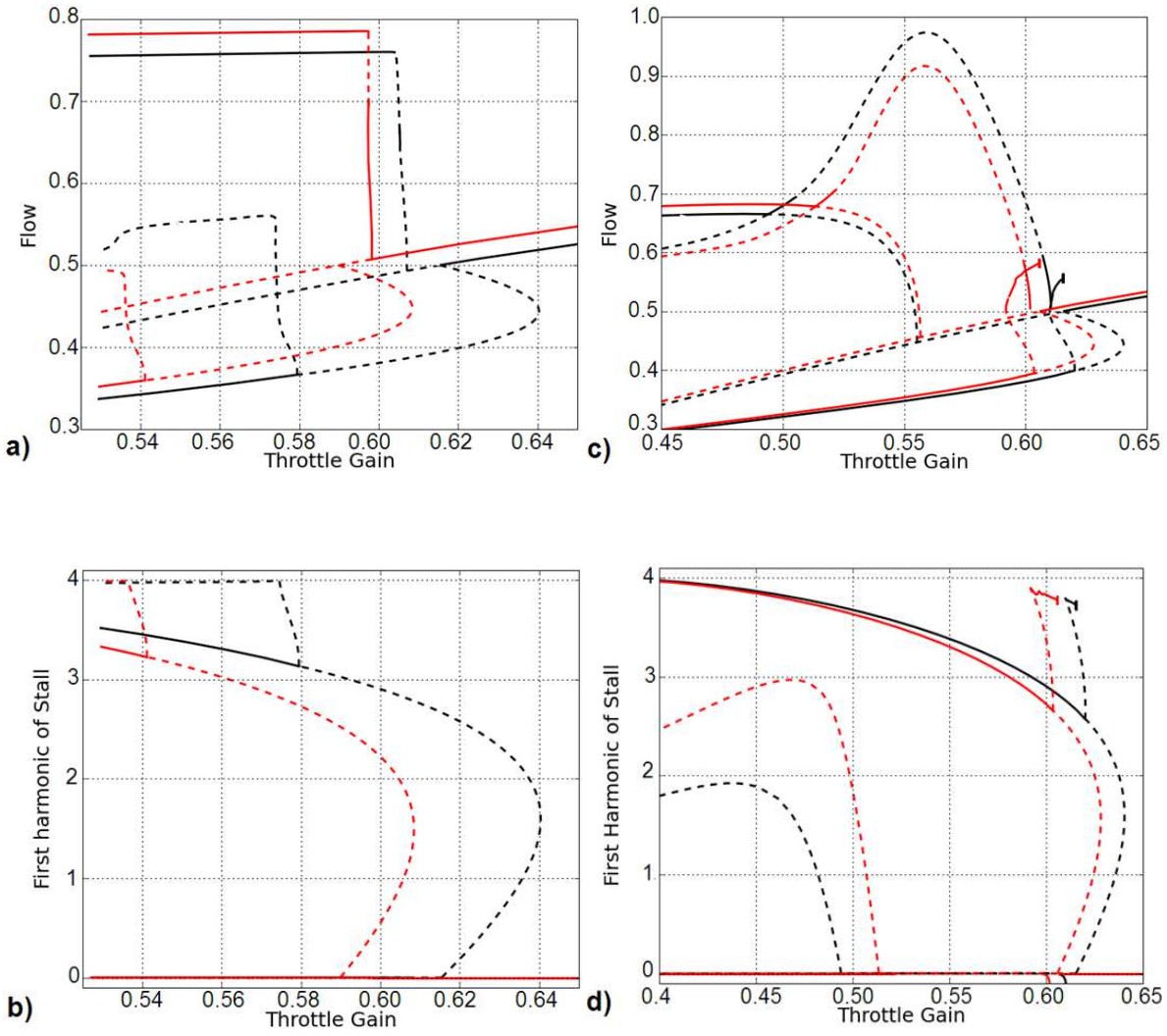

Figure 4.7: The impact of the acceleration rate on the bifurcation diagrams.

a), b): $U_d = 165$, c), d): $U_d = 65$

Black: periodic and stationary solutions for $C_S = 0.1$

Red: periodic and stationary solutions for $C_S = 30$

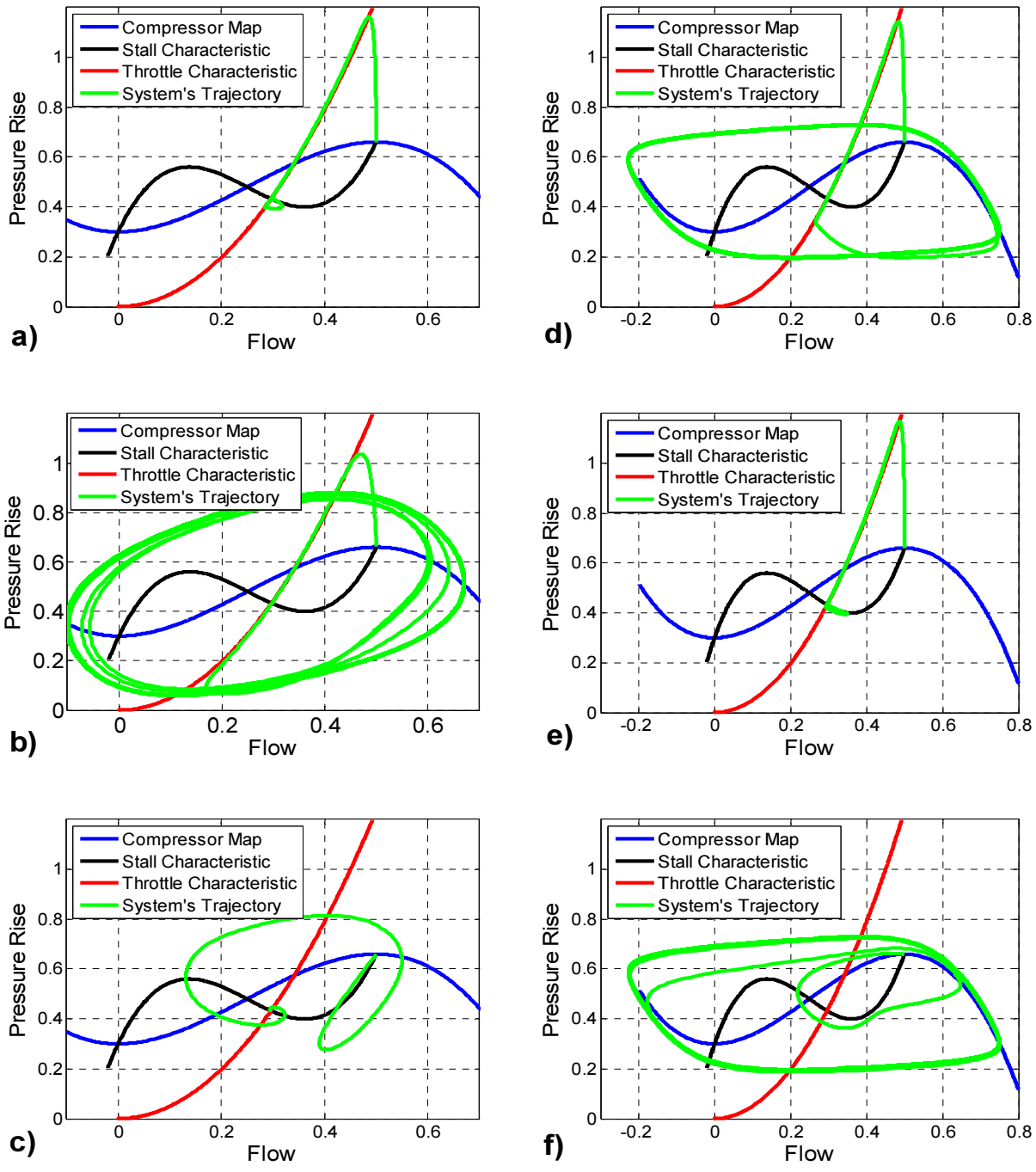

Figure 4.8: Effect of the acceleration rate (C_s) and initial speed (U_i) on instabilities

Blue: Compressor map, Red: Throttle characteristic ($\gamma_T = 0.45$) , Black: Stall characteristic, Green: System trajectory

a) $C_s = 1, U_d = 60, U_i = 2$, b) $C_s = 15, U_d = 60, U_i = 2$, c) $C_s = 15, U_d = 60, U_i = 30$

d) $C_s = 1, U_d = 165, U_i = 2$, e) $C_s = 0.1, U_d = 165, U_i = 2$, f) $C_s = 0.1, U_d = 165, U_i = 75$

Sensitivity to the initial speed can be explained in term of the domain of attraction. Figure 4.9 shows two different initial conditions in the state space of the system. By starting from the initial speed $U_i = 45$, the system converges to a deep surge while by initializing the system speed at $U_i = 2$, system converges to a fully developed rotating stall. In both cases the desired speed, the throttle gain, and the acceleration rate remain constant.

4.4.2 Effect of the Desired Speed

Another factor, which modifies the depth of speed transition and consequently affects speed dynamics, is the desired speed. Study on the effect of this factor was partially performed in MG3. In MG3, *B*-parameter involves the desired speed in the model without including the speed dynamics during the transition. First of all the impact of high and low value of *B*-parameter were indicated by surge and stall development respectively [36]. Then, the variation of *B*-parameter in the high value range was investigated [37, 139] to show its effect on the inception of surge. In the sequel, we study the effect of the desired speed U_d as the second bifurcation parameter of the Gravdahl model.

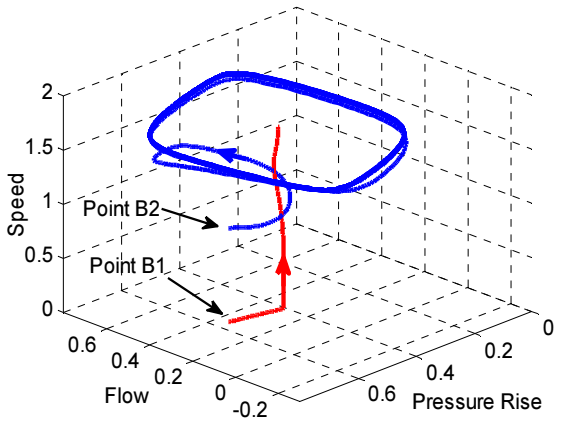

Figure 4.9: Effect of initial speed on the qualitative behavior of the system

$C_s = 0.1$, $U_d = 165$, $U_{iB1} = 2$ and $U_{iB2} = 45$.

(Deep surge: Blue trajectory, Rotating Stall: Red trajectory)

Figure 4.10 displays the bifurcation diagram of the mass flow. In this figure, the second Hopf bifurcation point (HB2) shows the inception of surge where the corresponding periodic solution begins. A family of this periodic solution is depicted for different values of the desired speed (when U_d varies from 105 to 165). By increasing the desired speed, surge is initiated in higher values of the throttle gain. Higher desired speeds also imply higher oscillation amplitudes. The variation of this parameter does not influence the position of the branch point (BP) or the limit point (LP) and does not cause any deformation in contrast to the effect of the acceleration rate. To study the movement of Hopf bifurcations due to the desired speed variation, the continuation of Hopf bifurcations is also calculated by AUTO. In this case, AUTO firstly computes the stationary and periodic solutions and then starts from bifurcation points being indicated as Hopf and varies the second parameter in the specified range. The new position of the Hopf bifurcation point is depicted at the same time. In Figure 4.11, the L2-Norm of states clearly shows the variation of the first and second Hopf bifurcation points when the desired speed gradually increases (dashed blue lines). HB1 shows the point where the unstable fully developed rotating stall equilibrium changes to a stable equilibrium. Throttle gains less than this value can lead to a stable fully developed rotating stall depending on the initial values of the system.

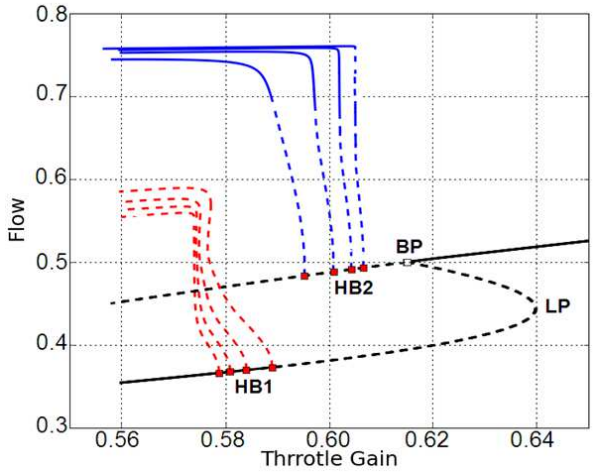

Figure 4.10: The impact of the desired speed on the position of HB2, left to right the desired speed is increasing ($U_d = 105,125,145,165$)

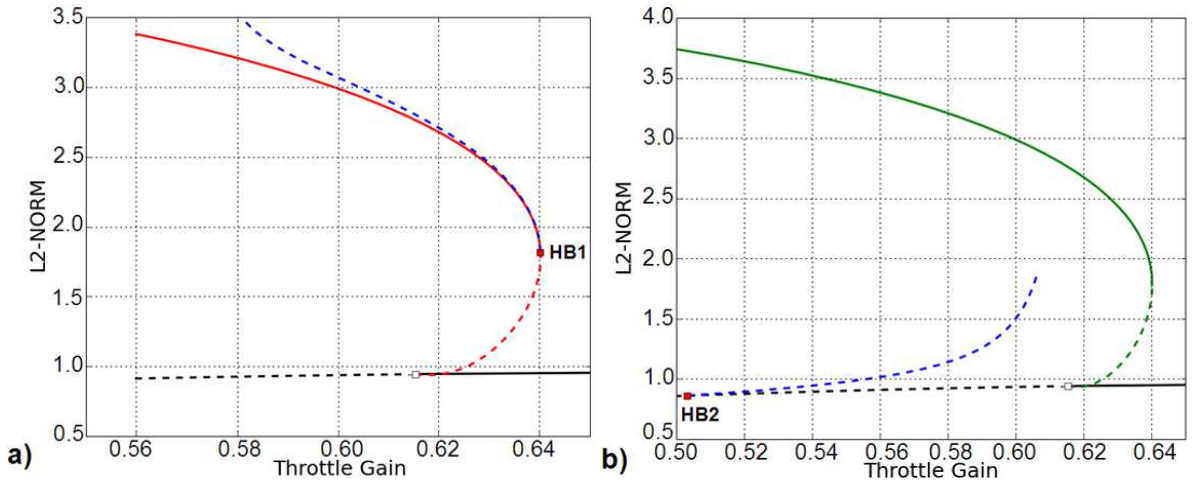

Figure 4.11: Continuation of Hopf bifurcation points (dashed-blue) when the desired speed as the second bifurcation parameter varies from 40 to 185

4.5 Conclusion

Aside from the theoretical and practical interest of the research about the performance limiting phenomena (surge and stall), an in-depth model analysis can help us to reject the infeasible control approaches and improve the formulation of the control design in next chapters. In this chapter, we focused firstly on the investigation of the developed nonlinearities in VSACs. Our results showed a richness of the model dynamics in comparison with the constant speed MG3. Bifurcation analysis based on continuation methods indicated new periodic solutions of mild surge and stall oscillation, however, the main contribution of the chapter is about the impact of speed transition. The detailed bifurcation analysis in a 2-parameter space revealed that the qualitative behavior of the system mainly depends on speed dynamics. Meanwhile, speed dynamics globally affecting the system are influenced by key factors such as the acceleration rate, the desired speed, and the initial speed.

The acceleration rate changes the rise time of the compressor speed and modify the bifurcation diagrams as a novel bifurcation parameter. It not only moves the critical points, but also deforms periodic and stationary solutions. This implies that surge or stall developments take place according to the way the speed of compressor varies. Time-domain simulations corroborate this hypothesis and show that slow or rapid speed variations can change the developed nonlinearities. We finally investigated the effect of the desired speed and the initial speed to

complete our study about the impacts of speed dynamics. These two key factors change the range of speed variation and modify the system behavior.

Next chapter will particularly concentrate on the contribution of higher order harmonics. As initially presented in Chapter 3, higher harmonics can temporarily dominate the main harmonic during speed transition. Chapter 5 explores also the impact of speed dynamics on the harmonics growth and rightly emphasizes the need for a multi-mode controller eliminating all modes of rotating stall.

CHAPTER 5

CONTRIBUTION OF ROTATING STALL MODES IN THE DYNAMICAL BEHAVIOR OF VARIABLE SPEED AXIAL COMPRESSORS

5.1 Introduction

Since compressors are variable speed machines, it is of interest to investigate the influence of speed transients on the system behavior and particularly on the higher order harmonics. Gravdahl's model for VSAC presented in Chapter 3 includes multi-modes of rotating stall and compressor speed as the states. The importance of higher order harmonics, which was explored in the literature for CSACs [40, 42, 143], has been an open problem for VSACs. The early work of Gravdahl [47] briefly addressed the qualitative properties of the model by performing time-domain simulations without exploring the contribution of rotating stall modes. This chapter stressed the need for detailed model analysis to assess the high-order modes dynamics of rotating stall. Gravdahl also suggested a novel multi-mode control design being capable of achieving fast speed transition and actively suppressing rotating stall as future work.

For the first time, the investigation of the transient behavior of Gravdahl's model reveals that the choice of parameters can change the amplitude of stall modes. Acceleration rate, desired speed, and initial speed as main factors determining speed dynamics can also significantly influence the number of dominant harmonics during temporary stall inception. Furthermore, the continuation of critical bifurcation points demonstrates that viscosity greatly changes the qualitative properties of higher modes of stall. These findings show the richness of the dynamical behavior that lies beyond the complex form of the model including the spool dynamics.

5.2 Methodology

The problem is to investigate the multi-mode rotating stall dynamics and to detail the involved key factors. To conduct this model-based study, Gravdahl's model for VSACs being recalled in Chapter 3.5 by (3-10)-(3-13) and the numerical values in Table 3.1 are used here. Our main objective is to investigate the effect of speed dynamics, which are deeply affected by the choice of parameters, on the multi-mode rotating stall dynamics. In order to explore the key issues of concern, numerical bifurcation and time domain simulation are both used. In this work,

MATCONT [144] and AUTO [145] packages based on continuation method are employed to study steady state behavior of the system and a set of time-domain model simulations is performed to investigate the transient response of the model.

5.3 Impact of Speed Dynamics on the Contribution of Stall Modes

In the previous chapter, the review of the bifurcation diagrams formed a novel hypothesis that the involved parameters of speed dynamics can modify the transient response of the model. Here, we test this hypothesis by performing a set of time-domain simulations. Among the model parameters, the desired speed and the acceleration rate directly modify the speed dynamics. The initial speed is another key factor which determines the range of speed variations and changes the system trajectories. Furthermore, we include the effect of throttle gain as the main bifurcation parameter of the model to complete our study. Four sets of time-domain simulation are performed to achieve this goal. Figures 5.1, 5.2, and 5.3 show the impact of the acceleration rate on the amplitude, and on the number of dominant stall modes temporarily developed during speed transitions. These figures are depicted for different values of the acceleration rate C_S while other parameters are kept constant ($U_d = 165$, $\mu = 0.01$, $U_i = 1$, and $\gamma_T = 0.65$). The results show that higher C_S increases the amplitude of stall modes. The number of higher harmonics, which dominate the main harmonic, is also increased for higher C_S. Consequently, the output pressure drops more dramatically for the case of rapid speed variation. Figures 5.1e-5.3e show that the operating points are adequately far from unstable area throughout the simulations. It is worth noting that slow speed variation yields an infeasible solution to temporary stall developments and pressure drops in many applications such as aeronautics.

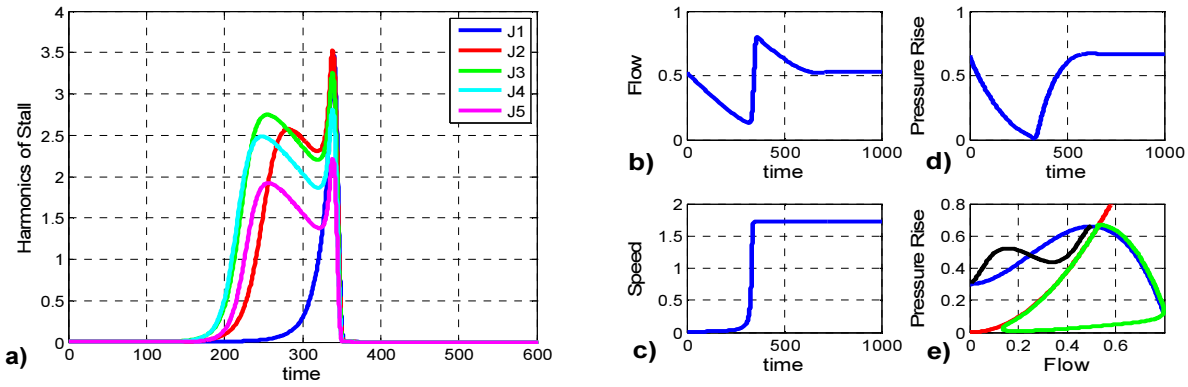

Figure 5.1: Dominant stall modes for temporary stall development $C_S = 8$

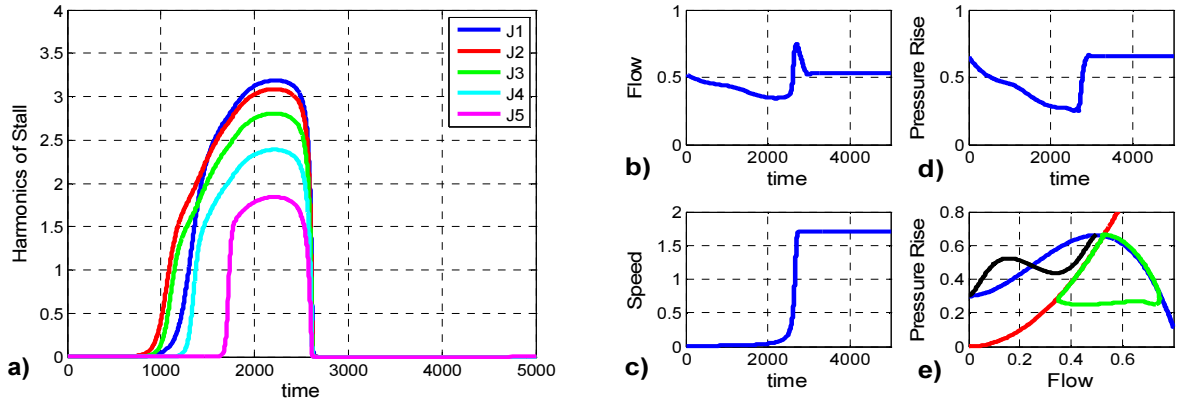

Figure 5.2: Dominant stall modes for temporary stall development $C_S = 1$

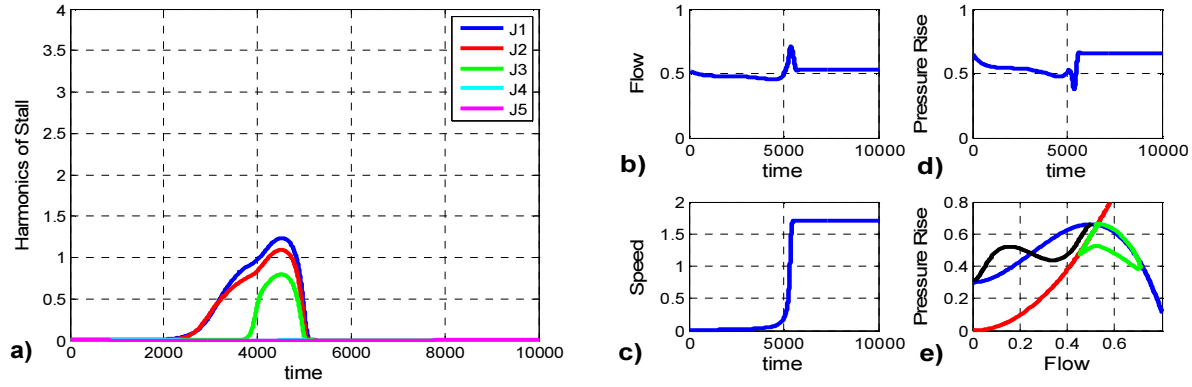

Figure 5.3: Dominant stall modes for temporary stall development $C_S = 0.5$

The desired speed is another involved factor which changes the range of speed variation and modifies speed dynamics as a result. The impact of the desired speed on the contribution of temporary developed stall modes is studied in Figure 5.4 where all of other parameters are constant ($C_S = 2$, $\mu = 0.01$, $U_i = 1$, and $\gamma_T = 0.65$). In Figure 5.4, the harmonics of rotating stall up to the 5th harmonic are depicted. Lower desired speeds dictate lower amplitude of harmonics. The number of higher modes dominating the main harmonic is also decreased for lower desired speeds. The initial speed can modify the transient response of the model as well. Figure 5.5 briefly shows the effect of this key factor on the temporary stall development. This figure clearly indicates that lower initial values cause higher amplitudes of stall modes and a higher number of dominant harmonics. For the simulations of Figure 5.4, all other parameters are kept constant ($C_S = 2$, $\mu = 0.01$, $U_d = 150$, and $\gamma_T = 0.65$).

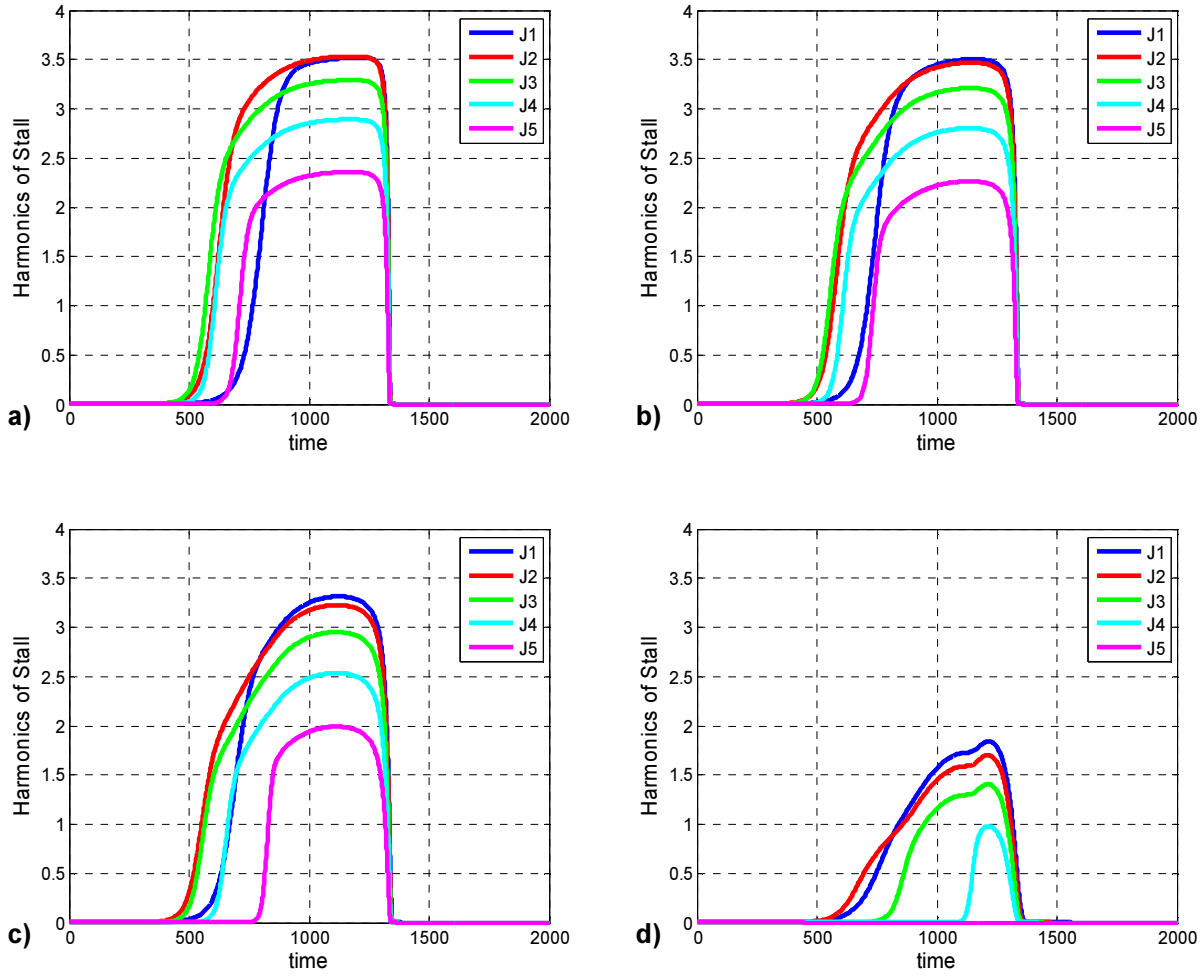

Figure 5.4: the effect of desired speed on the amplitude and number of dominant stall harmonics a) $U_d = 200$, b) $U_d = 150$, c) $U_d = 100$, d) $U_d = 50$

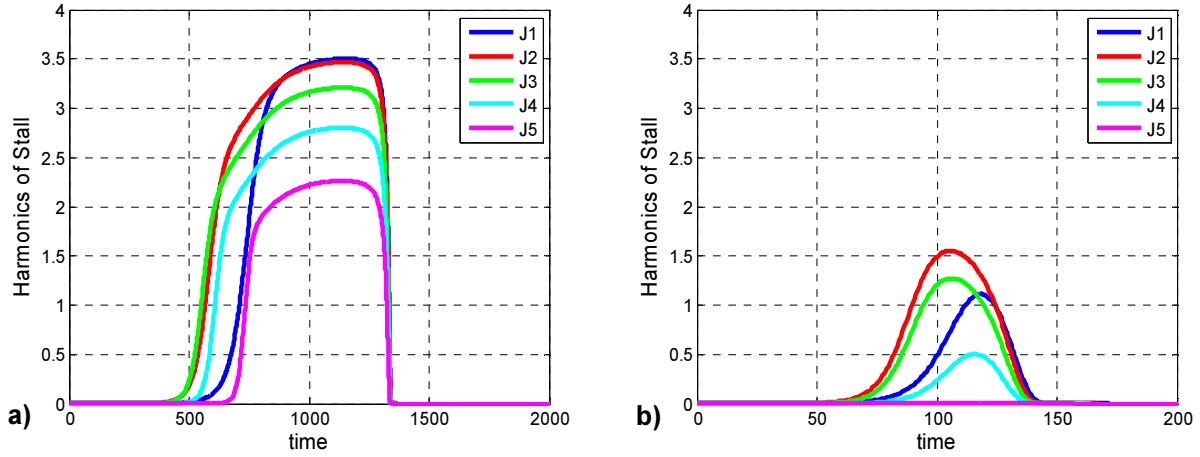

Figure 5.5: The effect of initial speed on transient behavior: a) $U_i = 1$, b) $U_i = 10$

Last but not least in this section, the effect of throttle gain on the temporary stall development is studied. Figures 5.6 and 5.7 show that the higher throttle gain γ_T , which leads to work far from stall line, causes lower amplitude of temporary developed stall (other key factors are kept constant: $C_S = 2,\ \mu = 0.01,\ U_d = 150,$ and $U_i = 1.$). The number of dominant harmonics is also reduced for the higher throttle gain. Again, an easy solution to deal with temporary stall developments and pressure drops is operating far from stall line. However, this comes at the expense of performance because at such operating points pressure rise is not high enough (compare Figure 5.6e and 5.7e).

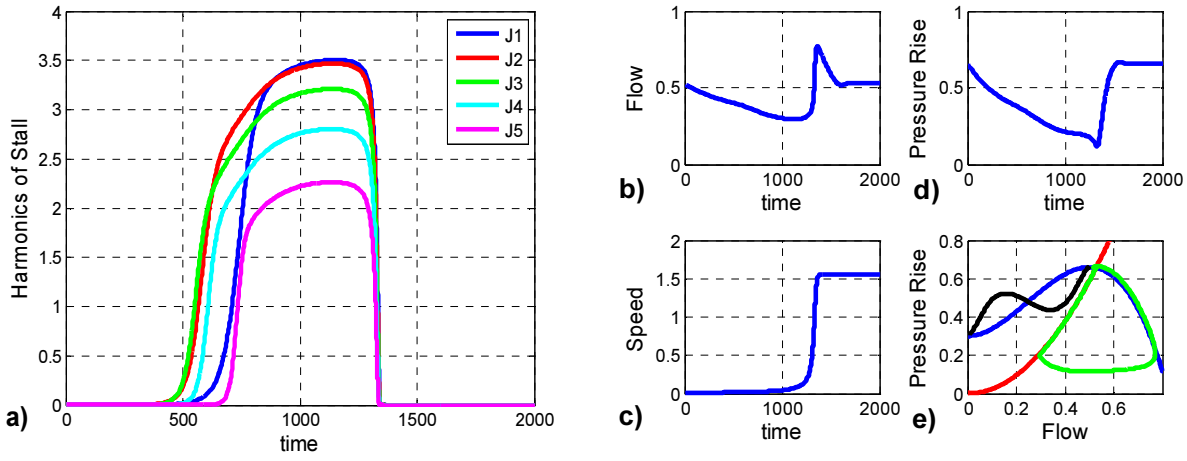

Figure 5.6: Low throttle gain leads to large number of dominant modes $\gamma_T = 0.65$

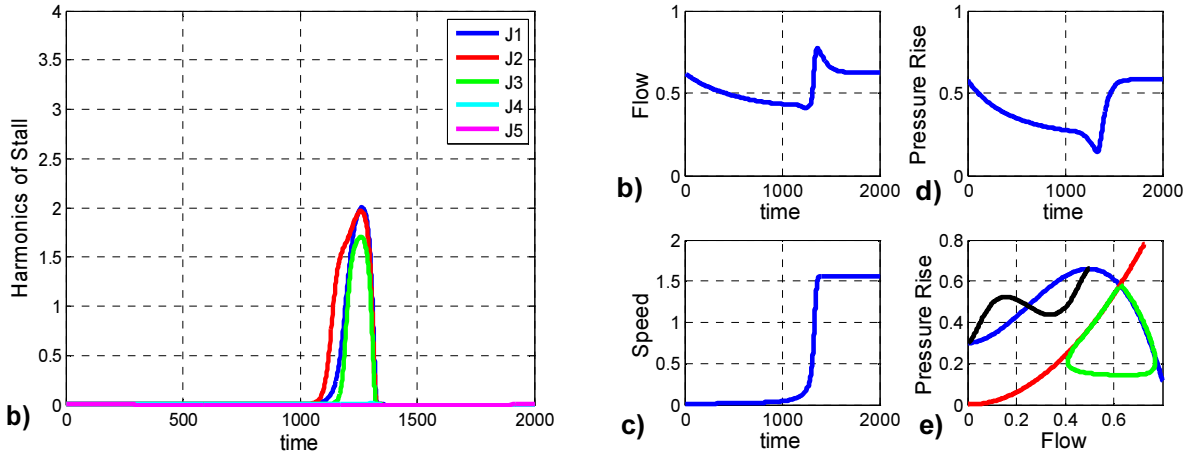

Figure 5.7: High throttle gain leads to a small number of dominant modes $\gamma_T = 0.82$

5.4 Impact of Viscosity on the Stall Modes

Another key parameter, which affects the qualitative behavior of the system, is gas viscosity. This parameter was first introduced in Moore-Greitzer model by Adomatis and Abed [42] and its effects were investigated by Gu et al. [37] and Hendrickson and Sparks [48]. Adomatis and Abed [42] demonstrated that large velocity gradients associated with higher modes will be damped out by viscous effect. In other words, the number of stall modes is determined by gas viscosity. Gas viscosity μ is also taken into account in the Gravdahl model.

It is shown here that μ is a bifurcation parameter for MG3 since its smooth variation can change the qualitative behavior of the model. It can affect both the transient and steady state behavior of stall modes in the same way. In sequel, the bifurcation diagrams of stall harmonics for VSACs and Gravdahl's model are studied in a two parameter-space. At first, bifurcation diagrams are depicted for throttle gain as the main bifurcation parameter and zero viscosity, then the continuation of limit points LP are traced due to the variation of μ as the second bifurcation parameter (red curves). The loci of limit points indicate that when μ increases in a normal range (e.g. $\mu \in [0\,,0.01]$), the nature of the transcritical bifurcation point BP changes from subcritical with hysteresis to supercritical without hysteresis for fourth and fifth harmonics (see [150] for more information on sub/super critical bifurcations.). In other words the deference between γ_{LP} the throttle gain at LP and γ_{BP} the throttle gain at BP ($\delta\gamma = \delta\gamma_{LP} - \delta\gamma_{BP}$), which defines the depth of rotating stall hysteresis (see [151] for stall recovery hysteresis), decreases by increasing gas viscosity.

In Figure 5.8, a family of bifurcation diagrams for different values of viscosity is depicted for the fifth harmonic of stall. The variation of limit point in Figure 5.8f corresponding with Figure 5.8e shows that higher μ can lead to fully damped higher order harmonics. This is in accordance with known results of constant speed compressors model presented in the literature, and is shown here to be also valid for VSACs.

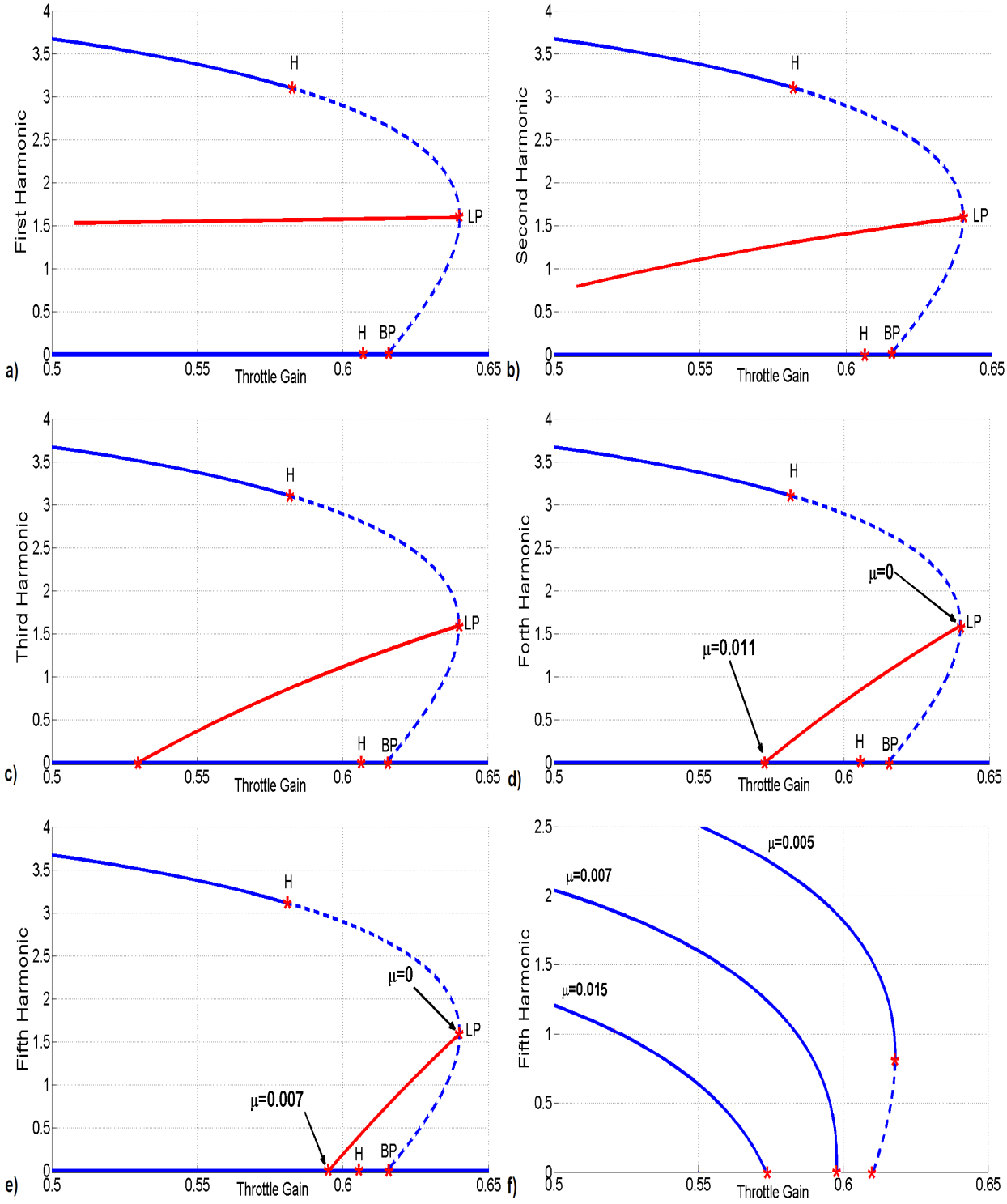

Figure 5.8: Continuation of limit point due to the variation of viscosity as second bifurcation parameter $C_s = 1, U_d = 165,$ and $U_i = 1$

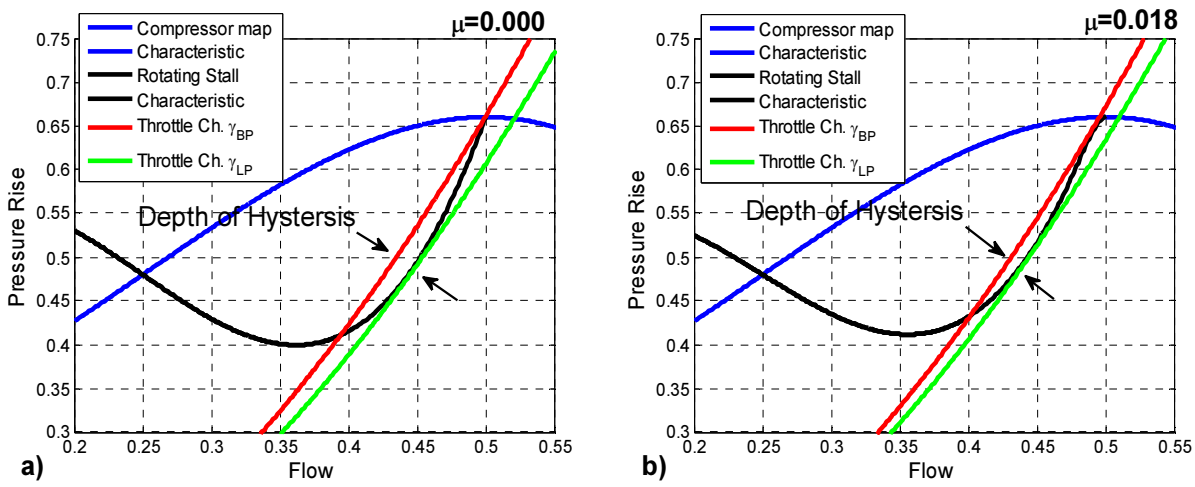

Figure 5.9: The Growth of gas viscosity decreases the depth of hysteresis

a) $\delta\gamma = \gamma_{BP} - \gamma_{LP} = 0.03$, b) $\delta\gamma = \gamma_{BP} - \gamma_{LP} = 0.015$

The time-domain simulations in Figure 5.9 corroborate through bifurcation analysis results. In this figure, γ_{LP} corresponds to the value of throttle gain where throttle characteristic is tangent to the rotating stall characteristic (green curve) and γ_{BP} corresponds to the value of throttle gain where throttle characteristic intersects the stall characteristic at the top of compressor map (red curve). By increasing μ the depth of hysteresis in Figure 5.9b is decreased. It is worth noting that the defined hysteresis in time-domain simulation is due to the average of all stall harmonics ($J = {}^{1}/_{N} \sum_{n=1}^{N} J_n$).

5.5 Temporary Rotating Stall Leading to Steady Rotating Stall Development

As discussed, at operating points far from stall line, temporary stall can finally be damped out when the speed reaches the desired value. However, this is not usually the case. In order to increase pressure rise and efficiency, the operating point should be selected near the top of the compressor map. As is well known, at such an operating point, small perturbation can lead to fully developed rotating stall or surge. This conveys the idea that speed variations and temporarily developed stall (as a perturbation) threaten the stability of VSACs in efficient working points. The dependency of temporary stall amplitude on parameters especially the acceleration rate suggests a tightly coupled interaction between throttle gain and the acceleration

rate in this issue. In the following, we examine the formed hypothesis by time-domain simulations.

Figure 5.10 shows that a slow speed variation cannot drive the system to the unstable zone, because temporary stall harmonics are not high enough (maximum 0.2, Figure 5.10e). In Figure 5.10a, the trajectory of the system returns to the initial operating point after a while. The quickly damped stall is manifested as a negligible temporary pressure drop in Figure 5.10c, which is cleared when stall harmonics are completely damped out in Figure 5.10e. Figure 5.10b shows speed variations where the slope of the curve depends on the acceleration rate. Harmonics of rotating stall (up to 5^{th}) are depicted in Figure 5.10d where the second and the third harmonics of stall dominate the first harmonic during the stall inception. Figure 5.11 shows the simulation for a rapid speed variation (High C_S) that causes high enough temporary stall harmonics and drives the system to steady-state rotating stall. The initial speed U_i, the desired speed U_d, gas viscosity μ, and throttle gain γ_T are kept constant for these two simulations ($\mu = 0.01, U_d = 10, U_i = 1, \text{and } \gamma_T = 0.62$). In Figure 5.11a, the system trajectory finally settles down at a new operating point (OP) where stall is steadily developed. Figure 5.11d focuses on a dramatic pressure drop as the effect of undamped rotating stall.

Figure 5.12 shows that a small smooth change made to the acceleration rate results in a sudden change in the system behavior. The rest of parameters are kept constant ($\gamma_T = 0.63,\ \ \mu = 0.01,\ U_d = 35,\ U_i = 2$). In Figure 5.12a, for $C_s \geq 1.032$, temporary stall leads to fully developed stall as discussed before. Figure 5.12b shows that for $C_s \geq 3.2$, stall is damped out again. This outcome is supported by the bifurcation analysis in Chapter 4 (see Figure 4.7) where the higher acceleration rates shifts the diagrams to the left and causes temporary stall for $\gamma_T = 0.63$.

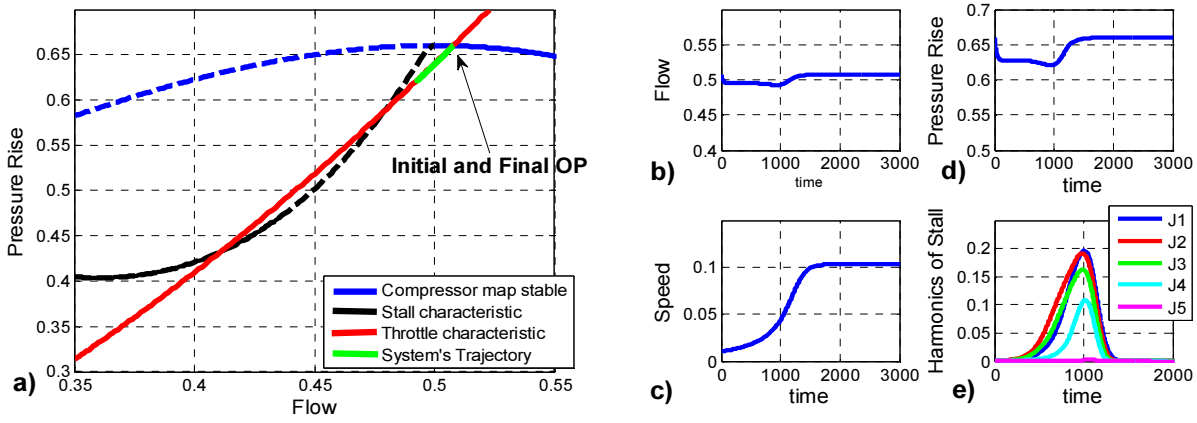

Figure 5.10: Temporary stall development is damped out $C_S = 2.5$

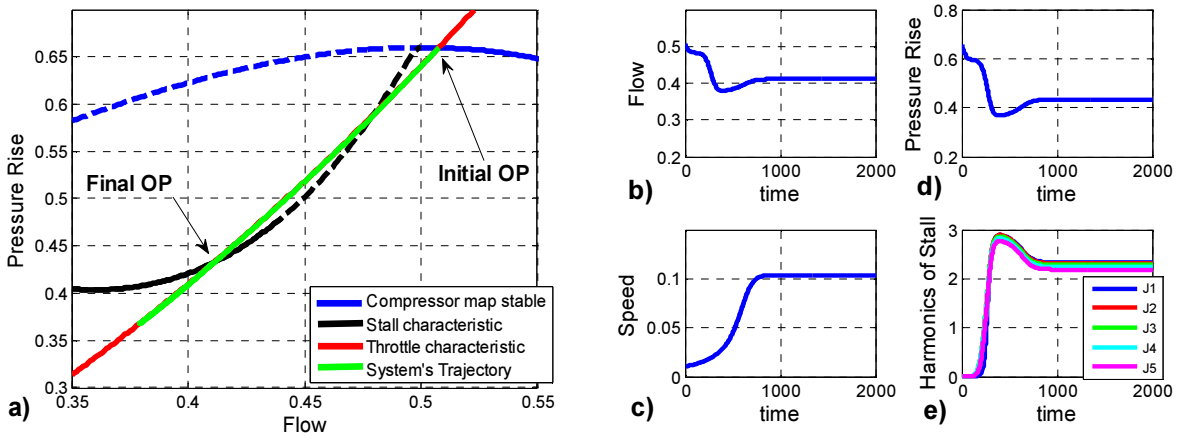

Figure 5.11: Temporary stall development causes fully developed stall $C_S = 5$

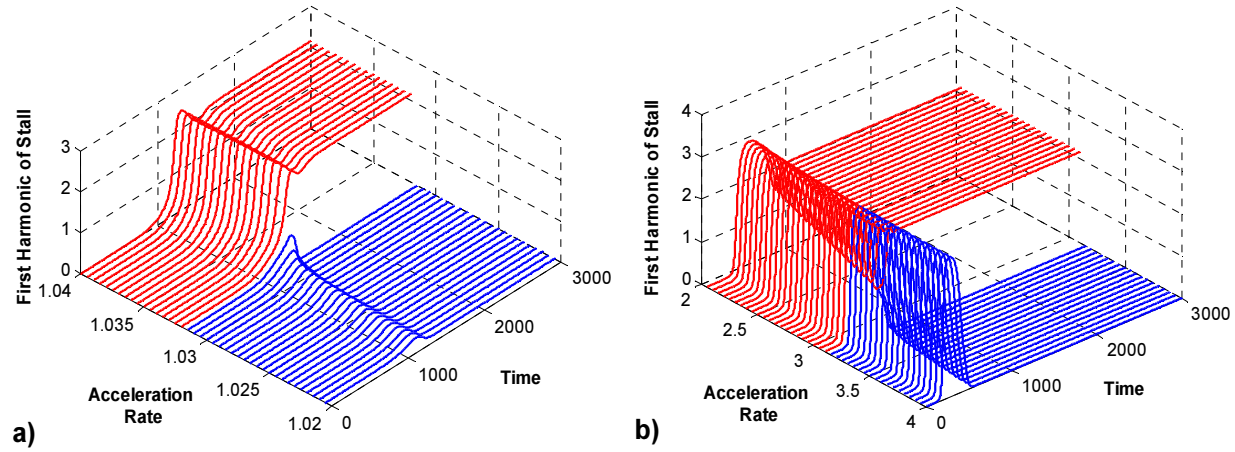

Figure 5.12: Increasing the acceleration rate results in different stall development

The well-known effect of throttle gain and the above results apparently shape a new idea about the interaction of throttle gain, the acceleration rate, and the threshold of transient perturbation leading to fully developed stall. Figure 5.13 shows this relationship. This figure indicates that higher γ_T requires higher C_S to develop steady stall. For lower γ_T however, even a slow speed variation leads to steady stall development. In other words, efficient operating points (e.g. $\gamma_T \leq 0.62$) are not robustly stable and speed variation easily destabilizes VSACs. In Figure 5.13, the upward sloping of developed stall recalls that as throttle gain drops, the amplitude of developed stall slightly increases.

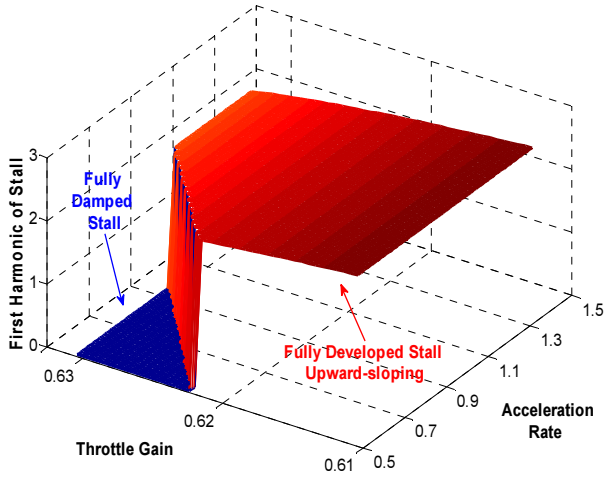

Figure 5.13 Thresholds of C_S for steady stall is influenced by γ_T ($\mu = 0.01,\ U_d = 35,\ U_i = 2$)

5.6 Conclusion

The common use of variable speed axial compressors clearly underlines the need for a detail analysis of model behavior including the multi-mode of rotating stall as performance limiting phenomenon. The impact of speed dynamics on the contribution of rotating stall modes in VSACs has been an open problem since the early work of Gravdahl. In this chapter, we address this problem to broaden the scope of mode's contribution and to consider the impact of key parameters of the model on the stability of the system. Simulation results supported by bifurcation analysis reveal that speed dynamics deeply affect the amplitude of harmonics and the number of dominant modes. The nature of this phenomenon and the topological behavior of the

model show the influence of many parameters such as gas viscosity, throttle gain, the desired speed, and acceleration rate.

This study demonstrated that speed variations at an efficient working point in the vicinity of unstable area can lead to fully developed stall causing serious operational trouble. This emphasizes the need for a stabilizing multi-mode controller to suppress temporary rotating stall developments and simultaneously achieve rapid speed variation in future work.

This research question is addressed in the next chapters. In Chapter 6, we firstly developed a robust controller and show that it can guarantee the boundedness of the model's states in error coordinates. This simple controller tackles the main control design problems of CSACs. To improve the control method, in Chapter 7, we explore again the stability of CSACs. By using a chattering-free sliding mode controller, we guarantee the asymptotic stability of the origin in error coordinates in the presence of external perturbations and model uncertainties. This controller is easy-to-implement and does not require full-state feedback. The finding of Chapter 6 and 7 shed some light on the VSACs' control design. Finally, in Chapter 8, we introduce a new method to simultaneously control speed and nonlinearities in these machines. This controller robustly control all of VSACs' instabilities being explored in chapter 4 and 5. The following chapters are submitted as research papers.

CHAPTER 6

ARTICLE 1: ROBUST PASSIVITY-BASED CONTROL OF SURGE AND ROTATING STALL IN AXIAL FLOW COMPRESSORS

Gholam-Reza Sari
École Polytechnique, University of Montreal, Montreal, Quebec, H3T 1J4, Canada

Ouassima Akhrif
École de Technologie Superieure, University of Quebec, Montreal, Quebec, H3C 1K3, Canada
and
Lahcen Saydy
École Polytechnique, University of Montreal, Montreal, Quebec, H3T 1J4, Canada

Submitted to Journal of Vibration and Control on May 2014

Abstract: In this work, we address the stability of compression systems and the active control of performance limiting phenomena: surge and rotating stall. Despite considerable efforts to stabilize axial compressors at efficient operating points, preventing and suppressing rotating stall and surge are still challenging problems. Due to certain passivity properties of the widely used Moore and Greitzer model for axial compressors, a robust passivity-based control approach is applied here to tackle the problem. The main advantage of this approach is that robust stabilization and high performance control can be achieved by simple control laws and limited control efforts. Analytical developments and time-domain simulations demonstrate that the developed control laws can effectively damp out rotating stall and surge limit cycles by throttle and close-coupled valve actuations. The robust performance of the controller is validated in the presence of bounded mass flow and pressure disturbances, as well as model uncertainties.

Key words: Passivity-based Control, Axial Compressor, Rotating Stall and Surge Control

6.1 Introduction

Passivity theory, which provides an energy based perspective in control theory, has been the subject of much research over the last decades [152-154] . The essential role of energy in the stability and performance of physical systems has resulted in the increasing attention to passivity. Basically, passive systems are a class of processes that dissipate a certain type of physical or virtual energy described by Lyapunov-like functions [155]. The concept of passivity especially plays an important role in robust control. Since passive systems are easy to control, the first step in passive system theory is to render a process passive via either feedback or feedforward.

Sufficient robustness to model uncertainties, parameter variations, and external disturbances can be ensured by passivity-based control (PBC) which guarantees the passivity of the system for the whole range of parameters. Achieving passivity with feedback is an appealing issue due to its input-output concept. However, one of the major challenges in feedback passification designs is to make it constructive. The key part of the design procedure is to select a proper output satisfying the required conditions [152]. In 1991, Byrnes et al. [154] derived the conditions under which a nonlinear system can be rendered passive via smooth state feedback and in 2009, Tsai and Wu [11] presented a constructive method for robust PBC (RPBC) of a certain class of weakly minimum phase nonlinear uncertain systems. They proposed a control law that renders the system passive and asymptotically stabilizes the closed loop system; however the perturbations were supposed to be vanishing.

In this work, we utilize RPBC to effectively stabilize nonlinear phenomena in compression systems. Compression systems suffer from two types of nonlinearities with different natures: surge and rotating stall. Rotating stall is a non-axisymmetric perturbation that travels around the annulus of the compressor, while surge is a violent limit-cycle in compressor characteristic that can lead to flow reversal and large axial oscillations (see [37] for more information). Despite the considerable efforts that have been made to investigate these phenomena, different aspects of the problem such as sensing, actuating and model-based control are still challenging issues.

From a control point of view, the nonlinear 2D model developed by Moore and Greitzer [36] for constant speed axial compressors (CSACs) dominates recent studies on rotating stall and surge control [37]. The lumped parameter Moore and Greitzer model (so-called MG3) is based on the first harmonic approximation of rotating stall. This model was developed by using Galerkin procedure applied to the original PDE form. In spite of the simple form of the model, it can capture surge and rotating stall nonlinearities and qualitative behavior of the system including bifurcations (see [142] for more information).

Remarkable efforts channeled into augmenting MG3 in different ways; among them obtaining higher order accurate models and including the force of actuators [40, 143, 156]. One of the most promising actuators is the close-coupled valve (CCV). The early work of Dussourd in 1977 [157] and the work of Simon and Valavani in 1991 [124] addressed CCV in compression

system control. In 1998, Gravdahl introduced an augmented MG3 model including CCV in error coordinates [47]. Recently, once again, this actuator attracted close attention of researchers in surge control ([94, 123, 131]).

Gravdahl demonstrated that the two-state simplified form of MG3 including CCV shows certain passivity properties and then applied PBC to develop a surge controller [158]. This simple proportional PBC law effectively stabilized surge limit cycles. Although the controller was not able to damp out rotating stall, it showed promise for suppressing this hard-to-control nonlinearity. This interesting open problem was suggested as future work by Gravdahl and to the best of our knowledge it has not been addressed since then.

Here, we address this problem and design a RPBC to suppress rotating stall in CSACs. The simple proportional and low order form of the developed controller is the first advantage of the applied method. It is not based on full-state feedback (the square amplitude of rotating stall as the third state of MG3 is practically hard to measure) and does not require the detailed knowledge of model parameters, which cannot be accurately estimated. The controller actuates the system with feedback from mass flow and pressure rise by using both the throttle valve and CCV. Furthermore, we relax assumptions on perturbations, which are usually supposed to be vanishing ([11, 12], by introducing bounded non-vanishing disturbances. Simulation results corroborating the analytical developments demonstrate that the applied RPBC effectively damps out the developed rotating stall and stabilizes efficient operating points (OPs) in the presence of bounded non-vanishing external disturbances and model uncertainties. The utilized approach eliminates surge limit cycles as well.

The rest of the paper is organized as follows. In Section 2, we start by reviewing the Gravdahl model representing CSACs comprising CCV. Section 3 presents the control design and section 4 reports time-domain simulations. Finally, some conclusions about this work are drawn in Section 5.

6.2 Axial Compressor Model

Here, we briefly review Gravdahl model for CSACs including CCV and throttle actuators. The compressor comprising CCV is shown in Figure 6.1 where the pressure rise over the equivalent compressor is the sum of the pressure rise of the compressor and the pressure drop over CCV: $\Psi_{ec}(\Phi) = \Psi_c(\Phi) - \Psi_v(\Phi)$. Φ is the circumferentially averaged flow coefficient and

Ψ is the total-to-static pressure rise coefficient. $\Psi_c(\Phi)$ is known as the compressor characteristic (map) which describes a nonlinear relationship (assumed cubic in [47]) between Φ and Ψ:

$$\Psi_c(\Phi) = \psi_{c0} + H\left(1 + 1.5\left(\frac{\Phi}{W} - 1\right) - 0.5\left(\frac{\Phi}{W} - 1\right)^3\right) \tag{6.1}$$

Here, H is the compressor characteristic height factor, W is the compressor characteristic width factor, and ψ_{c0} is shut-off head. The CCV characteristic that describes the pressure drop over CCV as a function of flow is given by $\Psi_v(\Phi) = \frac{1}{\gamma_v^2}\Phi^2$ where γ_v is the gain of CCV. The throttle characteristic $\Psi_T(\Phi) = \frac{1}{\gamma_T^2}\Phi^2$ gives the pressure over the throttle as a function of flow, where γ_T is the throttle gain. The throttle can be thought of as a simplified model of a power turbine.

For a given operating point (OP) (ϕ_0, ψ_0), the dynamic model is developed in the form of state-space equations $\dot{z} = f(z,u)$ equations (6.2)-(6.4), where $z \in \mathbb{R}^3, u \in \mathbb{R}^2$. $z = (\phi,\ \psi,\ J)^T$ represents the state vector of the system and $u = (u_1, u_2)$ is the control vector. It is defined in error coordinates with respect to the coordinates of the operating point (ϕ_0, ψ_0). In this model, $\phi = \Phi - \phi_0$, and $\psi = \Psi - \psi_0$. J is the squared amplitude of the first harmonic of rotating stall.

$$\dot{\psi} = k_1\left(\phi + \phi_0 - u_1\sqrt{\psi + \Psi_0} - \Delta_\phi\right) \tag{6.2}$$

$$\dot{\phi} = k_2\left(\psi_c - \psi - u_2 + \Delta_\psi - \frac{3H}{4}J\left(\frac{\phi+\phi_0}{W} - 1\right) - \frac{W^2 J}{2\gamma_v^2}\right) \tag{6.3}$$

$$\dot{J} = \varrho J\left(1 - \left(\frac{(\phi+\phi_0)}{W} - 1\right)^2 - \frac{J}{4} - \frac{4W(\phi+\phi_0)}{3H\gamma_v^2}\right) \tag{6.4}$$

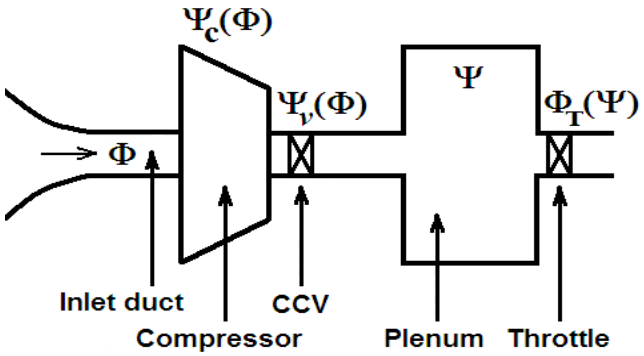

Figure 6.1: Compression system comprising CCV

Control variables $u_1 = \gamma_T$ and $u_2 = \psi_v(\phi)$ include the effect of throttle and the pressure drop over CCV (in error coordinates) respectively. A partially closed CCV during normal operation of the compressor leads to a bidirectional control law u_2 .The compressor characteristic given in (6.1) in global coordinates can be expressed in error coordinates as:

$$\psi_c(\phi) = -M_3\phi^3 - M_2\phi^2 - M_1\phi \tag{6.5}$$

where $M_1 = \frac{3H\phi_0}{2W^2}(\frac{\phi_0}{W} - 2)$, $M_2 = \frac{3H}{2W^2}\left(\frac{\phi_0}{W} - 1\right)$, and $M_3 = \frac{H}{2W^3} > 0$.

All derivatives are calculated with respect to a normalized time $\xi := {Ut}/{R}$ where t is the actual time, R is the mean compressor radius, and U is the constant compressor tangential speed. Here, $k_1 = \frac{1}{4B^2 l_c}$, $k_2 = \frac{1}{l_c}$, and l_c is the effective flow-passage nondimensional length of the compressor and ducts. B is a positive parameter (so-called Greitzer's B-parameter). The type of the developed nonlinear behavior to a great extent depends on the value of this parameter (small B can lead to rotating stall, and large B can cause surge).

In the model, $\Delta_\phi = \Phi_d + d_\phi$ and $\Delta_\psi = \Psi_d + d_\psi$ include model uncertainties and external disturbances. Mass flow disturbance $\Phi_d(\xi)$ and pressure disturbance $\Psi_d(\xi)$ are both considered as defined by Simon and Valavani [124]. The disturbances are time varying, non-vanishing, and bounded ($\|\Phi_d\|_\infty$ and $\|\Psi_d\|_\infty$ exist). In addition to time varying disturbances, constant or slow varying offsets d_ψ and d_ϕ are also introduced. These can be respectively thought of as an uncertainty in the compressor and throttle characteristics.

Setting $\dot{\phi} = \dot{\psi} = \dot{J} = 0$ leads to two equilibrium points: $J_{e1} = 0$ where the compressor is in its active operating point (ϕ_0, ψ_0) or $J_{e2} = 4(1 - \left(\frac{\Phi}{W} - 1\right)^2 - \frac{4W\Phi}{3H\gamma_v^2})$ when the system is in fully developed rotating stall. By using J_{e2} in (6.3), one can obtain the equivalent stall characteristic $\Psi_{\mathrm{es}}(\Phi)$, which is affected by pressure drop over CCV as can be seen in (6.6) (see [47] for more information).

$$\Psi_{es}(\Phi) = \psi_{c0} + H\left(1 - \frac{3}{2}\left(\frac{\Phi}{W} - 1\right) + \frac{5}{2}\left(\frac{\Phi}{W} - 1\right)^3\right) + \frac{5}{H}\Psi_v(\Phi) - \frac{8W}{H\gamma_v^2}\left(1 - \frac{W^2}{3H^2\gamma_v^2}\right)\Phi \tag{6.6}$$

Figure 6.a plots these characteristics: $\Psi_c(\Phi)$ (compressor map without CCV), $\Psi_{ec}(\Phi)$ (equivalent compressor map with CCV), $\Psi_v(\Phi)$ (pressure drop over CCV), $\Psi_T(\Phi)$ (pressure drop over throttle), $\Psi_s(\Phi)$ (stall characteristic without CCV), and $\Psi_{es}(\Phi)$ (equivalent stall

characteristic with CCV) in (Φ, Ψ) plane. The OP of the compression system (ϕ_0, ψ_0) is the intersection of the throttle characteristic and the equivalent compressor map. An efficient and stable OP is normally located near the peak of the equivalent compressor map (corresponding to a high pressure rise). Moreover, it can be shown that this OP corresponds to fully damped stall [142].

Figure 6.2a shows how the pressure drop over CCV can modify the equivalent compressor map and equivalent stall characteristic as well (see [47] for more details). This actuator can therefore be used to stabilize an unstable OP. Roughly speaking, when an OP is located in the negative slope area of the equivalent compressor map, it is stable [65]. Figure 6.2b shows that due to the pressure drop over CCV an unstable initial OP in the positive slope area of the compressor map is changed to a stable OP in the negative slope area of the equivalent compressor map. Furthermore, throttle control can also be applied to move the OP. In this work, these two actuators are used to stabilize the system and eliminate rotating stall and surge.

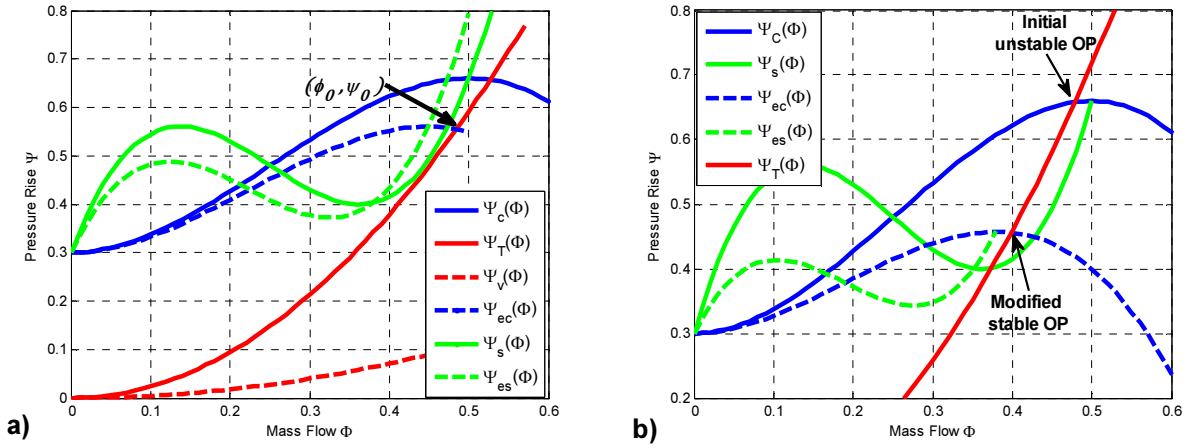

Figure 6.2: a) throttle characteristic, CCV pressure drop, original and equivalent compressor and stall characteristic

b) Effect of pressure drop over CCV on the equivalent compressor characteristic and the stability of the OP

6.3 Passivity-based Control

The main objectives of this section are, firstly, to passificate the axial compression system model and, secondly, to achieve disturbance rejection. In [154], the conditions under which a nonlinear system can be rendered passive via smooth state feedback are explained. Based on this work, several authors have proposed to include uncertain terms (model uncertainties and external disturbances) in order to develop a RPBC [11, 12, 159]. These works are based on assumptions on uncertainties (vanishing perturbations) or measurable states (full-state feedback with stall as a state-variable) which are not applicable here. Consequently, we remove certain restrictions that are imposed on the uncertainties and propose a new Lyapunov function stability analysis. We demonstrate that the control law developed in *Theorem 3.1* below ensures robust asymptotic stabilization of the compression system model. Furthermore, this easy-to-implement RPBC does not require a full-state feedback.

Theorem 3.1:

Consider the following disturbed system:

$$\Sigma 1: \begin{cases} \dot{x} = f_0(x,0) + f_1(x,y)y \\ \dot{y} = b_0(x,y) + a_0(x,y)u + D(x,y) + \Delta(x,y) \end{cases} \tag{6.7}$$

Where y is the output, $f_0(x,y)$, $f_1(x,y)$, $b_0(x,y)$, and $a_0(x,y)$ are smooth functions and $a_0(x,y)$ is invertible for all $x \in R^n$, $y \in R^m$, and $u \in R^m$. $\Delta(x,y)$ is the system uncertainty and $D(x,y)$ is the external disturbance.

If $\Delta(x,y)$ and $D(x,y)$ are bounded and if the zero dynamics of the system are stable (i.e. there exists a positive storage function $S(x)$ such that: $S(0) = 0$ and $\frac{\partial S}{\partial x} f_0(x,0) \leq 0$) and assuming that $\frac{\partial S}{\partial x} f_1(x,y)$ is bounded then feedback control law (6.8) guarantees the global boundedness of variable states of Σ_1 and (x,y) converges to a residual set. The size of the residual set can be arbitrarily made small by the choice of design parameters.

$$u = -a_0(x,y)^{-1}\{b_0(x,y) + p(y)\} \tag{6.8}$$

where $p(y)$ satisfies $y^T p(y) > 0$.

Proof:

Given a positive storage function for the system $\Sigma 1$ as:

$$V(x,y) = S(x) + \frac{1}{2}y^T y \tag{6.9}$$

differentiating $V(x,y)$ gives:

$$\dot{V}(x,y) = \frac{\partial S}{\partial x}(f_0(x,0) + f_1(x,y)y) + y^T b_0(x,y) + y^T a_0(x,y)u + y^T(D+\Delta) \tag{6.10}$$

Since $\frac{\partial S}{\partial x} f_0(x,0) \leq 0$, the substitution of the control law (6.8) into (6.10) gives that:

$$\dot{V}(x,y) \leq -y^T p(y) + y^T \eta \tag{6.11}$$

where

$$\eta = [\eta_1 \dots \eta_n]^T = [\frac{\partial S}{\partial x} f_1(x,y)]^T + (D+\Delta) \tag{6.12}$$

Now, we use the simplified form of Young's inequality which states that for all $C > 0$ and all $(q_1, q_2) \in \mathbb{R}^2$:

$$q_1 q_2 \leq C q_1^2 + \frac{1}{4C} q_2^2 \tag{6.13}$$

By applying (6.13) to each term of $y^T \eta$, we have:

$$y_i \eta_i \leq C y_i^2 + \frac{1}{4C}\eta_i^2 \quad \forall C > 0, i = 1, \dots, n \tag{6.14}$$

Following the boundedness of uncertainties and assuming that $\left\| \frac{\partial S}{\partial x} f_1(x,y) \right\|_\infty$ exists, we have:

$$y^T \eta \leq C y^T y + \frac{n}{4C} \|\eta\|_\infty^2 \tag{6.15}$$

therefore:

$$\dot{V}(x,y) \leq -y^T p_1(y) + \frac{n}{4C} \|\eta\|_\infty^2 \tag{6.16}$$

where

$$p_1(y) = p(y) - Cy \tag{6.17}$$

Appropriate choice of $p(y)$ can satisfy the condition $y^T p_1(y) > 0$ (e.g. $p(y) = Ky$ with $K - CI$ positive definite). Since $y^T p_1(y)$ and $V(x,y)$ are radially unbounded and positive definite, according to the work of Krstic et al. (Lemma 2.26) [160], we can demonstrate that the control law of (6.8) guarantees the global uniform boundedness of Σ_1

variable states at origin and (x, y) convergences to residual set U_Δ, outside which $\dot{V}(x, y) < 0$.

$$U_\Delta = \left\{ y: |y| \leq \alpha_1^{-1}.\alpha_2.\alpha_3^{-1}\frac{n}{4C}\|\eta\|_\infty^2 \right\} \tag{6.18}$$

where α_1, α_2, and α_3 are $class - \mathcal{K}_\infty$ functions such that:

$$\alpha_1(|(x, y)|) \leq V(x, y) \leq \alpha_2(|(x, y)|) \tag{6.19}$$

$$\alpha_3(|y|) \leq y^T p_1(y) \tag{6.20}$$

The size of this set depends on $\|\eta\|_\infty^2$ and C as the design parameter. A smaller size of U_Δ requires a large C parameter, which implies higher controller gain.

6.4 PBC Design for MG3

Here, it is supposed that mass flow ϕ and pressure rise ψ in the error coordinates can both be measured. Then $y = [\phi \quad \psi]^T$ and the model (6.2)-(6.4) can be rewritten in the form of system Σ1 including matched uncertainties. Since J cannot be practically measured, the idea in this paper is to consider all the terms containing J as part of the disturbances. This simplifies the control design and allows us to have an output feedback strategy. Here, a_0 and b_0 do not depend on J and the assumptions of perturbation boundedness of *Theorem 3.1* are satisfied.

$$\begin{cases} \dot{J} = f_0(J, 0) + f_1(J, y)y \\ \dot{y} = b_0(y) + a_0(y)u + D(J, y) + \Delta(y) \end{cases} \tag{6.21}$$

where

$$a_0 = \begin{bmatrix} 0 & -k_2 \\ -k_1\sqrt{\psi + \psi_0} & 0 \end{bmatrix} \tag{6.22}$$

$$b_0 = \begin{bmatrix} k_2(-\psi + \psi_c) \\ k_1(\phi + \phi_0) \end{bmatrix} \tag{6.23}$$

$$D = \begin{bmatrix} -k_1\Phi_d \\ k_2\left(-\frac{3HJ}{4}\left(\frac{\phi+\phi_0}{W} - 1\right) - \frac{W^2 J}{2\gamma_v^2} + \Psi_d\right) \end{bmatrix} \tag{6.24}$$

$$\Delta = \begin{bmatrix} -k_1 d_\phi \\ k_2 d_\psi \end{bmatrix} \tag{6.25}$$

a_0 is nonsingular in the domain of interest where $\psi + \psi_0 > 0$. Furthermore, Gravdahl showed that the squared amplitude of rotating stall and mass flow have upper bounds [47]:

$\exists\, J_{max} < \infty$ such that $J(\xi) \leq J_{max}\ \forall\, \xi > 0$, and $\phi_{min} \leq \Phi \leq \phi_{choke}$, where ϕ_{choke} is the choking value of the mass flow and ϕ_{min} is the negative flow during deep surge. The CCV gain is practically limited as well, in other words $\gamma_v \in [\gamma_{min}, \gamma_{max}]$. Consequently, D and Δ are both bounded. Similarly, $\left\|\frac{\partial S}{\partial x} f_1(x,y)\right\|_\infty$ exists since:

$$f_1(J,y) = \varrho J\phi\left(-\frac{\phi+2\phi_0}{W^2} + \frac{2}{W} - \frac{4w}{3H\gamma_v^2}\right) \tag{6.26}$$

where W, H, and γ_v are nonzero.

To investigate the stability of zero dynamics, suppose that a nominal OP is initially located at the peak of the compressor map (which is ideally the case). It can be seen that the peak of the compressor map in (6.1) is located at $(\Phi, \Psi) = (2W, 2H + \psi_{c0})$. Therefore, $\phi_0 = 2W$ at this OP:

$$f_0(J,0) = \varrho J\left(-\frac{J}{4} - \frac{4W\phi_0}{3H\gamma_v^2}\right) \tag{6.27}$$

Considering $S = \frac{1}{2\varrho J_{max}} J^2$, one can show that:

$$\frac{\partial S}{\partial J} f_0(J,0) = \frac{J^2}{J_{max}}\left(-\frac{J}{4} - \frac{4W\phi_0}{3H\gamma_v^2}\right) \tag{6.28}$$

In (6.28) the parameters (W, H), ϕ_0, and J are all positive.

Hence $\frac{\partial S}{\partial J} f_0(J,0) \leq 0$, this satisfies the first condition of *Theorem 3.1*. By choosing $p(y) = Ky$, *Theorem 3.1* states that the following control law (6.29) can stabilize the OP in the presence of the external disturbances and the model uncertainties.

$$u = [u_1, u_2]^T = \begin{bmatrix} \frac{\phi+\phi_0+k_1^{-1}P_2\psi}{\sqrt{\psi+\psi_0}} \\ -\psi + \psi_c + k_2^{-1}P_1\phi \end{bmatrix} \tag{6.29}$$

In the developed control law, $K = \begin{bmatrix} P_1 & 0 \\ 0 & P_2 \end{bmatrix}$ consists of two high enough positive design parameters (P_1 and P_2) that guarantee the convergence to U_Δ and limit the size of this residual convergence set.

Note that the control law (6.29) cancels all the nonlinearities in the model. Since the term M_3 is always positive in (6.5), we propose the following modification to avoid canceling the stabilizing nonlinearities ($-M_3\phi^3$):

$$u = [u_1, u_2]^T = \begin{bmatrix} \frac{\phi+\phi_0+k_1^{-1}P_2\psi}{\sqrt{\psi+\psi_0}} \\ -\psi - M_2\phi^2 - M_1\phi + k_2^{-1}P_1\phi \end{bmatrix} \tag{6.30}$$

It is worth noting that all uncertainties in the model parameters are considered in the terms of Δ, therefore the parameter set used in (6.30) is only a reasonable estimation.

Remark:

In the case of deep surge, the system does not include the zero dynamics and the simplified form of control system can be derived by putting $J = 0$ in (6.21). It can be seen that $J = 0$ considerably relaxes the boundedness conditions; however, the developed control laws (6.30) remains effective.

6.5 Results and Discussions

All of the numerical constants and model parameters, which are used in this section, are mentioned in Table 6.1. At first, we demonstrate that external disturbances and model uncertainties can lead to rotating stall when the controller is deactivated (B-parameter in this case is 0.1). The system initially starts from OP1 (the intersection of throttle characteristic $\gamma_T = 0.62$ and compressor map at $(\phi_i, \psi_i) = (0.51, 0.66)$ (see Figure 6.3). This OP is located in the negative slope area and the system is initially stable. As seen in Figure 6.4f, we test the controller for non-vanishing disturbances including time varying sinusoidal and constant offsets, which are applied at $\xi = 50$. Consequently, the system develops rotating stall (Figure 6.4c) and output pressure drops (Figure 6.4a). This spells trouble for normal operation of the axial compressor. In Figure 6.3, the disturbed trajectory (blue line) settles down at OP2 consisting of the effect of rotating stall and disturbances. The disturbances last until $\xi = 200$, but due to the hysteresis in the qualitative behavior of the system, rotating stall cannot be automatically removed (see Figure 6.4c). When disturbances disappear, uncontrolled trajectory (magenta line) ends up in OP3 which is located on the stall characteristic where pressure is considerably reduced.

At $\xi = 300$, the controller starts and rapidly damps out rotating stall and imposes the controlled trajectory (green line) toward the initial efficient OP1 where output pressure is high. In this simulation, $P_1 = 10$ and $P_2 = 0.2$. Figure 6.4d and 6.4e respectively report the control laws u_1 and u_2.

To investigate the effectiveness of the controller in the presence of perturbations, long lasting disturbances are applied to the system for $\xi > 50$ (Figure 6.6f). Again, Figure 6.5 and 6.6 show that the controller, which is activated at $\xi = 300$, stabilizes the system at the desired OP1. In Figure 6.5, the controlled system trajectory finally reaches to the initial desired OP1.

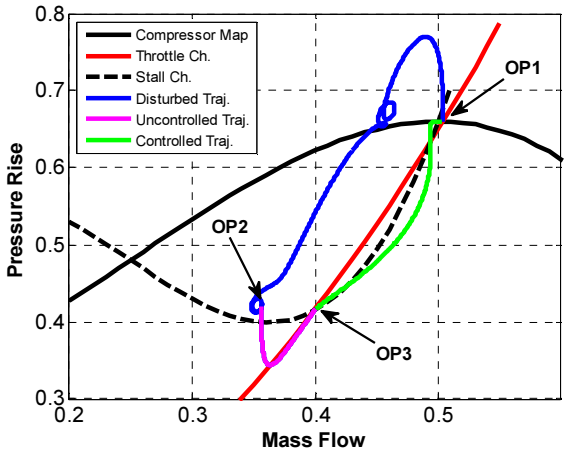

Figure 6.3: Perturbations lead to rotating stall, but RPBC effectively damps it out, OP1: efficient OP, OP2: developed rotating stall and disturbances, OP3: rotating stall OP

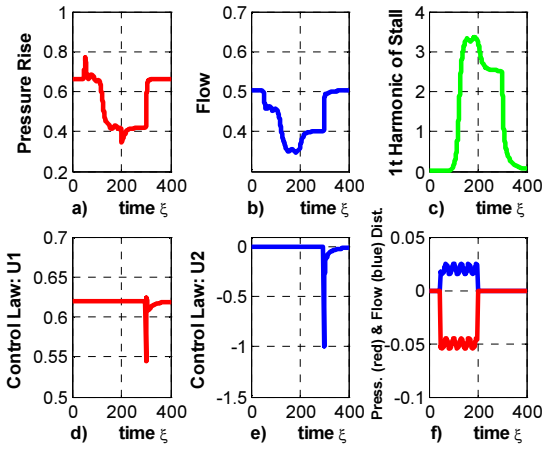

Figure 6.4: RPBC returns the system to its initial efficient OP and removes rotating stall

Figure 6.6c shows that rotating stall is rapidly damped out and Figure 6.6a reports the corresponding pressure increase after the activation of the controller at $\xi = 300$. In this case, $P_1 = P_2 = 20$. These two design parameters also modify the transient response of the system (e.g. the fall time of rotating stall). The scale of Figure 6.6d and 6.6e are adjusted to show the variation of control laws due to the time varying sinusoidal disturbances.

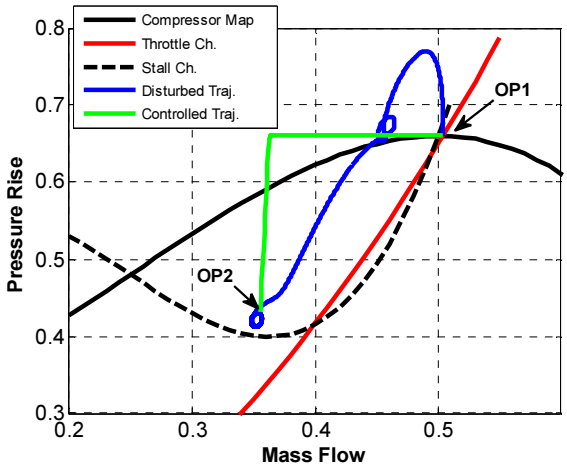

Figure 6.5: RPBC removes rotating stall and returns the system to its desired initial OP1, OP1: initial efficient OP, OP2: OP including rotating stall and disturbances

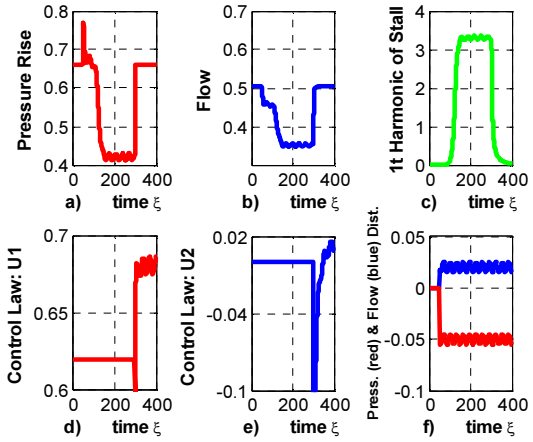

Figure 6.6: RPBC increases the output pressure and eliminates rotating stall

Compressors suffer from deep surge as well. For surge simulations, the system initially starts at an efficient OP at the peak of compressor map. In this case, at $\xi = 50$, we apply only the offset disturbances (thought of as model uncertainties) that move the system toward surge condition. Deep surge can be simulated by choosing a high enough value of B-parameter (e.g. $B = 2$ leads to surge). During deep surge, flow reversal occurs (see Figure 6.8b with negative flow values). Although perturbations are removed at $\xi = 2000$, the system remains in surge condition (see Figure 6.8f and 6.8b). Then at $\xi = 3000$, the controller starts and quickly stabilizes deep surge as shown in Figure 6.8a and 6.8b. Control efforts are shown in Figure 6.8d and 6.8e.

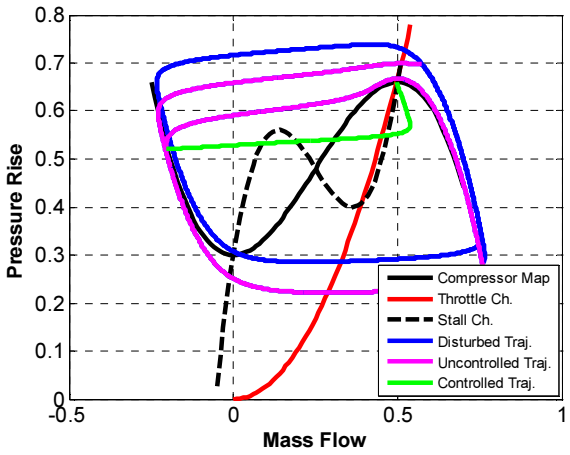

Figure 6.7: RPBC stabilizes the compression system and eliminates deep surge

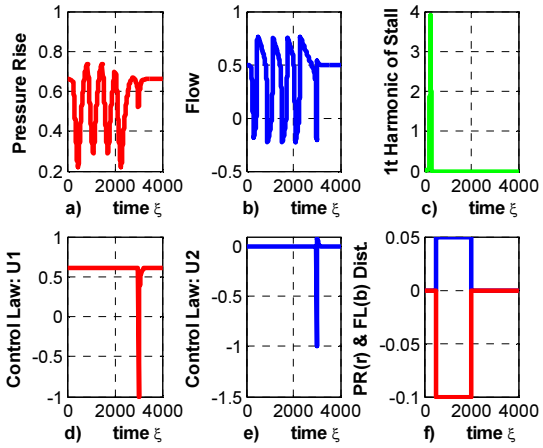

Figure 6.8: Deep surge including flow reversal and pressure oscillation is damped out due to RPBC activation

Figure 6.7 reports disturbed and uncontrolled trajectories showing a limit cycle. Finally, when the control is applied at $\xi = 3000$, the controlled system trajectory settles down at the initial efficient OP1 (green trajectory). This time-domain simulation shows that the developed control law (6.30) can robustly stabilize deep surge as well.

6.6 Conclusion

In this paper, the effectiveness of RPBC in stabilizing compression systems is demonstrated. Here, surge and rotating stall being potentially able to cause mechanical damages and performance reduction are robustly controlled in the presence of external disturbances and model uncertainties. The controller derives the control signal from pressure and flow measurements and applies it to the system by CCV and throttle actuations. The main contribution of this paper is to propose a simple and easy-to-implement RPBC algorithm that only relies on a small number of design parameters and does not require accurate knowledge of the model parameters and full state feedback. Furthermore, it can effectively reject non-vanishing bounded perturbations.

Analytical developments demonstrate that RPBC accomplishes the stability of the closed-loop disturbed system. The size of the residual convergence set and the transient response can be adjusted by control parameters. Time-domain simulation evaluates the performance of the control system and widely supports analytical outcomes.

This brings us to the conclusion that by taking advantage of control methods based on the passivity properties of compression systems, a wide range of machines using compressors can obtain higher performance and greater operational reliability. Among these machines, gas turbines play an essential role both in aerospace and energy industries.

Table 6.1: Numerical values used in simulations

l_c	3	ϱ	0.425
W	0.25	d_ϕ	-0.05
H	0.18	d_ψ	0.02
B for rotating stall	0.1	$\Psi_d(\xi)$	$0.01sin(0.2\xi)$
B for deep surge	2	$\Phi_d(\xi)$	$0.01sin(0.2\xi)$

CHAPTER 7

ARTICLE 2: VARIABLE STRUCTURE CONTROL OF ROTATING STALL AND SURGE IN AXIAL FLOW COMPRESSORS

Gholam-Reza Sari
École Polytechnique, University of Montreal, Montreal, Quebec, H3T 1J4, Canada

Ouassima Akhrif
École de Technologie Superieure, University of Quebec, Montreal, Quebec, H3C 1K3, Canada
and
Lahcen Saydy
École Polytechnique, University of Montreal, Montreal, Quebec, H3T 1J4, Canada

Submitted to Journal of Control Science and Engineering on May 2014

Abstract: In this work, we address the robust control of performance limiting nonlinearities: surge and rotating stall in constant speed axial compressors. This topic has been the subject of ongoing studies over the years and is still a challenge for researchers. Here, the third-order Moore-Greitzer model (MG3) comprising close-coupled valve and including parameter uncertainties and external disturbances is considered. Second order sliding mode control and input output feedback linearization using throttle and close-coupled valve actuations are applied to control the model. The applicability of the method is proved by including the rotating stall harmonic in disturbance terms and ensuring the boundedness of perturbations. Time-domain simulations corroborate theoretical analysis and demonstrate that this chattering-free controller can effectively stabilize the nonlinearities and robustly reject external perturbations and model uncertainties.

Key words: Second Order Sliding Mode Control, Axial Compressor, Rotating Stall and Surge Control, Throttle Control, Close-Coupled Valve, Model Uncertainty and Disturbance Rejection

7.1 Introduction

A wide range of machines benefits from the high efficiency and the large mass flow capacity of axial compressors. Among these machines, gas turbines play an essential role in both aerospace and energy industries. Axial compressors suffer however from two kinds of nonlinearities: rotating stall and surge. Rotating stall is a nonaxisymmetric perturbation that turns around the axis of compressors and reduces average mass flow and pressure rise. This nonlinear

phenomenon in its fully developed case spells operational troubles and causes mechanical vibrations and damages. It can also lead to deep surge, another violent nonlinear phenomenon which represents an axisymmetric limit cycle of mass flow including flow reversal. Deep surge can damage mechanical parts of axial compressors in only a few cycles (see [37] for more details). Working far from such nonlinearities and unstable zones is a simple solution to the problem, but this is achieved at the expense of performance. Another solution is active control, which simultaneously guarantees stability and performance.

Axial compressors have been the subject of much research for years. Despite tremendous efforts on modeling, sensing, actuating, and control of axial compressors, these key issues are still challenging problems. From the modeling point of view, a nonlinear 2D model introduced by Moore and Greitzer [36] dominates recent studies on rotating stall and surge. This lumped model (so-called MG3) is developed for constant speed axial compressors (CSACs) based on the first harmonic approximation of rotating stall. In spite of the simple form of MG3, it captures surge and rotating stall developments and explains the qualitative behavior of compression systems. Later, researchers proposed different extensions to the model [40, 42, 161].

Several studies and experimental results have been performed on different types of actuators for surge and rotating stall control. In 1977, Dussourd [157] and in 1991, Simon and Valavani [124] addressed close-coupled valve (CCV) as an actuator in compression system control. Among the different actuation methods, CCV remains one of the most promising [162, 163]. In 1998, Gravdahl introduced an augmented MG3 model including CCV in error coordinates [47]. This augmented model has recently attracted increasing attention in the control of compression systems [94, 123, 131].

From the control point of view, model uncertainties reflect a key challenge that confronts researchers. The precise estimation of model parameters, especially in the unstable zone, is difficult. Therefore, control approaches that require the accurate knowledge of the compression system parameters cannot be robustly implemented. Another problem is that the squared amplitude of stall as a state of MG3 is experimentally difficult to measure and control methods that need full state feedback cannot practically overcome this problem. Although, mass flow measurement is a challenge as well, it is surmountable [113]. Mass flow is frequently used in the literature to develop control design methodologies [114, 115], and there exist some implemented

controllers that use this measurement [116]. Furthermore, nonlinear observers are proposed to estimate mass flow [117, 118]. The last but not least problem is the effect of external disturbances that can drive the system toward instabilities. Pressure and mass flow disturbances were taken into account in the model by Simon and Valavani [124].

In recent years, sliding mode control (SMC) has gained increasing acceptance by research communities, due to its potential insensitivity to model errors, parametric uncertainties, and external disturbances. The drawback of SMC in terms of chattering is overcome by chattering-free methods, among them higher order SMC. A constructive method was newly proposed to develop higher order SMCs for a class of multi-input multi-output nonlinear uncertain systems [164]. The reasonable computation load and the fairly straightforward firmware implementation of SMC make it an excellent choice in such applications. Over the past decade, SMC has been increasingly applied to stabilize compression system nonlinearities. In 2001, Liaw and Huang [95] applied a first order SMC (FOSMC) to robustly stabilize axial-flow compressor dynamics by CCV actuation. They showed that the domain of attraction for an unstalled operating equilibrium is enlarged to a great extent. This control approach needed full state feedback (i.e. rotating stall measurements) and suffered from chattering. In 2008, Bartolini et al. (Bartolini G., Muntoni A., Pisano A., & Usai E., 2008) proposed a second order SMC (SOSMC) to stabilize surge in compression systems by CCV and throttle actuation. Although this control approach coped with chattering, it was developed for surge stabilization only (two-state simplified form of the Moor-Greitzer model) and could not be used to damp out rotating stall. It also required the zero crossing knowledge of sliding variables derivatives. In 2009, Song et al. used SMC to control a centrifugal compressor with spool dynamics, which does not include rotating stall [92].

Here, we propose a SMC combined with feedback linearization control design to robustly stabilize both surge and rotating stall in MG3 model comprising CCV in the presence of external disturbances and model uncertainties. We are inspired by the higher order sliding mode control method proposed by Defoort et al. [165], which is based on classical feedback linearization, and develop our chattering free SOSMC for the multi-input multi-output nonlinear uncertain compressor model. However, here, the proposed classical feedback linearization by defoort et al. is appropriately modified to avoid eliminating the stabilizing nonlinearities. In the control design, we reformulate the problem and propose the terms consisting of rotating stall as disturbances. This approach, which is supported by the proof of perturbations boundedness, greatly simplifies

the design. As a consequence, a full state feedback including rotating stall amplitude is not assumed and the control is only driven from pressure and mass flow measurements. Furthermore, the control scheme does not require the accurate knowledge of the compression system parameters. Finally, the information of initial conditions and zero crossing of sliding variables derivatives are not used in the control design. Our time-domain simulations corroborating the analytical analysis reveal that the global asymptotic stabilization of the closed-loop system can be achieved in finite time by adjusting only a small number of control parameters.

The rest of this paper is organized as follows. In Section 7.2, we recall MG3 model comprising CCV and define the feasible region of actuation. Section 7.3 explains the control method and underlines assumptions. We first develop FOSMC and finally propose SOSMC as the main contribution of the paper. Section 7.4 shows time-domain simulation results and opens up related discussions. Finally, some conclusions about this work are drawn in Section 7.5.

7.2 Axial Compressors' Model Comprising CCV

The compression system with CCV considered is presented in Figure 7.1. An extension to MG3 comprising CCV, which is introduced in [47], is briefly reviewed in this section. The model dynamics are:

$$\dot{\Psi} = \frac{1}{4l_c B^2}(\Phi - \Phi_T) \tag{7.1}$$

$$\dot{\Phi} = \frac{1}{l_c}\left[-\Psi + \Psi_C - \frac{3HJ}{4}\left(\frac{\Phi}{W} - 1\right) - \frac{1}{\gamma^2}\left(\frac{W^2 J}{2} + \Phi^2\right)\right] \tag{7.2}$$

$$\dot{J} = J\left(1 - \left(\frac{\Phi}{W} - 1\right)^2 - \frac{J}{4} - \frac{1}{\gamma^2}\frac{4W\Phi}{3H}\right)\varrho \tag{7.3}$$

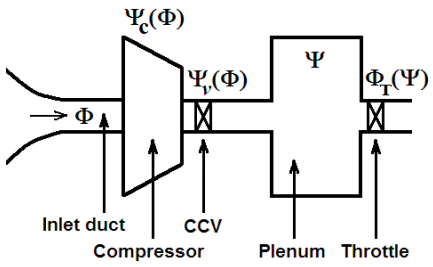

Figure 7.1: Compression system with CCV

Where, Φ is the circumferentially averaged mass flow coefficient, Ψ is the total-to-static pressure rise coefficient, and J is the squared amplitude of rotating stall. Ψ_c is the compressor characteristic (map), Ψ_v and Ψ_T are the pressure drop over CCV and throttle respectively.

l_c (the effective flow-passage nondimensional length of the compressor), ϱ, and B (so-called Greitzer's B-parameter) are constant parameters. The nonlinear behavior of the model depends to a great extent on the value of Greitzer's B-parameter (small B can lead to rotating stall, and large B can cause surge).

The pressure rise of the compressor $\Psi_c(\Phi)$ is a nonlinear function of the mass flow and a cubic form of this function (7.4) is widely used in the literature.

$$\Psi_c(\Phi) = \psi_{c0} + H\left(1 + \frac{3}{2}\left(\frac{\Phi}{W} - 1\right) - \frac{1}{2}\left(\frac{\Phi}{W} - 1\right)^3\right) \tag{7.4}$$

where H is the compressor characteristic height factor, W is the compressor characteristic width factor, and ψ_{c0} is shut-off head (they are all constant [47]).

γ is the gain of CCV which is proportional to the valve opening and determines its characteristic $\Psi_v(\Phi) = \frac{1}{\gamma^2}\Phi^2$, while the throttle characteristic, which can be thought of as a simple model of a power turbine, is given by $\Psi_\mathrm{T}(\Phi) = \frac{1}{\gamma_\mathrm{T}^2}\Phi^2$. In Fig. 2; the three characteristics Ψ_c, Ψ_v, and Ψ_T as well as the so-called equivalent compressor characteristic (defined as $\Psi_{ec}(\Phi) = \Psi_c(\Phi) - \Psi_v(\Phi)$: the sum of the pressure rise of the compressor and the pressure drop over CCV) are presented. It can be seen how the pressure drop over CCV can modify the pressure rise over the equivalent compressor from the blue to the green line.

Figure 7.2 shows also the operating point (OP) of the compression system which is the intersection of the throttle characteristic and the equivalent compressor map. The pressure drop over CCV and throttle can be used to change the OP and stabilize the system. Generally speaking, when an OP is located in the negative slope area of the equivalent compressor map, it is stable [65]. It can be seen that the initially unstable OP (P1) in the positive slope area of the

original compressor map is changed to a stable OP (P2) in the negative slope area of the equivalent compressor map due to the pressure drop over CCV. The locus of the peak of equivalent compressor maps for a variation range of CCV is depicted in Figure 7.2. All of the OPs at the right side of this locus are stable. Throttle control can also change the slope of the throttle characteristic and move the OP. Furthermore, because the gain of throttle and CCV are practically limited ($\gamma_T \in [\gamma_{Tmin}, \gamma_{Tmax}]$, $\gamma \in [0, \gamma_{max}]$) , the stable operating zone is also limited to these boundaries (see SOP in Fig. 3). In this work, these two actuators are used to eliminate nonlinearities in the presence of external disturbances and model parameter variations at an efficient OP located at the top of the compressor map.

Setting $\dot{\Phi} = \dot{\Psi} = \dot{J} = 0$ leads to two equilibria: $J_{e1} = 0$, where the compressor is in its active operating point, or $J_{e2} = 4\left(1 - \left(\frac{\Phi}{W} - 1\right)^2 - \frac{4W\Phi}{3H\gamma^2}\right)$ when the system is in fully developed rotating stall. By using J_{e2} in (2), one can obtain the equivalent stall characteristic $\Psi_{es}(\Phi)$ given by:

$$\Psi_{es}(\Phi) = \psi_{c0} + H\left(1 - \frac{3}{2}\left(\frac{\Phi}{W} - 1\right) + \frac{5}{2}\left(\frac{\Phi}{W} - 1\right)^3\right) + \frac{5}{H}\Psi_v(\Phi) - \frac{8W}{H\gamma^2}\left(1 - \frac{W^2}{3H^2\gamma^2}\right)\Phi \qquad (7.5)$$

Note that this characteristic is also modified by pressure drop over CCV. The original and equivalent stall characteristics (with and without CCV) are both depicted in Figure 7.2 and 7.3.

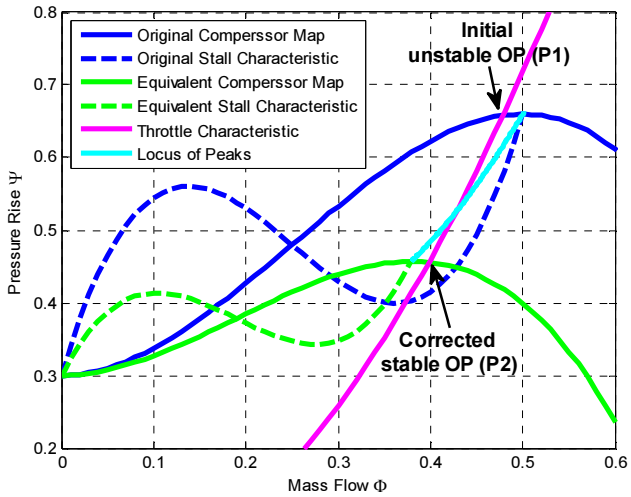

Figure 7.2: Pressure drop over CCV corrects the equivalent compressor characteristic and stabilizes the OP

For control proposes, the model (7.1)-(7.3) can be redefined in error coordinates with respect to the coordinates of an OP (Φ_0, Ψ_0) ideally located at the peak of the compressor characteristic where $J = 0$ and the pressure rise is high enough for the normal operation of the compression system. The model becomes in the form of $\dot{z} = f(z,u)$ ((7.6)-(7.8) below) where $z \in \mathbb{R}^3, u \in \mathbb{R}^2$. $z = (\phi,\ \psi,\ J)^T$ represents the state vector of the system with $\phi = \Phi - \Phi_0$ and $\psi = \Psi - \Psi_0$, and $u = (u_1, u_2)$ is the control vector. The control variables $u_1 = \gamma_T$ (throttle gain) and $u_2 = \psi_v(\phi)$ include the effect of throttle and the pressure drop over CCV respectively. A partially closed CCV during normal operation leads to a bidirectional control u_2 . All derivatives are calculated with respect to a normalized time $\xi := {Ut}/{R}$ where t is the actual time, R is the mean compressor radius, and. U is the constant compressor tangential speed.

$$\dot{\psi} = k_1\left(\phi - u_1\sqrt{\psi + \Psi_0} + \Phi_0 - \Delta\phi\right) \tag{7.6}$$

$$\dot{\phi} = k_2\left(\psi_c - \psi - u_2 - \frac{3H}{4}J\left(\frac{\phi+\Phi_0}{W} - 1\right) - \frac{W^2 J}{2\gamma^2} + \Delta\psi\right) \tag{7.7}$$

$$\dot{J} = \varrho J(1 - \left(\frac{\phi+\Phi_0}{W} - 1\right)^2 - \frac{J}{4} - \frac{4W(\phi+\Phi_0)}{3H\gamma^2}) \tag{7.8}$$

where , $k_1 = \frac{1}{4B^2 l_c}$, $k_2 = \frac{1}{l_c}$.

In this model $\Delta\phi(\xi)$ includes external mass flow disturbances and model uncertainties as well. $\Delta\psi(\xi)$ consists of pressure disturbances and model uncertainties as considered by Simon and Valavani [124]. These terms are assumed to be time varying and bounded (i.e. $\|\Delta\phi\|_\infty$ and $\|\Delta\psi\|_\infty$ exist).

The throttle, CCV, and compressor characteristics in the error coordinates are respectively defined as:

$$\phi_T(\psi) = \gamma_T\sqrt{\psi + \Psi_0} - \Phi_0 \tag{7.9}$$

$$\psi_v(\phi) = \Psi_v(\Phi) + \Psi_0 \tag{7.10}$$

$$\psi_c(\phi) = -M_3\phi^3 - M_2\phi^2 - M_1\phi \tag{7.11}$$

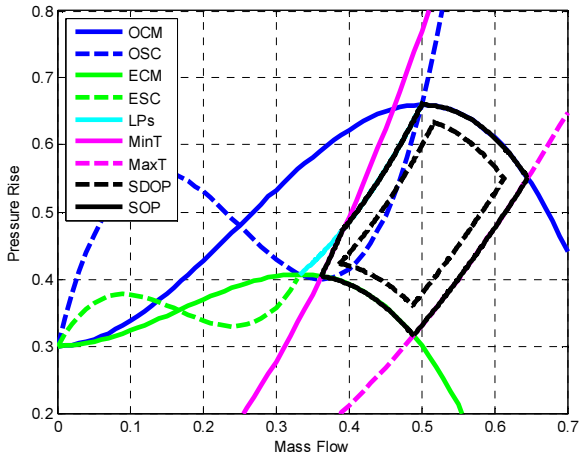

Figure 7.3: Black lines show the boundaries of stabilizable area

OCM: original compressor map, OSM: original stall characteristic, ECM: equivalent compressor map, ESC: equivalent stall characteristic, LPs: locus of peaks, MinT: Throttle characteristic for minimum throttle gain, MaxT: Throttle characteristic for maximum throttle gain,

SOP: stabilizable OP, SDOP: stabilizable disturbed OP

where the constants: $M_1 = \frac{3H\Phi_0}{2W^2}(\frac{\Phi_0}{W} - 2)$, $M_2 = \frac{3H}{2W^2}\left(\frac{\Phi_0}{W} - 1\right)$, and $M_3 = \frac{H}{2W^3} > 0$.

Going back to Figure 7.3, it can be seen that including bounded disturbances further limits the stabilizable area to stabilizable disturbed OPs (SDOP) in Figure 7.3, approximately depicted by the black dashed line. The width of this area directly depends on $\|\Delta\phi\|_\infty$ and $\|\Delta\psi\|_\infty$.

7.3 Control Design

Let us consider the model (7.6)-(7.8) as a square MIMO nonlinear affine uncertain system:

$$\Sigma 1: \begin{cases} \dot{x} = f(x) + \sum_{i=1}^{m} g_i(x)u_i \\ y_i = \sigma_i(x) \end{cases} \tag{7.12}$$

where the state variable $x = (\phi,\ \psi, J)$ belongs to $\mathbb{R}^3$ and the control input $u = (u_1, u_2) \in \mathbb{R}^2$. Here, $f(x)$ and $g(x)$ are uncertain smooth functions and $\sigma(x) \in \mathbb{R}^2$ is a smooth measurable output vector. Σ1 is defined in error coordinates and in the regulation problem, the objective is to make the outputs vanish in finite time.

We next apply two control approaches for our application, a FOSMC and a SOSMC which are inspired by the work of Defoort et al. [165]. To this end, we need to demonstrate that the two assumptions in Defoort's work are satisfied in our case. The control design is then performed in four steps. In the first step, we judiciously reformulate the regulation problem to a sliding mode design problem. In the second step, we partially decouple the nominal system by applying a preliminary feedback. In this step, contrary to the work of Defoort, the cancellation of stabilizing terms is avoided in order to reduce the control effort. Later, in third step, a controller stabilizes the nominal system. Finally, in the fourth step, a discontinuous feedback rejects the perturbations and guarantees the global asymptotic stabilization of the uncertain disturbed system in finite time.

7.3.1 First Order Sliding Mode Control (FOSMC)

Let us define outputs for system Σ1 as follows:

$$\sigma = [\sigma_1, \sigma_2]^T = [\psi, \phi]^T \tag{7.13}$$

Step1: Reformulating the problem

By considering $\sigma(x)$ as sliding variable, the manifold defined as:

$$S = \{x: \sigma_i(x) = 0\} \quad \forall\, i = 1,2 \tag{7.14}$$

is called the first order sliding set and the motion on S is called the first order sliding mode with respect to the sliding variable σ. The FOSMC allows the finite time stabilization of each output by defining a suitable discontinuous control law which is proposed in sequel. Here, the first time derivative of sliding variables yields:

$$\Sigma 2\text{: } [\dot{\sigma_1}(x), \dot{\sigma_2}(x)]^T = A(x) + B(x)u \tag{7.15}$$

with $A = \left[L_f\sigma_1(x), L_f\sigma_2(x)\right]^T$. Vector $A(x)$ and matrix $B(x)$ can be partitioned into nominal $(\bar{A}, \bar{B})$ and unknown parts (Δ_A, Δ_B) as follows:

$$\begin{cases} A(x) = \bar{A}(x) + \Delta_A(x) \\ B(x) = \bar{B}(x) + \Delta_B(x) \end{cases} \tag{7.16}$$

Nominal parts *($\bar{A}$* and *$\bar{B}$)* are known a priori. Δ_A and Δ_B traditionally comprise the model uncertainties and perturbations. In this work, however we consider all terms comprising J in Δ_A. Although J is a model state variable, it cannot be measured, moreover its nature as a perturbation conveys the idea that it can be thought of as uncertain terms. This approach simplifies the control design and makes the proposed control method applicable.

By calculating $\bar{A}$, $\bar{B}$, and Δ_A for the model at hand (7.6)-(7.8) we have:

$$\bar{B} = \begin{bmatrix} -k_1\sqrt{\psi + \Psi_0} & 0 \\ 0 & -k_2 \end{bmatrix} \tag{7.17}$$

$$\bar{A} = \begin{bmatrix} k_1\phi + k_1\Phi_0 \\ -k_2\psi - k_2M_2\phi^2 - k_2M_1\phi \end{bmatrix} \tag{7.18}$$

$$\Delta_A = \begin{bmatrix} -k_1\Delta\phi \\ -k_2\left(\frac{3HJ}{4}\left(\frac{\phi+\Phi_0}{W} - 1\right) - \frac{W^2J}{2\gamma^2} - \Delta\psi\right) \end{bmatrix} \tag{7.19}$$

For the applied model, Δ_B ends up being equal to zero.

Remark:

In order to avoid eliminating the stabilizing nonlinearities and replacing them with destabilizing terms, the proposed $\bar{A}$ in (7.18) has been properly modified. According to the classical feedback linearization, the term $k_2\psi_c$ where $\psi_c = -M_3\phi^3 - M_2\phi^2 - M_1\phi$ must be cancelled but the term $-k_2M_3\phi^3$, where $k_2M_3 > 0$, is a stabilizing term in (7.7), we do not, therefore, include this term in the decoupling control law (7.24). The term $-k_2M_3\phi^3$ is later considered in (7.25).

Assumption 1:

We assume that there is an a priori known constant ρ such that the uncertain function Δ_A satisfies the following inequality:

$$\|\Delta_A(x)\| \leq \rho \quad x \in X \subset R^3 \tag{7.20}$$

X is an open subset of $\mathbb{R}^3$ within which the boundedness of Δ_A is ensured.

Gravdahl showed that the squared amplitude of rotating stall has an upper bound [47].

$$\exists\, J_{max} < \infty \text{ such that } J(\xi) \leq J_{max} \;\; \forall\, \xi > 0 \tag{7.21}$$

and an upper bound on mass flow is given by choking $\phi < \phi_{choke}$. Finally, the boundedness of external disturbances and model uncertainties implies the boundedness of Δ_A and the system satisfies the conditions of *Assumption 1*.

Assumption 2:

We assume that matrix $\bar{B}(x)$ is nonsingular and the associated zero dynamics of $\Sigma 2$ are asymptotically stable.

To examine this assumption, from (7.17), it can be seen that matrix $\bar{B}$ is nonsingular for the operation range of the compressor because k_1 are k_2 are non-zero model constants and $\psi + \Psi_0 > 0$. Furthermore, we suppose that the desired OP is located at the peak of the compressor map (where $\Phi_0 = 2\mathrm{W}$) , which is ideally the case due to maximum pressure rise (see [47] for more information). Zero dynamics can then be expressed as:

$$\dot{J} = \varrho J\left(-\frac{J}{4} - \frac{4W\Phi_0}{3H\gamma^2}\right) \tag{7.22}$$

Taking into account $V = \frac{1}{2}J^2$, one can show that:

$$\dot{V} = \varrho J^2\left(-\frac{J}{4} - \frac{4W\Phi_0}{3H\gamma^2}\right) \tag{7.23}$$

where parameters (ϱ, W, H), Φ_0, and J (squared amplitude of stall) are all positive then $\forall J > 0 \rightarrow \dot{V} < 0$. Therefore the system satisfies the condition of *Assumption 2*.

Step2: Normal Form Representation

By applying the following preliminary feedback to system $\Sigma 2$:

$$u = \bar{B}^{-1}(-\bar{A} + w) \tag{7.24}$$

where $w = [w_1, w_2]^T \in \mathbb{R}^2$ is the auxiliary control input, one can partially decouple the nominal system (the system without uncertainties). Consequently, system Σ2 can be expressed as follows:

$$\Sigma 3: [\dot{\sigma_1}(x), \dot{\sigma_2}(x)]^T = \Delta_A + w + [0, -k_2 M_3 \phi^3]^T \tag{7.25}$$

Now, the design problem of the FOSMC of system Σ1 with respect to the sliding variable $\sigma(x)$ is equivalent to the finite time stabilization of the multivariable uncertain system Σ3. In what follows, this problem is tackled in two further steps.

Step3: Stabilization of the Nominal System

At first, we stabilize the nominal part of system Σ3 ($\Delta_A = 0$). The nominal system can be represented by two independent integrators as follows:

$$\Sigma_{nom}: [\dot{\sigma_1}, \dot{\sigma_2}]^T = [w_{nom1}, w_{nom2} - k_2 M_3 \phi^3]^T \tag{7.26}$$

In this case, the stabilization of Σ_{nom} can directly be achieved by $w_{nom,i} = -C_i \sigma_i$, $\forall i = 1,2$ where $C_i > 0$ is a control parameter.

$$w_{nom}: \begin{cases} w_{nom1} = -C_1 \sigma_1 = -C_1 \psi \\ w_{nom2} = -C_2 \sigma_2 = -C_2 \phi \end{cases} \tag{7.27}$$

Step4: Rejection of Uncertainties and Stabilization of Σ3

To stabilize uncertain system Σ3, at first, we define an augmented sliding variable $S_a \in \mathbb{R}^2$and its associated discontinuous control law as follows:

$$S_a(\sigma, z_{aux}) = [\sigma_1, \sigma_2]^T + z_{aux} \tag{7.28}$$

$$\begin{cases} w(\sigma) = w_{nom}(\sigma) + w_{disc}(\sigma, z_{aux}) \\ \dot{z}_{aux} = -w_{nom}(\sigma) \end{cases} \tag{7.29}$$

where auxiliary function $z_{aux} \in \mathbb{R}^2$ is used in the design of the augmented sliding variable and discontinuous control law $w_{disc}(\sigma, z_{aux}) \in \mathbb{R}^2$. The nominal control law $w_{nom}(\sigma) \in \mathbb{R}^2$ is given in the previous step.

The time derivative of $S_a(\sigma, z_{aux})$ along the system trajectories can be expressed as:

$$\dot{S_a} = [\dot{\sigma_1}, \dot{\sigma_2}]^T + \dot{z}_{aux} = w + \Delta_A - w_{nom} = w_{disc} + \Delta_A \tag{7.30}$$

Now, it can be seen that the discontinuous control law w_{disc} defined below, can ensure the sliding mode on $(x \in X: S_a = 0)$ and consequently on S in spite of uncertainties.

$$w_{disc} = -Gsign(S_a) \tag{7.31}$$

$$\begin{cases} \dot{z}_{aux1} = -w_{nom1} \\ \dot{z}_{aux2} = -w_{nom2} \end{cases} \tag{7.32}$$

$$\begin{cases} w_{disc1} = -Gsign(\sigma_1 + z_{aux1}) = -Gsign(\psi + z_{aux1}) \\ w_{disc2} = -Gsign(\sigma_2 + z_{aux2}) = -Gsign(\phi + z_{aux2}) \end{cases} \tag{7.33}$$

where the notation $sign$ $([S_{a1}, S_{a2}]^T)$ denotes $[sign(S_{a1}), sign(S_{a2})]^T)$ and the gain satisfies:

$$G \geq \rho + \eta\ ,\ \eta > 0 \tag{7.34}$$

Following these steps, now we can propose *theorem1* to control the system.

Theorem 1:

Consider nonlinear system Σ1 and assume that *Assumptions1-2* are fulfilled. Then, the control law:

$$u = \bar{B}^{-1}\left(-\bar{A} + w_{nom}(\sigma) + w_{disc}(\sigma, z_{aux})\right) \tag{7.35}$$

ensures the establishment of FOSMC in Σ2 with respect to σ in finite time. In this control law, $\dot{z}_{aux} = -w_{nom}(\sigma)$, with $w_{nom}(\sigma)$ and $w_{disc}(\sigma, z_{aux})$ given by (7.27) and (7.33) respectively.

Proof of Theorem 1: See [164].

7.3.2 Second Order Sliding Mode Control

Although FOSMC can robustly stabilize the system, it suffers from chattering. To raise the control smoothness degree, we consider $\dot{u}_1$ and $\dot{u}_2$ as new control signals (see Figure 7.4). In other words, a second order sliding mode is defined here.

Let us consider the sliding variables as:

$$\begin{cases}\sigma_1 = \psi - \psi_{ref} \\ \sigma_2 = \phi - \phi_{ref}\end{cases} \tag{7.36}$$

Here terms ϕ_{ref} and ψ_{ref} include the desired set points. Consequently, the developed control law guarantees the evolution of system trajectories to the desired manifolds in finite time and robustly stabilizes the system there.

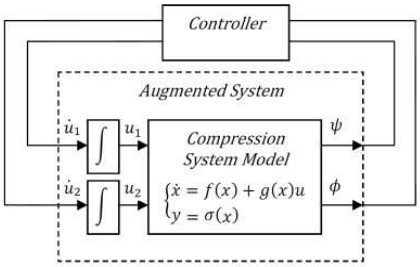

Figure 7.4: SOSMC

Step1: Reformulating the problem

By considering $\sigma(x)$ as sliding variable, the manifold defined as:

$$S = \{x: \sigma_i(x) = \dot{\sigma}_i(x) = 0\} \quad \forall\, i = 1,2 \tag{7.37}$$

is called the second order sliding set and the motion on S is called the second order sliding mode with respect to the sliding variable σ. The SOSMC allows the finite time stabilization of each output by defining a suitable discontinuous control law. To reformulate the problem, the second derivatives of sliding variables yields:

$$\Sigma 4: [\ddot{\sigma}_1(x), \ddot{\sigma}_2(x)]^T = A(x) + B(x)\tilde{u} \tag{7.38}$$

where $x = [\psi, \phi, u_1, u_2]$ is the new state vector and $\tilde{u} = (\dot{u}_1, \dot{u}_2)$ is the new input vector of the system. In this system, the new vector $A(x)$ and matrix $B(x)$ can be partitioned into nominal $(\bar{A}, \bar{B})$ and unknown parts (Δ_A and Δ_B).

Assumptions:

After some algebraic manipulations, we obtain $\bar{A}$, $\bar{B}$, Δ_A, and Δ_B in this case as follows:

$\bar{A} = \begin{bmatrix} \bar{A}_1 \\ \bar{A}_2 \end{bmatrix}$:

$$\bar{A}_1 = k_1 k_2(-\psi - M_3\phi^3 - M_2\phi^2 - M_1\phi - u_2) - k_1^2\left(\frac{u_1\phi}{2\sqrt{\psi+\Psi_0}} - \frac{u_1^2}{2} + \frac{u_1}{2\sqrt{\psi+\Psi_0}}\Phi_0\right) - \ddot{\psi}_{ref} \quad (7.39)$$

$$\bar{A}_2 = k_1 k_2\left(-\phi + \sqrt{\psi+\Psi_0}u_1 - \Phi_0\right) + k_2^2(\psi + M_3\phi^3 + M_2\phi^2 + M_1\phi + u_2)(3M_3\phi^2 + 2M_2\phi + M_1) - \ddot{\phi}_{ref} \quad (7.40)$$

$$\bar{B} = \begin{bmatrix} -k_1\sqrt{\psi+\Psi_0} & 0 \\ 0 & -k_2 \end{bmatrix} \quad (7.41)$$

$$\Delta_A = \begin{bmatrix} \Delta_{A1} \\ \Delta_{A2} \end{bmatrix} \quad (7.42)$$

$$\Delta_B = 0 \quad (7.43)$$

Δ_{A1}, Δ_{A2} are polynomial functions of uncertainties, disturbances, and J (see appendix). Again, due to the boundedness of J and ϕ, *Assumption 1* is satisfied.

Equation (7.41) shows that the matrix $\bar{B}$ is nonsingular and the stability of zero dynamics can be proved as before, so *Assumption 2* is also satisfied.

Step2: Normal Form Representation

The preliminary feedback:

$$u = \bar{B}^{-1}(-\bar{A} + w) \quad (7.44)$$

where $w = [w_1, w_2]^T \in \mathbb{R}^2$ partially decouples the system and consequently Σ5 can be expressed as follows:

$$\Sigma 5: [\ddot{\sigma_1}(x), \ddot{\sigma_2}(x)]^T = w + \Delta_A \quad (7.45)$$

Now, the design problem of the second order SMC of system Σ1 with respect to the sliding variable $\sigma(x)$ is equivalent to the finite time stabilization of multivariable uncertain system Σ6:

$$\Sigma 6: \begin{cases} \dot{z}_{1,1} = z_{2,1} \\ \dot{z}_{1,2} = z_{2,2} \\ \left[\dot{z}_{2,1}, \dot{z}_{2,2}\right]^T = w + \Delta_A \end{cases} \tag{7.46}$$

where $z_{1,1} = \psi - \psi_{ref}, z_{1,2} = \phi - \phi_{ref}$.

As before, we follow two additional steps to tackle the problem.

Step3: Stabilization of the Nominal System

The nominal part of Σ6 ($\Delta_A = 0$) can be represented by two double independent integrator chains as follows:

$$\Sigma_{nom2}: \{\ddot{\sigma}_i = w_{nom,i} \; \forall \; i = 1,2\} \tag{7.47}$$

In what follows, the proposed control law by [166] is used to asymptotically stabilize the nominal system at the origin in finite time. Bhat and Bernstein demonstrated that there is $\varepsilon_i \in (0,1)$ such that, for every $v_i \in (1 - \varepsilon_i, 1)$, Σ_{nom2} is stabilized at the origin in finite time under the feedback:

$$\begin{cases} w_{nom1} = -C_{11} sign(\sigma_1)|\sigma_1|^{v_{11}} - C_{21} sign(\dot{\sigma}_1)|\dot{\sigma}_1|^{v_{21}} \\ w_{nom2} = -C_{12} sign(\sigma_2)|\sigma_2|^{v_{12}} - C_{22} sign(\dot{\sigma}_2)|\dot{\sigma}_2|^{v_{22}} \end{cases} \tag{7.48}$$

where $v_{1,i} = \frac{v_i}{2 - v_i}$ and $v_{2,i} = v_i$. Here, C_{11}, C_{21}, C_{12}, and C_{22} are positive constants.

Step4: Rejection of Uncertainties and Stabilization of Σ5

To stabilize the uncertain system Σ5, the following control law is defined:

$$\begin{cases} w(z) = w_{nom}(z) + w_{disc}(z, z_{aux}) \\ \dot{z}_{aux} = -w_{nom}(z) \end{cases} \tag{7.49}$$

where $z_i = \left[z_{1,i}, z_{2,i}\right]^T$, $z = [z_1^T, z_2^T]$, and

$$\begin{cases} \dot{z}_{aux1} = -w_{nom1} \\ \dot{z}_{aux2} = -w_{nom2} \end{cases} \tag{7.50}$$

$$w_{disc}: \begin{cases} w_{disc1} = -Gsign(\dot{\sigma}_1 + z_{aux1}) \\ w_{disc2} = -Gsign(\dot{\sigma}_2 + z_{aux2}) \end{cases} \quad (7.51)$$

Auxiliary function $z_{aux} \in \mathbb{R}^2$ is used in the design of the augmented sliding variable $S_a(z) \in \mathbb{R}^2$ associated with the discontinuous control law $w_{disc}(z, z_{aux}) \in \mathbb{R}^2$as bellow:

$$S_a(z, z_{aux}) = \left[z_{2,1}, z_{2,2}\right]^T + z_{aux} \quad (7.52)$$

The time derivative of $S_a(z, z_{aux})$ along the system trajectories can be expressed as:

$$\dot{S_a} = \left[\dot{z}_{2,1}, \dot{z}_{2,2}\right]^T + \dot{z}_{aux} = w + \Delta_A - w_{nom} = w_{disc} + \Delta_A \quad (7.53)$$

The following discontinuous control law w_{disc} is defined to ensure the sliding mode on $(x \in X: S_a = 0)$ in spite of uncertainties.

$$w_{disc} = -Gsign(S_a) \quad (7.54)$$

where the notation $sign$ ($[S_{a1}, S_{a2}]^T$) denotes $[sign(S_{a1}), sign(S_{a2})]^T$) and the gain satisfies:

$$G \geq \rho + \eta\ ,\ \eta > 0 \quad (7.55)$$

Theorem 2:

Consider nonlinear system Σ1 and assume that *Assumptions1-2* are fulfilled. Then, the control law:

$$\dot{u} = \bar{B}^{-1}\left(-\bar{A} + w_{nom}(\sigma) + w_{disc}(\sigma, z_{aux})\right) \quad (7.56)$$

with:

$$\begin{cases} \dot{u}_1 = -\frac{1}{k_1\sqrt{\psi + \Psi_0}}(-\bar{A}_1 + w_{nom1} + w_{disc1}) \\ \dot{u}_2 = -\frac{1}{k_2}(-\bar{A}_2 + w_{nom2} + w_{disc2}) \end{cases} \quad (7.57)$$

where $\bar{A}_1$ and $\bar{A}_2$ are given by (7.39) and (7.40) respectively, ensures the establishment of the second order sliding mode for Σ5, with respect to σ in finite time. In this control law, $\dot{z}_{aux} = -w_{nom}(\sigma)$, with $w_{nom}(\sigma)$ and $w_{disc}(\sigma, z_{aux})$ given by (7.48) and (7.51) respectively.

Proof of Theorem 2:

See [164].

7.3.3 Surge Control

Regarding that $J = 0$ in surge cases, the model (7.6)-(7.8) can be simplified to the following two-state model:

$$\dot{\psi} = \frac{1}{4B^2 l_c}\left(\phi - u_1\sqrt{\psi + \Psi_0} + \Phi_0 - \Delta\phi\right) \tag{7.58}$$

$$\dot{\phi} = \frac{1}{l_c}(\psi_c - \psi - u_2 + \Delta\psi) \tag{7.59}$$

It is obvious that $J = 0$ considerably relaxes the conditions imposed by *Assumption 1*; however, the developed control laws (7.35) and (7.57) remain effective. Therefore, the control design of FOSMC in section 3.1 and the one of SOSMC in section 3.2 can be directly applied to the model to stabilize surge.

7.3.4 Actuator Dynamics

Suppose that in Σ_4 the actuators are non-ideal and include additional first-order dynamics as follows:

$$\mu_i\dot{\tilde{u}}_i + \tilde{u}_i = \hat{u}_i \ , i = 1,2 \tag{7.60}$$

where $\hat{u}_i$ is a new actuation force and μ_i is the actuator time constant. Then SOSMC converges in finite time to the following invariant boundary layers of the sliding surface (defined by (7.37)):

$$\begin{cases} |\psi| < \rho_{\psi 1}\mu_1^2 \\ |\phi| < \rho_{\phi 1}\mu_2^2 \end{cases} \tag{7.61}$$

$$\begin{cases} |\dot{\psi}| < \rho_{\psi 2}\mu_1 \\ |\dot{\phi}| < \rho_{\phi 2}\mu_2 \end{cases} \tag{7.62}$$

where $\rho_{\phi 1}$, $\rho_{\psi 1}$, $\rho_{\phi 2}$, and $\rho_{\psi 2}$ are positive constants independent of μ_1, μ_2.

The proof of this statement is provided in [167]. This was also shown by Bartolini et al. [94] for SOSMC and the two-state simplified form of the model which is only valid for surge development.

Here, by time domain simulations, we investigate the effect of the non-ideal CCV and throttle in SOSMC of rotating stall (the full-state MG3 model).

7.4 Results and Discussions

All of the numerical constants and model parameters, which are used in this section, are mentioned in Table 7.1.

7.4.1 First Order Sliding Mode Control

Figure 7.5 reports the time-domain simulation results of FOSMC given by (7.35). The system initially starts from an efficient OP at the peak of the compressor map (OP1), where pressure rise is high and stall amplitude is zero. The controller is disabled until $\xi = 300$.

Figure 7.5e shows the pressure $\Delta\psi = \Psi_d(\xi) + d\psi$ and mass flow $\Delta\phi = \Phi_d(\xi) + d\phi$ perturbations. These perturbations consist of two terms: 1- Time varying sinusoidal disturbances $\Phi_d(\xi)$, $\Psi_d(\xi)$ and constant offsets $d\phi$ and $d\psi$ that can be thought of as model uncertainties (see Table 7.1 for the selected values).

By including perturbations at $\xi = 100$, the uncontrolled system develops rotating stall and J increases as shown in Figure 7.5d. This imposes a trajectory (cyan in Figure 7.5a) toward the unstable area and finally leads to fully developed rotating stall at OP2. Correspondingly, the output pressure drops as seen in Figure 7.5b.

Although, the perturbations last to the end of simulation, as soon as the controller starts at $\xi = 300$, the developed stall is damped out and pressure rise is corrected (Figure 7.5d and 7.5b respectively). Figure 7.5a shows that the controlled system trajectory (green) returns to OP1 in finite time. Due to the presence of perturbations on the sliding surface ($\phi = 0, \psi = 0$), the control laws continuously switch to compensate their effect. Therefore chattering can be seen in Figure 7.5f-7.5g. Figure 7.5 is reported for $G = 5$ and $C_1 = C_2 = 125$.

Our outcomes demonstrate that the choice of control design parameters (G, C_1 , and C_2) can modify the transient response of the system.

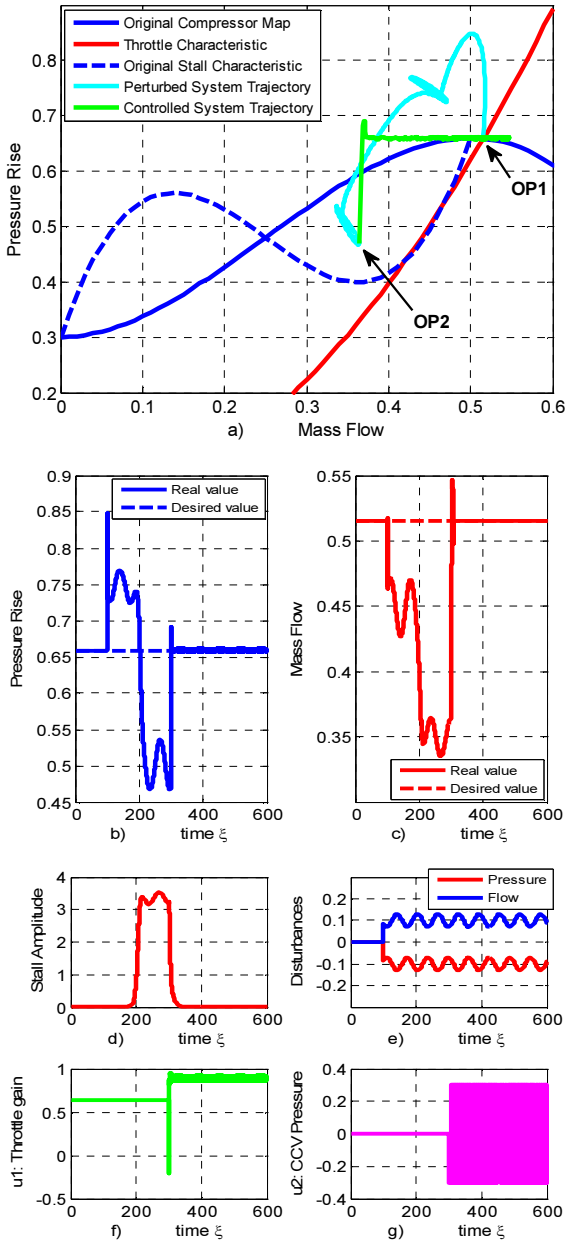

Figure 7.5: FOSMC of rotating stall in the presence of external disturbances and model uncertainties

7.4.2 Second Order Sliding Mode Control

In this case, we investigate the effectiveness of the SOSMC developed in (7.57). The system initially starts from OP1 when the controller is disabled to show the destabilizing effect of perturbations. The same perturbations as in the previous section are applied to the system. They push the system toward instabilities and the system settles down at a fully developed rotating stall OP (OP2) (see magenta trajectory in Figure 7.6a). At $\xi = 500$, the controller starts and rapidly damps out rotating stall (see Figure 7.6d). Consequently, the system returns to the efficient OP1 in finite time (see cyan trajectory in Figure 7.6a).

Now, the system has converged to the defined sliding surface $\phi_{ref} = 0$ and $\psi_{ref} = 0$. On the sliding surface, control laws reject the effect of perturbations. At $\xi = 800$, time varying set points are applied to the system as follows:

$$\phi_{ref} = 0.09\left(1 - e^{0.05(\xi - 800)}\right)$$

$$\psi_{ref} = -0.07\left(1 - e^{0.05(\xi - 800)}\right)$$

As can be seen in Figure 7.6a-7.6c, the system smoothly follows the variations of setpoints and remains at the time varying sliding surface. The investigation of Figure 7.6f and 7.6g reveals that the chattering disappears as expected in the analysis.

In this simulation the control design parameters are $G = 2$, $C_{11} = C_{12} = C_{21} = C_{22} = 180$, and $\nu_i = 0.75$ $(i = 1,2)$.

7.4.3 SOSMC of Surge

Here, the system is initially stable at OP1. At $\xi = 100$, the same disturbances as before (see Figure 7.7e) lead to deep surge due to the selected value for B-parameter ($B = 2$). As shown in Figure 7.7a and 7.7c deep surge causes flow reversal. SOSMC given by (7.57) starts at $\xi = 350$, immediately damps out surge oscillations, and stabilizes the system at desired initial OP. It is worth noting that although perturbations last until the end of simulation, chattering-free control laws effectively reject them. In this simulation the control design parameters are $G = 2$, $C_{11} = C_{12} = C_{21} = C_{22} = 180$, and $\nu_i = 0.75$ $(i = 1,2)$.

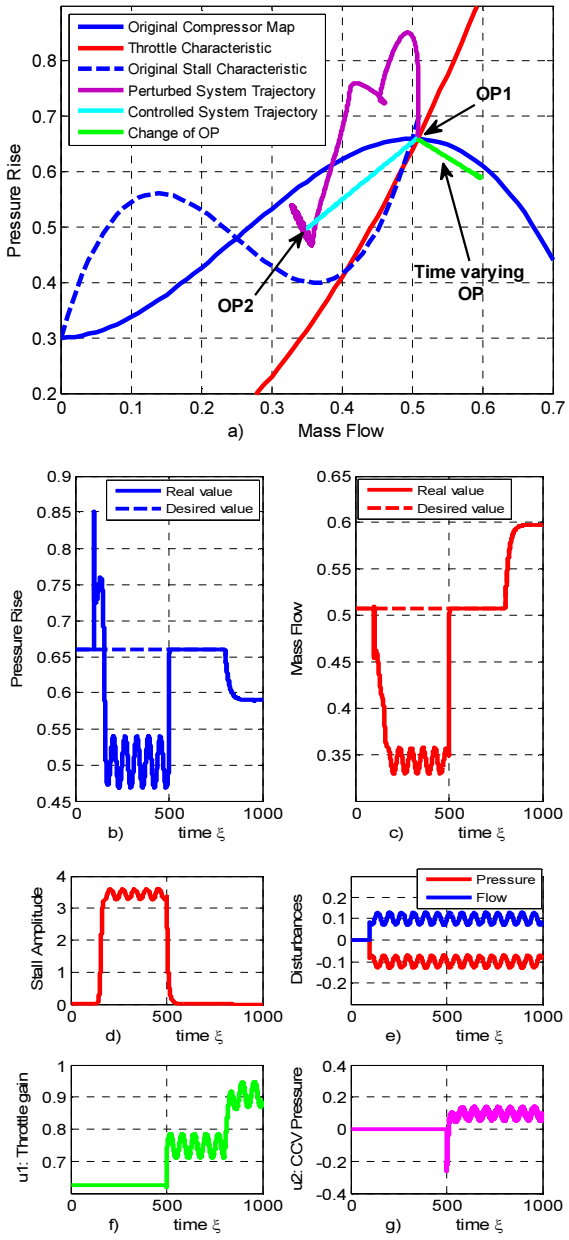

Figure 7.6: Chattering-free SOSMC of rotating stall in the presence of external disturbances, model uncertainties and setpoint variations

7.4.4 Unmodeled Actuator Dynamics and SOSMC

Figure 7.8 clearly shows that stable linear actuators (CCV and throttle valve) leads to the convergence to invariant boundary layers of sliding surface in finite time. In this case, asymptotic convergence to the sliding surface ($\phi = \dot{\phi} = 0$ and $\psi = \dot{\psi} = 0$) is destroyed and a stable limit cycle around this surface is initiated. In this simulation ($\mu_1 = \mu_2 = 15$).

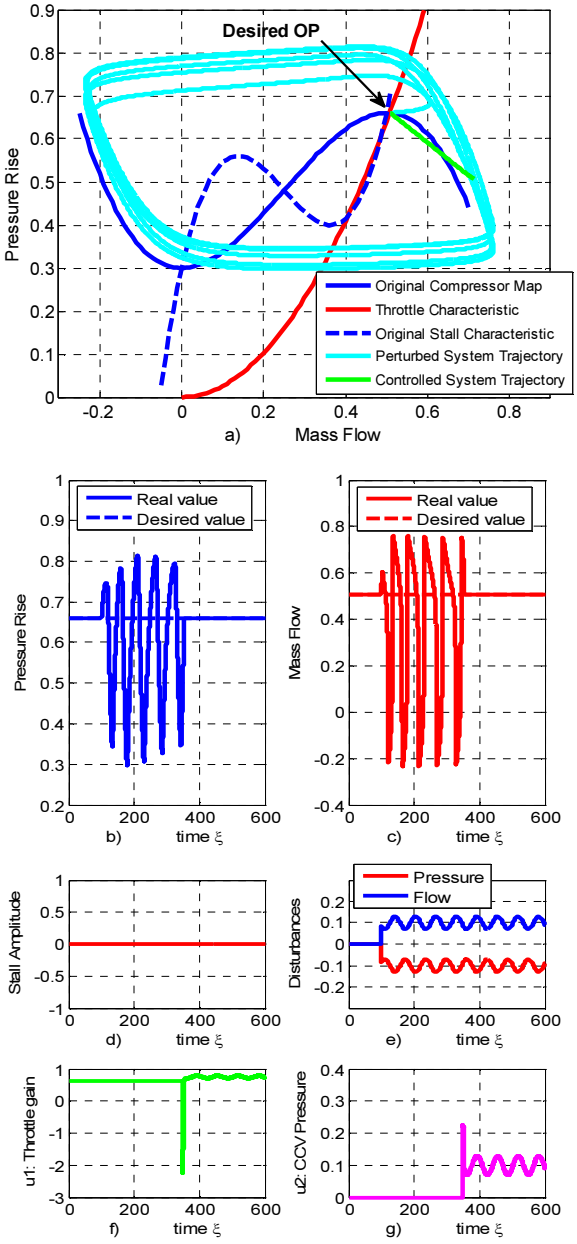

Figure 7.7: Chattering-free SOSMC of surge

7.5 Conclusion

In this paper, we tackle the problem of rotating stall and surge in axial compressors. This is performed by driving the control from pressure and mass flow measurements, and using throttle and CCV actuations. The square form of the control system makes a new robust chattering-free SOSMC combined with feedback linearization applicable to the problem. This method, which does not require the accurate knowledge of the compression system parameters,

guarantees the exponential stablility of the tracking control design. The idea of considering the terms including rotating stall in the disturbances simplifies the control design and the proof of perturbation boundedness satisfies the conditions of the applied theorems.

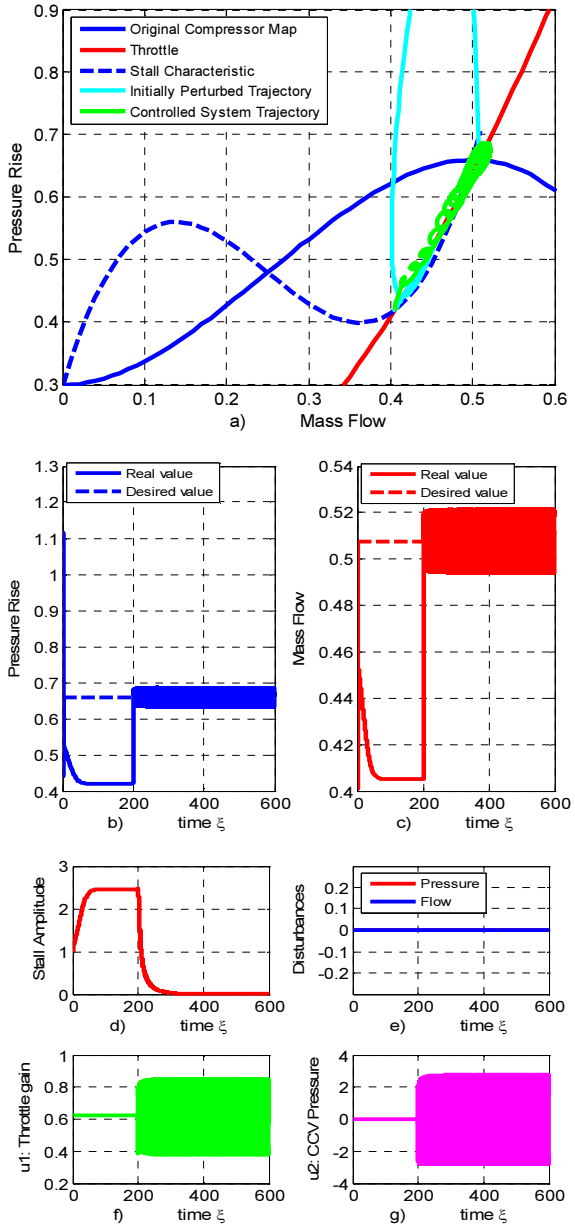

Figure 7.8: First order actuator dynamics and their effects on SOSMC as a limit cycle around the desired OP

The analytical analysis is corroborated by time-domain simulations reveals that the global asymptotic stabilization of the uncertain disturbed model can be achieved using a small number of control parameters. These parameters can determine transient response in reaching phase and perturbation rejection in sliding phase. The reasonable computation load and the fairly straightforward firmware implementation of developed chattering-free SOSMC make it an excellent choice for this application. Even a small enlargement in the domain of attraction of efficient OPs leads to a remarkable increase in performance and reliability of axial compressors and brings benefits to a wide range of users.

Appendices

A.

Table 7.1: Numerical values used in simulations

l_c	3	ϱ	0.425
W	0.25	d_ϕ	-0.05
H	0.18	d_ψ	0.02
B for rotating stall	0.1	$\Phi_d(\xi)$	$0.01sin(0.2\xi)$
B for deep surge	2	$\Psi_d(\xi)$	$0.01sin(0.2\xi)$

B.

$$\Delta A_1 = k_1 k_2 \left(-\frac{3H}{4} J \left(\frac{\phi + \Phi_0}{W} - 1 \right) - \frac{W^2 J}{2\gamma^2} + \Delta\psi \right) + \frac{1}{2} k_1^2 u_1 (\psi + \Psi_0)^{-\frac{1}{2}} \Delta\phi - k_1 \Delta\dot{\phi}$$

$$\Delta A_2 = k_2^2 (-M_1 - 2M_2\phi - 3M_3\phi^2) \left(-\frac{3H}{4} J \left(\frac{\phi + \Phi_0}{W} - 1 \right) - \frac{W^2 J}{2\gamma^2} + \Delta\psi \right) + k_1 k_2 \Delta\phi + k_2 \Delta\dot{\psi}$$
$$-\varrho J \left(\frac{3k_2 H}{4} \left(\frac{\phi + \Phi_0}{W} - 1 \right) + \frac{k_2 W^2}{2\gamma^2} \right) \left(1 - \left(\frac{\phi + \Phi_0}{W} - 1 \right)^2 - \frac{J}{4} - \frac{4W(\phi + \Phi_0)}{3H\gamma^2} \right)$$
$$-\frac{3k_2^2 HJ}{4W} \left(\psi_C - \psi - u_2 - \frac{3H}{4} J \left(\frac{\phi + \Phi_0}{W} - 1 \right) - \frac{W^2 J}{2\gamma^2} + \Delta\psi \right)$$

CHAPTER 8

ARTICLE 3: SIMULTANEOUS SPEED AND SURGE/STALL CONTROL IN VARIABLE SPEED AXIAL COMPRESSORS

Gholam-Reza Sari
École Polytechnique, University of Montreal, Montreal, Quebec, H3T 1J4, Canada

Ouassima Akhrif
École de Technologie Superieure, University of Quebec, Montreal, Quebec, H3C 1K3, Canada
and
Lahcen Saydy
École Polytechnique, University of Montreal, Montreal, Quebec, H3T 1J4, Canada

Submitted to International Journal of Flow Control on June 2014

Abstract

Gas turbines are internal combustion engines, which require pressurized air, and are widely used in industrial and aeronautic applications. The pressurized air is delivered by air compressors suffering from two kinds of aerodynamic instabilities, namely, surge and rotating stall. These instabilities are deeply affected by speed dynamics. Indeed, speed transitions develop temporary rotating stall and cause pressure drop at the output. The pressure drop limits the performance and spells troubles for normal operation of gas turbines even far from unstable zone usually defined in terms of stall point or surge line. Despite considerable efforts to stabilize axial compressors based on a constant speed assumption, the simultaneous control of speed and instabilities in variable speed axial compressors has been an open problem. The highly nonlinear and uncertain model of compressors including external perturbations forms a complex problem to control design. Furthermore, the lack of a full-state feedback makes the problem more challenging. In the present work, this problem is tackled by using a nonlinear robust controller based on output feedback linearization. The controller initially transforms the system into a controllable canonical form and then guarantees the disturbance rejection and asymptotical boundedness of the state variables. It drives a feedback from mass flow and pressure rise to stabilize the instabilities by actuating both the throttle valve and close-coupled valve. Time domain simulations corroborate analytical developments and show the effectiveness of the controller in the presence of bounded external perturbations and model uncertainties. Here, the impact of actuators' saturation is also studied.

8.1 Introduction

Gas turbines are commonly used in nowadays aircraft jet engines. Petroleum and chemical industries rely also on turbo compressor stations to pressurize products. Furthermore, gas turbines are effectively used to generate electricity across the power generation sector worldwide. These machines are known to suffer however from instabilities, namely, rotating stall and surge, which occur in the compressor stage and badly limit the performance of the system. Modeling the nonlinear behavior of compression systems and that of ensuing rotating stall and surge has been explored for decades. A wide variety of models exist for this purpose, each with its own strengths and limitations. Among these models, the lumped parameter Moore and Greitzer three-state model (so-called MG3) [36] describing both surge and rotating stall dominates the studies on control design of compression systems. Contrary to axial compressors, which are affected by both surge and rotating stall, the instability of centrifugal compressors is almost restricted to surge considerations [6, 104]. Consequently, in the case of centrifugal compressors, Greitzer model [18] which comprises only two state variables can capture the behavior of surge.

The main advantage of MG3 and its extensions is that they are not computational and can be used for control design purposes. On the other hand, they suffer from important limitations including a single-mode approximation of rotating stall and a constant-speed assumption. In 1997, Fink et al. [44] and subsequently Gravdahl and Egeland [45] presented a model for variable speed centrifugal compressors that incorporates the speed of the rotor as a state variable. However, these models were both developed for centrifugal machines, and did not capture rotating stall in axial compressors. In 1998, Gravdahl [46, 47] considered the speed of the rotor as a state variable and introduced a new model for variable speed axial compressors (VSACs). This extension of MG3 includes higher harmonics (modes) of rotating stall as well. The early work of Gravdahl [47] briefly reported some exclusive behavior of VSACs, which cannot be captured by constant-speed models such as MG3. His time-domain simulation results showed that contrary to what MG3 predicts, rotating stall can temporarily develop during speed transitions even while operating far from the unstable zone traditionally defined in term of stall point or surge line. The problem of variable speed compressor control design is one of the topics which is proposed for further research in Moore and Greitzer work [36] and Gravdahl's research [47]. Gravdahl

highlighted the need for simultaneous speed and surge/stall control to guarantee the performance of compression systems in both normal operation and during speed transitions. Despite devoted efforts on stabilizing axial compressors being based on the constant speed assumption and the reported achievements (see [47, 50, 123, 129, 134, 140, 141]) , the simultaneous control of speed and instabilities in VSACs has remained an open problem. The highly nonlinear model of VSACs represents a complex problem for control design. Furthermore, including model uncertainties (the precise estimation of model parameters, especially in the unstable zone, being difficult) and external perturbations make the problem even more challenging. Finally, the squared amplitude of stall modes used as state variables are experimentally difficult to measure and full-state feedback cannot be considered in control design.

Here, we propose a robust feedback linearization method to tackle the stability problems of VSACs. The control law is based on speed, pressure and mass flow measurements. Mass flow is frequently used in some control design methodologies in the literature [114, 115], and there exist some implemented controllers that use this measurement [116]. Nonlinear observers are also proposed to estimate mass flow [117, 118]. In this work, throttle and close-coupled valve (CCV) actuation are used to guarantee the stability, and a drive torque is applied to increase the speed of the rotor. CCV is considered to be one of the most promising actuation methods [92-94]. To develop the controller, the amplitude of rotating stall, which cannot be measured but is one of the state variables in Gravdahl's model, is considered as a disturbance. This assumption being supported by the proof of perturbations boundedness greatly simplifies the design. Furthermore, the control scheme does not require an accurate knowledge of model parameters. Simulation results corroborate analytical developments and demonstrate the disturbance rejection and the global ultimate boundedness of state variables which leads to surge and rotating stall control.

The rest of the paper is organized as follows. Section 8.2 recalls the Gravdahl model for VSACs. Section 8.3 describes the control design and considers the assumptions involved. Section 8.4 examines the hypotheses and investigates the applicability of the control design to VSACs. Section 8.5 reports time-domain simulation results and explores the effect of actuators' saturation. Conclusions about this work are drawn in Section 8.6.

8.2 Dynamic Equations for VSACs

In 1998, Gravdahl developed a model for VSACs and considered the speed of the rotor as a state variable [47]. Later, Zaiet et al. [168] modified the model to include the pressure drop over a CCV and to make it suitable for control applications. At an operating point $(\Phi_0, \Psi_0, \Omega_0)$, the dynamic model can be given in the form of state-space equations in error coordinates (see [47] for details). The model which is only includes the first harmonic of rotating stall and comprises actuator forces, is given in Σ_1: (8.1)-(8.4).

$$\dot{J}_1 = \rho_2 J_1 \left(1 - \left(\frac{(\phi+\Phi_0)}{W} - 1\right)^2 - \frac{J_1}{4} - \frac{\mu W}{3aH} + \frac{2\Omega_0 \Lambda_1 (m-1)W}{3bH}(c(\phi+\Phi_0)^2 - u_3) - \frac{4W}{3H\gamma_v^2}(\phi+\Phi_0)\right) \tag{8.1}$$

$$\dot{\phi} = \rho_1 \left(-\psi - \Psi_0 + \psi_{c0} + H + \frac{3H}{2}\left(\frac{\phi+\Phi_0}{W} - 1\right)\left(1 - \frac{J_1}{2}\right) - \frac{H}{2}\left(\frac{\phi+\Phi_0}{W} - 1\right)^3 - u_1 - \frac{W^2}{2\gamma_v^2} J_1 - \frac{l_E \Omega_0 \Lambda_1}{b}(\phi+\Phi_0)u_3 + \frac{l_E \Omega_0 \Lambda_1 c}{b}(\phi+\Phi_0)^3 + \Delta_\psi\right) \tag{8.2}$$

$$\dot{\psi} = \frac{\Lambda_2}{\omega+\Omega_0}\left(\phi + \Phi_0 - \sqrt{\psi+\Psi_0}u_2 - \Delta_\phi - \frac{2\Lambda_1}{\Lambda_2}(\psi+\Psi_0)(\omega+\Omega_0)^2(u_3 - c(\phi+\Phi_0)^2)\right) \tag{8.3}$$

$$\dot{\omega} = \Lambda_1(\omega+\Omega_0)^2(u_3 - c(\phi+\Phi_0)^2) \tag{8.4}$$

where ϕ, ψ, and ω denote respectively the annulus averaged mass flow coefficient, the non-dimensional plenum pressure, and the speed of the rotor in error coordinates. J_1 is the squared amplitude of the first harmonic of rotating stall. The actuators' forces are input variables u_1, u_2, and u_3 defined respectively as: the pressure drop over CCV, the throttle gain, and the non-dimensional drive torque being used to increase the speed. The definition of the remaining model parameters H, W, ψ_{c0}, γ_v, Λ_1, Λ_2, m, b, μ, a, ρ_1, and ρ_2, which are all positive non-zero parameters, can be found in [47]. To investigate the effect of uncertainties, we introduce Δ_ϕ and Δ_ψ in the model. Δ_ϕ consists of two terms : Φ_d which is a time varying mass flow disturbance and d_ϕ which introduces a constant or slow varying uncertainty in the throttle characteristic. Similarly, Δ_ψ consists of two terms: Ψ_d which is a time varying pressure disturbance and d_ψ which can be thought of as a constant or slow varying uncertainty in the compressor map. Furthermore, it is supposed that these uncertain terms are bounded.

Here, the domain of interest is a subset $D \subset \mathcal{R}^4$ where $\psi + \Psi_0 > 0$ and the mass flow of compressors is always limited to $\phi_{min} < \phi + \Phi_0 < \phi_{choke}$, where ϕ_{choke} is the choking value

of the mass flow and ϕ_{min} is the minimum negative mass flow during deep surge (see [47] for more details). In the literature [169, 170], there exist also other assumptions on the speed of rotor which state that $0 < \omega + \Omega_0 < \Omega_{max}$.

8.3 Control Design

The control objective is to stabilize Σ_1 at origin. By considering the following control inputs:

$$u_1 = -\psi - \Psi_0 + \psi_{c0} + H + \frac{3H}{2}\left(\frac{\phi+\Phi_0}{W} - 1\right) - \frac{H}{2}\left(\frac{\phi+\Phi_0}{W} - 1\right)^3 + \frac{l_E\,\Omega_0 \Lambda_1(\phi+\Phi_0)}{b} K_3\omega + \frac{K_1}{\rho_1}\phi \quad (8.5)$$

$$u_2 = \frac{(\phi+\Phi_0)}{\sqrt{\psi+\Psi_0}} + \frac{2\Lambda_1\sqrt{\psi+\Psi_0}(\omega+\Omega_0)^2 K_3\omega}{\Lambda_2} + \frac{1}{\sqrt{\psi+\Psi_0}} K_2\psi \quad (8.6)$$

$$u_3 = c(\phi + \Phi_0)^2 - K_3\omega \quad (8.7)$$

Σ_1 can be written as follows:

$$\Sigma_2: \begin{cases} \dot{J_1} = f(J_1, \phi, \omega) \\ \dot{\phi} = -K_1\phi + \delta_1 \\ \dot{\psi} = \frac{\Lambda_2}{\omega+\Omega_0}(-K_2\psi + \delta_2) \\ \dot{\omega} = -\Lambda_1(\omega + \Omega_0)^2 K_3\omega + \delta_3 \\ y = [\phi, \psi, \omega]^T \end{cases} \quad (8.8)$$

where K_i are design parameters.

δ and f are given by:

$$\delta = \begin{bmatrix} \delta_1 \\ \delta_2 \\ \delta_3 \end{bmatrix} = \begin{bmatrix} \rho_1\left(-\frac{3J_1H}{4}\left(\frac{\phi+\Phi_0}{W} - 1\right) - \frac{W^2}{2\gamma_v^2}J_1 + \Delta_\psi\right) \\ -\Delta_\phi \\ 0 \end{bmatrix} \quad (8.9)$$

$$f(J_1, \phi, \omega) = \rho_2 J_1\left(1 - \left(\frac{(\phi+\Phi_0)}{W} - 1\right)^2 - \frac{J_1}{4} - \frac{\mu W}{3aH} + \frac{2\Omega_0\Lambda_1(m-1)WK_3}{3bH}\omega - \frac{4W}{3H\gamma_v^2}(\phi + \Phi_0)\right) \quad (8.10)$$

Here $f(J_1, \phi, \omega)$ is continuously differentiable in the domain of interest and $f(0,0,0) = 0$.

Lemma 1: Consider system Σ_2, and suppose that δ is bounded ($\|\delta(J_1, \zeta)\| \leq \varepsilon$) and $\dot{J_1} = f(J_1, \phi, \omega)$ is globally in the domain of interest input-to-state stable, then by choosing positive

gains $(K_i > 0)$, the state variables (J_1, ζ) where $\zeta = [\phi, \psi, \omega]$ converge to a residual subset around the origin and are bounded.

In order to prove *Lemma 1*, we firstly test the two formed hypotheses.

Hypothesis 1: δ is bounded ($\|\delta(J_1, \zeta)\| \leq \varepsilon$).

Hypothesis 2: $\dot{J}_1 = f(J_1, \phi, \omega)$ is globally (in the domain of interest) input-to-state stable.

It is worth noting that here, u_3 is used to only change rotor speed and u_1 and u_2 guarantee the stability of the system during the speed variations.

Test of Hypothesis 1

The objective is to prove that δ is bounded. Recall that in the domain of interest, the averaged mass flow ϕ and the rotor speed are bounded, $\phi_{min} < \phi + \Phi_0 < \phi_{choke}$, $0 < \omega + \Omega_0 < \Omega_{max}$ so it remains to show that $J_1(t)$ is bounded as well.

To prove this, the dynamics of J_1 , i.e., (8.1) are first rewritten as:

$$\begin{cases} \dot{J}_1 = \rho_2 J_1 \left(\beta_1 - \frac{J_1}{4} + \beta_2 \omega + \beta_3 \phi\right) = \rho_2 J_1 \left(\beta_1 - \frac{J_1}{4} + f(t)\right) \\ J_1(0) = J_{10} \geq 0 \end{cases}$$

where $f(t) \triangleq \beta_2 \omega(t) + \beta_3 \phi(t)$,

$$\beta_1 \triangleq -\frac{\mu W}{3aH} - \frac{4W\Phi_0}{3H\gamma_v^2} - \frac{\phi^2 + \Phi_0^2}{W^2} + \frac{2\Phi_0}{W} < 0,$$

$$\beta_2 \triangleq \frac{2\Omega_0(m-1)WK_3}{3bH} > 0,$$

$$\beta_3 \triangleq -\frac{4W}{3H\gamma_v^2} + \frac{2}{W} - \frac{2\Phi_0}{W^2}.$$

Then:

$$\dot{J}_1 = \rho_2 \beta_1 J_1 - \frac{\rho_2 J_1^2}{4} + \rho_2 J_1 f(t) \leq \rho_2 \beta_1 J_1 - \frac{\rho_2 J_1^2}{4} + \rho_2 M J_1 \triangleq \alpha J_1 - \beta^2 J_1^2,$$

where $\beta^2 \triangleq \frac{\rho_2}{4}$ and M is such that $M \geq |f(t)|$ for all $t \geq 0$ and, without loss of generality, chosen so that, $\alpha \triangleq \rho_2(\beta_1 + M)$ is non zero.

It therefore follows from comparison theorems [171] that:

$J_1(t) \leq r(t) \quad \forall \ t \geq 0$

$$\begin{cases} \dot{r}(t) = \alpha r(t) - \beta^2 r^2 \\ r(0) = J_{10} \end{cases}$$

The solution of which is given by:

$$r(t) = \frac{\alpha}{\beta^2} \frac{e^{\alpha t}}{C_0 + e^{\alpha t}} \quad ; t \geq 0$$

$$C_0 \triangleq \frac{\alpha}{J_{10}\beta^2} - 1, \ (J_{10} \neq 0)$$

Now the upper bound of $r(t)$ is monotonous since:

$$\dot{r}(t) = \frac{\alpha^2}{\beta^2} \frac{C_0 e^{\alpha t}}{(C_0 + e^{\alpha t})^2}$$

Therefore $r(t)$ does not have a finite escape-time. Consequently:

$$J_1(t) \leq \max\left(J_{10}, \frac{\alpha}{\beta^2}\right)$$

The boundedness of Δ_ϕ, Δ_ψ,$\gamma_v \in [\gamma_{min}, \gamma_{max}]$, and J_1 lead to the boundedness of δ which confirms *Hypothesis 1.*

Test of Hypothesis 2

The objective here is to show that $\dot{J}_1 = f(J_1, \phi, \omega) = f(J_1, v)$ with $v \coloneqq [\phi, \omega]$, is input-to-state stable. Theorem 4.19 [172] states that if there is a continuously differentiable function $V_1 : R \to R$ such that

$$\alpha_1(\|J_1\|) \leq V_1(J_1) \leq \alpha_2(\|J_1\|)$$

$$\frac{\partial V_1}{\partial J_1} f(J_1, u) \leq -W(J_1), \qquad \forall \ \|J_1\| > \rho(\|v\|) > 0$$

where α_1, α_2 are class $\varkappa_\infty$ functions, ρ is a class $\varkappa$ function , and $W(J_1)$ is continuous positive definite function on R. Then $\dot{J}_1 = f(J_1, v)$ is input-to state stable.

Considering the Lyapunov function $V_1(J_1) = \frac{1}{2\rho_2} J_1^2$ then we have:

$$\dot{V}_1 = \frac{\partial V_1}{\partial J_1} f(J_1, \phi, \omega) = J_1^2 \left(\beta_1 - \frac{J_1}{4} + \beta_2 \omega + \beta_3 \phi\right) = \beta_1 J_1^2 + \frac{J_1^2}{4}\left(-J_1 + 4\beta_2 \omega(t) + 4\beta_3 \phi(t)\right)$$

where β_i are as above.

Let $g(t) \triangleq 4\beta_2\omega(t) + 4\beta_3\phi(t)$ then:

$g(t) \leq 4|\beta_2||\omega| + 4|\beta_3||\phi| \leq 4\max(|\beta_2|, |\beta_3|)\,\|v\|_\infty =: \sigma\|v\|_\infty$

then: $\dot{V}_1 \leq \beta_1 J_1^2 + \frac{J_1^2}{4}(-J_1 + \sigma\|v\|_\infty) \leq \beta_1 W(J_1)$

with $W(J_1) \triangleq J_1^2$, a positive definite function and $\beta_1 < 0$. Then provided that: $-J_1 + \sigma\|v\|_\infty \leq 0$, i.e., $J_1 = \|J_1\|_\infty \geq \sigma\|v\|_\infty = \sigma\rho(\|v\|_\infty)$ which proves input-to-state stability of the $\dot{J}_1 = f(J_1, \phi, \omega) = f(J_1, v)$.

Proof of Lemma 1:

Let $V_2(\zeta) = \frac{1}{2}\zeta^T\zeta$ which is a positive definite function of ζ then:

$$\dot{V}_2(\zeta) = -\zeta^T\dot{\zeta} = -K_1\phi^2 + \delta_1\phi + \frac{\Lambda_2}{\omega + \Omega_0}(-K_2\psi^2 + \delta_2\psi) - \Lambda_1 K_3(\omega + \Omega_0)^2\omega^2$$

$$\dot{V}_2(\zeta) \leq -\frac{1}{2}K_1\phi^2 - \frac{\Lambda_2 K_2}{2(\omega + \Omega_0)}\psi^2 - \Lambda_1 K_3(\omega + \Omega_0)^2\omega^2 - \left(\frac{K_1}{2}\phi^2 - \|\delta_1\|\|\phi\| + \frac{\Lambda_2}{(\omega + \Omega_0)}\left(\frac{K_2}{2}\psi^2 - \|\delta_2\|\|\psi\|\right)\right)$$

As a conservative choice, in a neighborhood of the origin where $\|\phi\| \geq \frac{2}{K_1}\|\delta_1\|$ and $\|\psi\| \geq \frac{2}{K_2}\|\delta_2\|$ then: $\dot{V}_2(\zeta) \leq -W_3(\phi, \psi, \omega)$

where $W_3(\phi, \psi, \omega) = \frac{1}{2}K_1\phi^2 + \frac{\Lambda_2 K_2}{2(\omega + \Omega_0)}\psi^2 + K_3\Lambda_1(\omega + \Omega_0)^2\omega^2$ is a positive definite function. Higher feedback gains K_i clearly imply a smaller size for this neighborhood of the origin.

By applying Theorem 4.18 in [172] and considering a bounded uncertainties $\|\delta(J_1, \zeta)\| \leq \varepsilon$, we can show that a finite time t_0 and a positive constant c exist such that: $\|\zeta\|_2 \leq c\varepsilon,\ \forall\, t \geq t_0$ and c can arbitrarily be small by an appropriate choice of K_i.

By input-to-state stability of $\dot{J}_1 = f(J_1, \phi, \omega)$, we have :

$$\|J_1(t)\|_2 \leq \beta(\|J_1(0)\|_2, t - t_0) + \gamma(\sup_{t \geq t_0}\|\zeta(t)\|_2) \leq \beta(\|J_1(0)\|_2, t - t_0) + \gamma(c\varepsilon)$$

where β and γ are class $\varkappa\mathcal{L}$ and class $\varkappa$ functions, respectively. The term $\beta(\|J_1(0)\|_2, t-t_0)$ satisfies $\beta \leq \varepsilon$ after some finite time. Therefore $\|J_1, \zeta\|_2$ is ultimately bounded by $c\varepsilon + \varepsilon + \gamma(c\varepsilon)$. Finally, *Lemma 1* states that by using the proposed controller u given in (8.5-7) the state variables converge to a neighborhood of the origin and consequently they are bounded.

8.4 Results and Discussions

In the following time-domain simulations, we compare two cases: 1- a system including u_3 changing the rotor speed but without surge and rotating stall control (u_1 and u_2) which is called open-loop and 2- a system including (u_1, u_2, u_3) where we simultaneously control the speed and surge/rotating stall which is called closed-loop.

The numerical values of the simulations are given in Table 8.1.

8.4.1 Temporary Stall Control in the Case of Unsaturated Actuators

The problem of temporary stall development is tackled in this section. Time-domain simulations compare open-loop and closed-loop systems and demonstrate the effectiveness of the controller in preventing the compressor from developing temporary rotating stall and pressure drop. Figures 8.1a, b, c, and d show the systems' trajectories $(\Phi, \Psi, \Omega, \mathrm{J}_1)$ during a speed transition without actuator saturation.

Table 8.1: Numerical values used in simulations

l_c	3	ϱ	0.425
W	0.25	μ	0.001
H	0.18	b	96.17
B for rotating stall	0.1	m	1.75
B for deep surge	2	l_I	2
Λ_1	2.1685e-4	Λ_2	0.0189
a	0.3	$0 < \rho_1 < 1,\ 0 < \rho_2 < 1$	

For the open-loop system and during the speed transition, dashed lines in Figure 8.1b and d report a pressure drop and a temporary rotating stall development respectively. For the closed-

loop system, the controller completely damps out the temporary stall and prevents the pressure from dropping (see Figure 8.1b and 8.1d bold trajectories). The variation of flow is reported for both system in Figure 8.1a and the speed variation is shown in Figure 8.1c.

Figure 8.2 shows the variables Φ and Ψ in the phase space along with equivalent compressor map and stall characteristic. Both open-loop and closed-loop systems start from an effective initial operating point (OP) at the top of the equivalent compressor map (i.e. compressor comprising CCV, see [47] for the exact definition). In Figure 8.1a, the open-loop system's trajectory (Φ, Ψ) goes back to the initial OP once the rotor speed reaches the desired value, but only after considerable variations due to temporary stall development. For the case of closed-loop system, thanks to the effective controller, this variation is negligible.

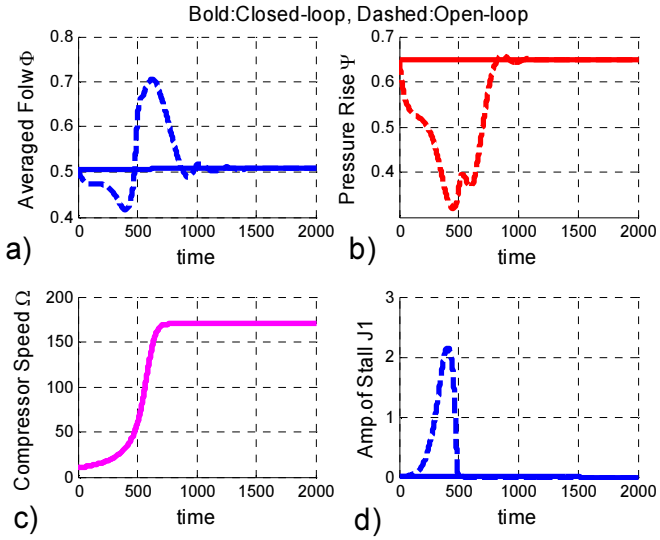

Figure 8.1: Open-loop system (dashed) and closed-loop system without saturation (bold)

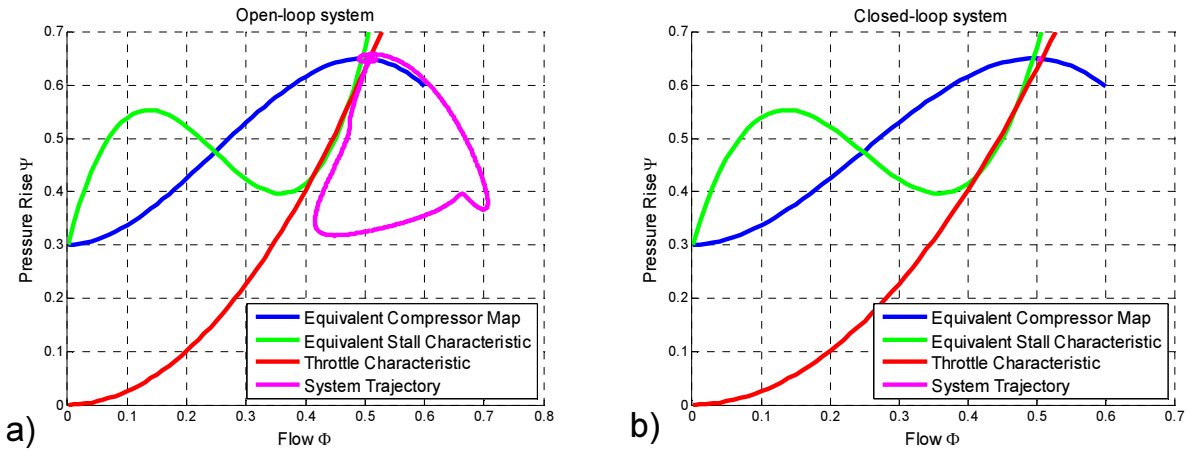

Figure 8.2: (a) Open-loop and (b) closed-loop (unsaturated actuators)

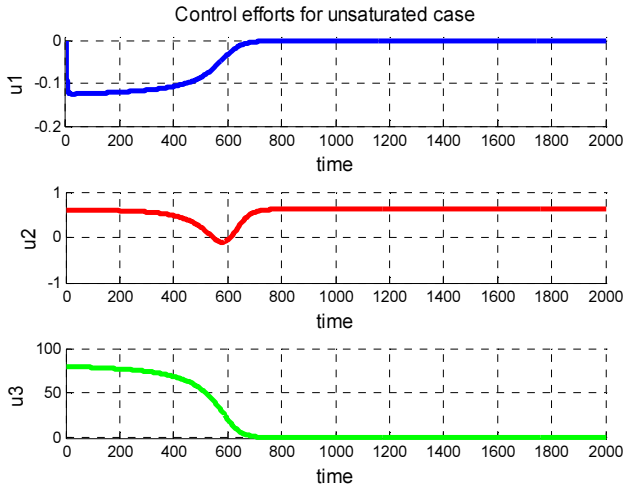

Figure 8.3: Control efforts for closed-loop system without actuators' saturations

Figure 8.3 finally shows the three control efforts of the closed-loop system with unsaturated actuators.

8.4.2 Temporary Stall Control in the Case of Saturated Actuators

Here, a saturation is added to each actuator to limit the control efforts. Figure 8.4 reports the impact of actuators' saturations on the closed-loop system.

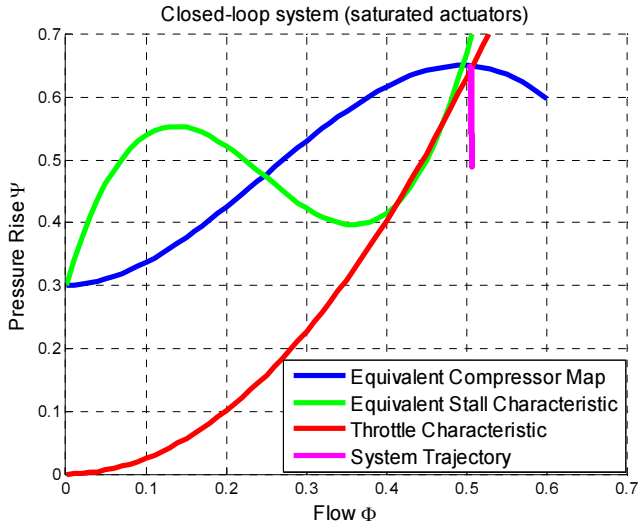

Figure 8.4: Closed-loop with saturated actuators

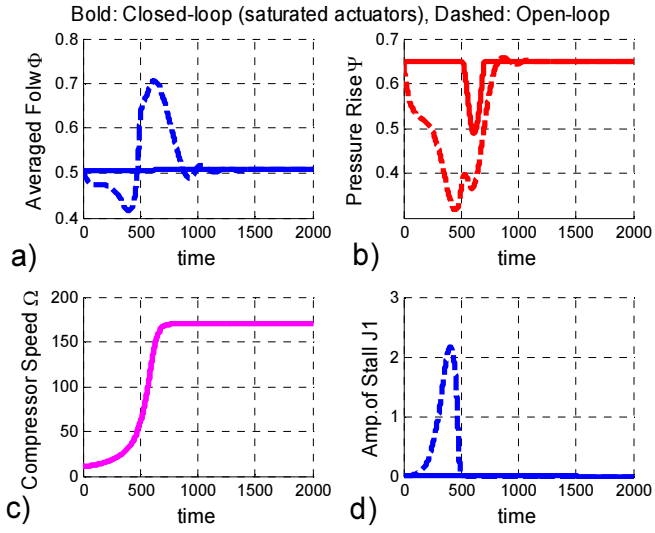

Figure 8.5: Open-loop system (dashed) and closed-loop system with saturation (bold)

Figure 8.5 compares the closed-loop and open-loop system state variables. It is interesting to note that, although the controller cannot completely prevent the pressure drop because of actuators' saturations, it still suppresses rotating stall and achieves a considerable improvement by comparison to the open-loop system. Again, Figure 8.6 shows the saturated control efforts.

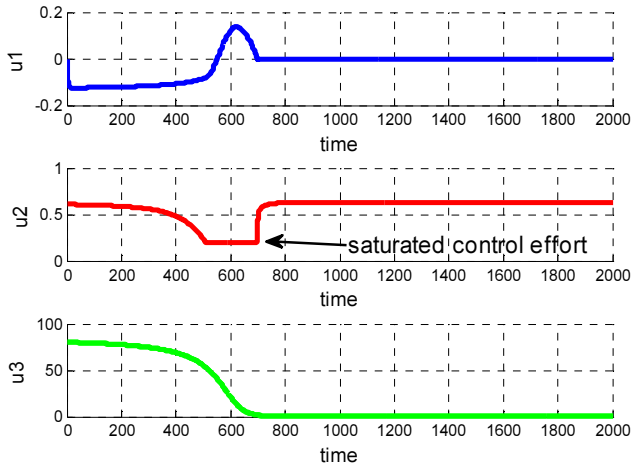

Figure 8.6: Control efforts for the closed-loop system with actuators' saturations

8.4.3 Fully developed Stall Due to Speed Variations

As reported in [173] when speed varies at an efficient operating point (e.g. at the peak of the equivalent compressor map), temporary stall developments can lead to a fully developed rotating stall. Here, we will show that the proposed controller prevents the system from developing such a rotating stall. Figure 8.7a firstly shows that the open-loop system moves from the initial OP to the final fully developed rotating stall OP due to a speed transition. Figures 8.7e and 8.7c show the stall development and the pressure drop at the output respectively.

Figure 8.8 shows that on the other hand in closed loop, the controller effectively stabilizes the compression system at the efficient OP and prevents it from developing a steady rotating stall due to the speed variation. Output pressure, rotor speed, rotating stall, and control efforts are respectively reported in Figure 8.8c to 8.8f.

8.4.4 Fully Developed Stall and Deep Surge Due to External Perturbations

Previously reported results in [47] show that pressure and flow external perturbations can destroy the stability of compressors at an efficient OP and lead to fully developed rotating stall or deep surge depending on the speed of the rotor (i.e. for low speeds the system goes to rotating stall and for high speeds it develops deep surge). Here, we first consider the case of low speed operation and demonstrate that the controller can effectively reject the perturbations and guarantee the stability of the system.

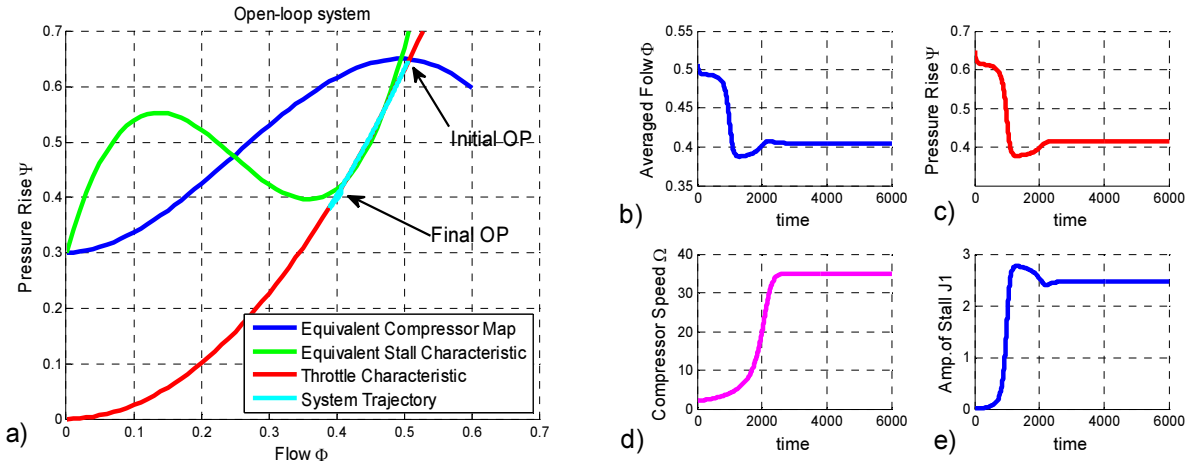

Figure 8.7: Open-loop system develops steady rotating stall due to a speed variation

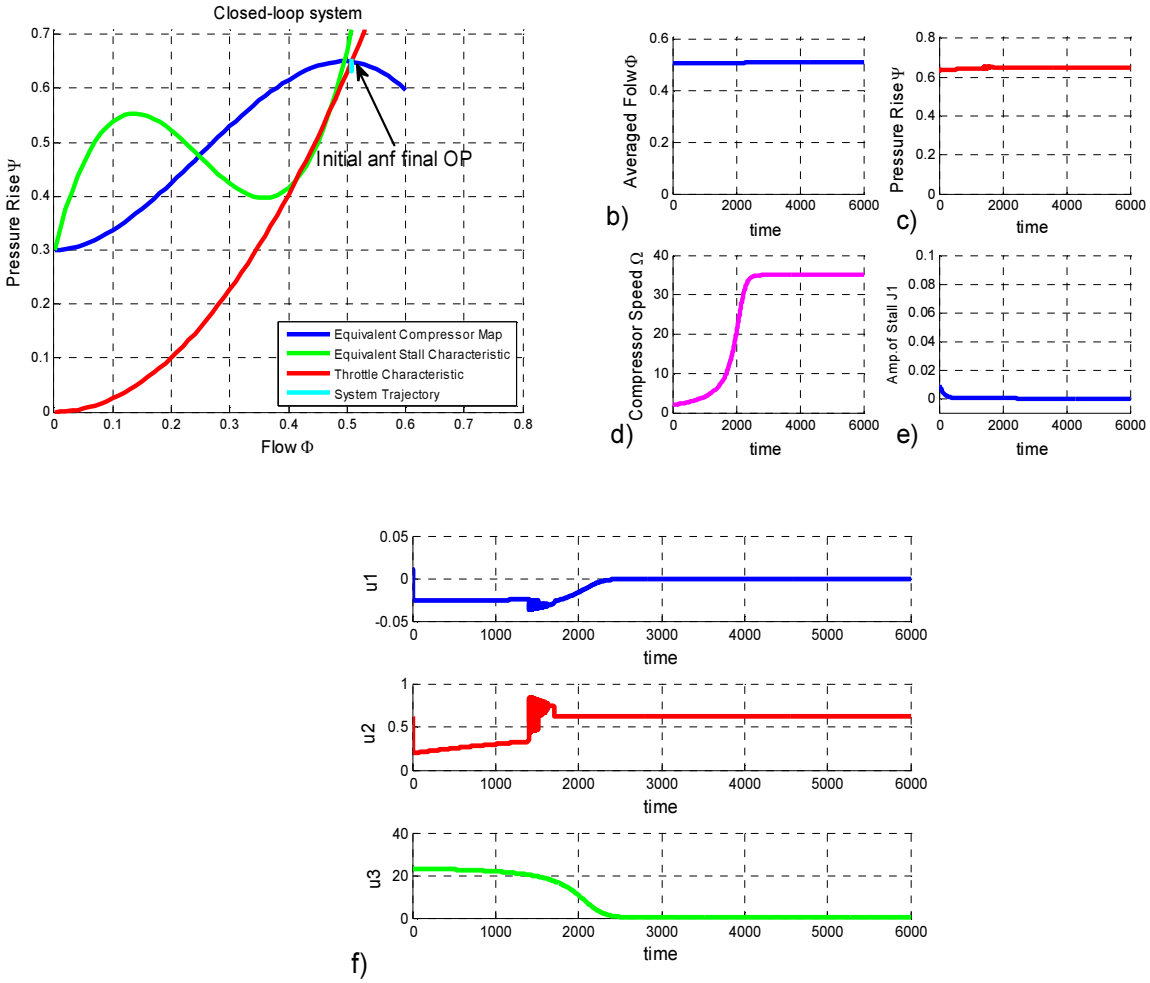

Figure 8.8: Controller prevents system from developing rotating stall due to a speed transition

To realize the simulations two types of perturbations are applied to the system denoted by Φ_d, Ψ_d, d_ψ, and d_ϕ. $\Phi_d = \Psi_d = 0.01sin(0.2\xi)$ are considered as mass flow and pressure disturbances respectively and $d_\psi = 0.02, d_\phi = -0.05$ which represents the uncertainty of compressor map and throttle characteristic.

In Figure 8.9a, the system initially starts from OP1 when the controller is not activated. Perturbations are applied to the system at $t = 10000$ (see Figure 8.9g). The system develops then rotating stall and goes to OP2 (i.e. in this case final speed is not high and implies stall development see Figure 8.9e). Although the perturbations are removed at $t = 12000$ the open-loop system remains at OP2 (see Figures 8.9c and 8.9e for pressure drop and amplitude of stall).

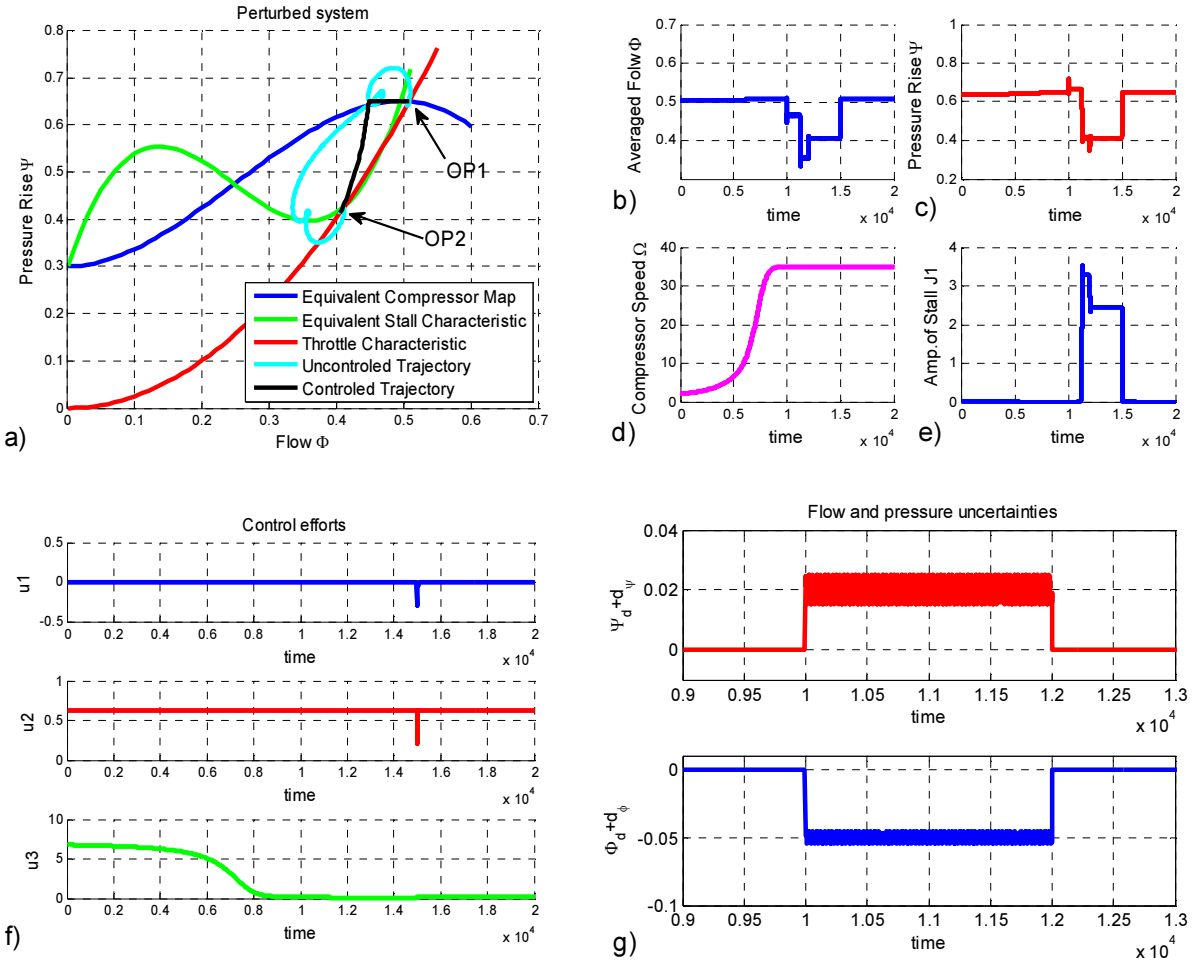

Figure 8.9: Effect of perturbation on open-loop and closed-loop systems

At $t = 15000$ the controller is activated and closes the loop. It immediately damps out rotating stall and increases the pressure. Consequently the system returns to its initial efficient OP (OP1) where the pressure is high enough for normal operation of the gas turbine.

Figure 8.10 reports the effectiveness of the controller for long-lasting perturbations. Here, the perturbations are applied at $t = 10000$ and remain until the end of the simulation (Figure 8.10g). Figures 8.10c and 8.10e show that when the controller is activated at $t = 15000$, the stall is damped out and the output pressure is stabilized. Therefore, the controller guarantees the stability of the compression system even in the presence of bounded external perturbations.

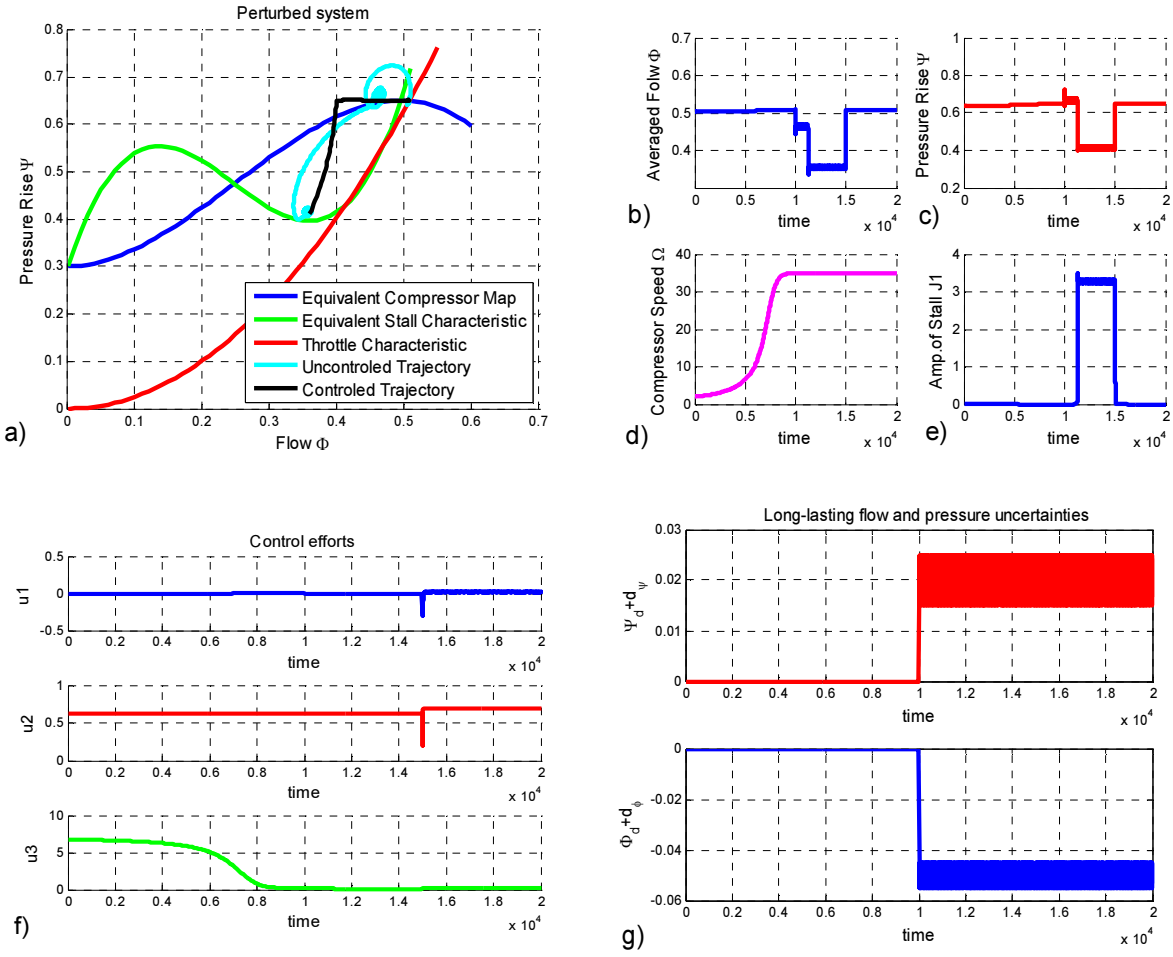

Figure 8.10: Effectiveness of the controller in the presence of perturbations

Last but not least is the case of deep surge. We run the same simulations but for high speed operations (Figure 8.11). The open-loop system initially starts at OP1. At $t = 3000$, perturbations are applied to the open-loop system. Due to the perturbation and the high rotor speed (see Figure 8.11d) the open-loop system goes to deep surge. A flow reversal can be seen in Figure 8.11a and 8.11b. At $t = 6000$, the controller is activated and immediately damps out deep surge oscillations. Again, this simulation shows the effectiveness of the proposed control law in surge control.

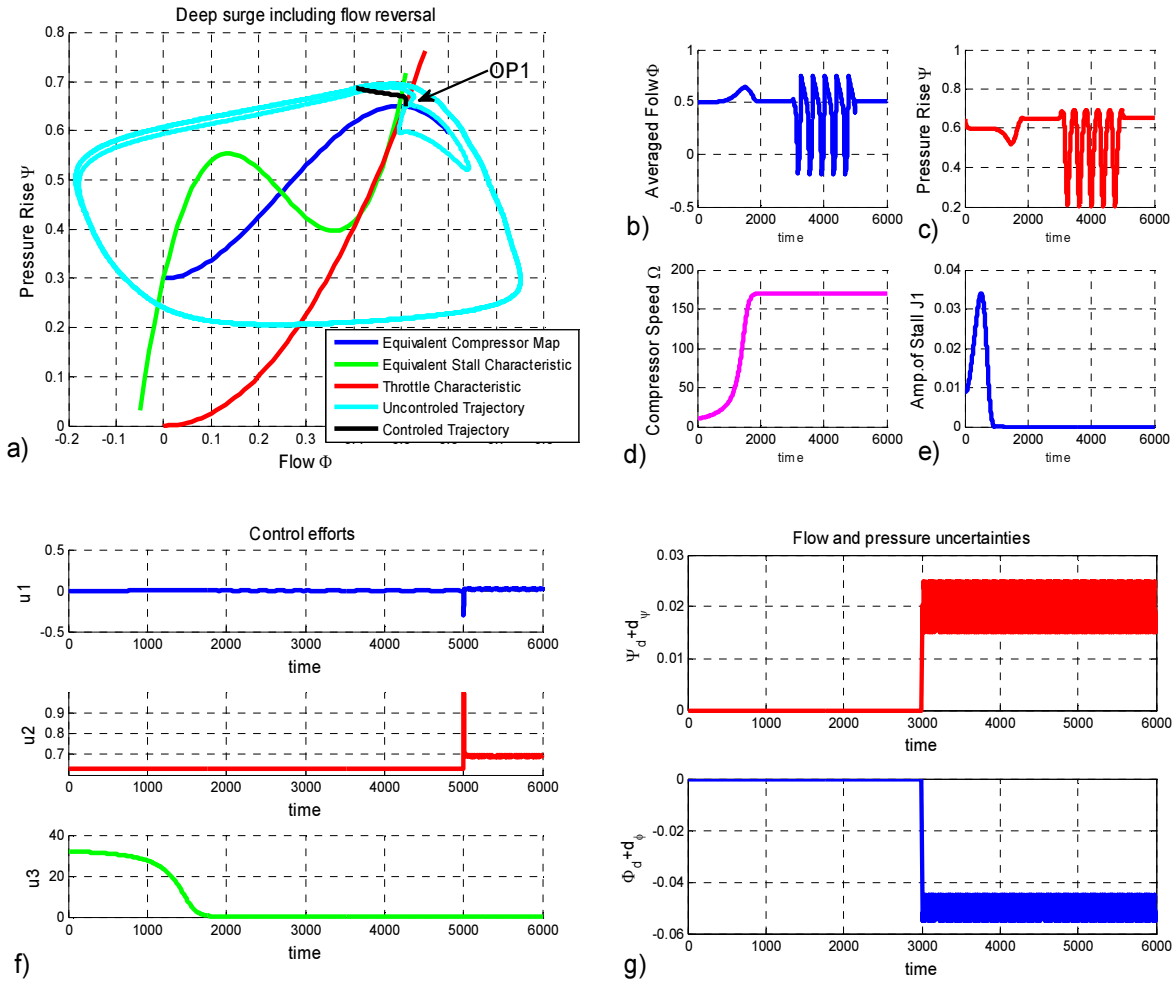

Figure 8.11: Surge control in the presence of perturbations

8.5 Conclusion

Surge and rotating stall limit compression systems performance and can cause mechanical damages. Furthermore speed transitions, which can lead to temporary stall development and pressure drop at the output, degrade the effective operation of compressors and consequently gas turbines. The pressure drop can be prevented by slow speed variations which introduce severe restrictions on the effective operation and results in large penalties in performance. This highlights the need for a simultaneous control of speed and instabilities in VSACs which are widely used in aeronautics and industries.

In the present work, a robust nonlinear control method based on feedback linearization is applied to tackle this open control problem. The proposed controller does not require the precise knowledge of the compressor map and does not use a full-state feedback. The only assumption made here is the boundedness of external perturbations and model uncertainties. Under this assumption the developed control law can guarantee global asymptotic boundedness of model state variables. Time-domain simulations demonstrate that the controller can damp out system instabilities including surge or rotating stall, prevent the system from developing temporary rotating stall during speed variations and effectively reject external perturbations. Time-domain simulations also show how the actuator saturations can affect the effectiveness of the controller. This highlights the need for an adaptive method to estimate the saturations and adapt the control parameter for optimal performance in future work.

Finally, by taking advantage of simultaneous speed and surge/stall control methods, one can stabilize VSACs in all operation conditions. A wide range of machines using compressors can then obtain higher performance and greater operational reliability.

CHAPTER 9

GENERAL DISCUSSION

The present work explores the qualitative behavior of VSACs' model by using detailed bifurcation analyses and time-domain simulations in Chapter 4 and 5. These chapters explore the effect of different model parameters and reveal the impact of speed transitions on the stability of compression systems. The results show that a compression system, which is variable speed in nature, suffers from temporarily developed instabilities which may lead to a steady and fully developed rotating stall or surge. Consequently, these machines need to be controlled even far from unstable zones and even in the absence of external perturbations. This shows that the simple industrial solutions being based on maintaining a sufficient stability margin far from the unstable zone, which reduces performance, cannot guarantee the stability during speed transitions.

The robust control of compression systems is a matter of importance. Including the model uncertainties and external perturbations forms a challenging problem. Furthermore due to the impracticality of full-state feedbacks, control approaches which require sensing the squared amplitude of rotating stall to form the feedback fail to be practically implemented. Chapter 6 and 7 tackles the robust stability of CSACs and propose solutions which guarantee the reliable operation of the system at efficient operating points in the vicinity of unstable areas. These methods drive the feedbacks only from flow and pressure measurements and apply control laws using throttle valve and CCV actuations. Time-domain simulations corroborate the analytical developments and report the effectiveness of the designs. External perturbations and model uncertainties, which destabilize the open-loop systems, are completely rejected in close-loop. Chapter 7 explores the effect of actuator dynamics to convey an idea about the impact of this key issue. Time-domain simulations show that first-order actuator dynamics can degrade the performance of SMC and lead to a limit cycle around the desired OP.

The robust control design of CSACs sheds some light on the problem of VSACs' control. The simultaneous speed control and rotating stall and surge stabilization is achieved in Chapter 8. A robust feedback linearization method is proposed to tackle the problem. The controller stabilizes all the developed instabilities being caused by speed transitions, model uncertainties and external perturbations. Finally, Chapter 8 also explores the effect of actuator saturations.

Time-domain simulation shows that the proposed method can cope with actuator saturations and damps out the rotating stall. Although the output pressure slightly drops during rapid speed transitions due to the saturation, it shows a great improvement in comparison with pressure drops in open-loop systems during the same variations.

CHAPTER 10

CONCLUSION

The stability of compression systems in different applications has been addressed by researchers for decades. Reliable and high performance compressors as integrated parts of gas turbines benefit turbo-compressor stations, turbo-generators and jet engines. In this work, the instabilities of axial compressors are investigated and the effect of speed dynamics on the behavior of compression systems is studied. This firstly broadens our knowledge about key issues in the context of compressors modeling, and secondly sheds some lights on the control of compression systems. Here, by defining the rate of speed variations as a new bifurcation model parameter, a new series of time-domain simulations and detailed bifurcation analysis are provided. They show that contrary to previous results, the speed transitions can cause deep surge and fully developed rotating stall even in the absence of external perturbations. This highlights the need for robust control approaches which guarantee rapid speed variations and safe operation of the system at an efficient OP.

From the control point of view, the proposed methods for CSACs achieve robust stability of the system which has been a challenging problem. Furthermore, a simultaneous speed and surge/stall control method stabilizes VSACs during the speed transitions. These robust methods reject the external perturbations and model uncertainties and do not need full-state feedbacks. By taking advantage of such robust control approaches a wide range of machines using compressors can then obtain higher performance, greater operational reliability, and less fuel consumption.

Although the impact of actuator dynamics and saturations is addressed here, it needs to be carefully investigated. The future work on this topic includes the development of an adaptive control method to satisfy the operational speed transition requirements and prevent the system from going to saturated zones of actuators which limit the performance of the controller.

APPENDIX A

Bifurcation

The literature on the theory of bifurcations is enormous: for example, the bibliography in [174] contains over 700 entries. Shiraiwa [175] collected a bibliography of 4405 entries on dynamical systems. The formal foundations of bifurcation theory were created by Andronov and his students. Their theory was motivated by their investigations of applied problems. In particular, they studied in detail the birth of cycles at bifurcations when an equilibrium loses its stability, the case of "Hopf bifurcation" [176].

When a system loses stability, the number of eigenvalues which are associated with this change is typically small. Hence bifurcation problems usually involve stable part "critical" modes which change from stable to unstable as the bifurcation parameter exceeds a threshold. The central idea of bifurcation theory is that the dynamics of the system near the onset of instability is governed by the evolution of these critical modes, while the stable modes follow in a passive fashion. In this work, to present the impact of parameters on qualitative behavior of the system a parameter vector is firstly introduced in the vector field as $\dot{x} = f(x, \mu)$ where $x \in R^n$, $\mu \in R^m$ represent respectively phase variables and parameters. Consider the phase portrait of the system. As the parameters vary, the phase portrait also varies. There are two possibilities: either the system remains topologically equivalent to the original, or its topology changes (i.e. two topologically equivalent systems must have the same orientation properties, e.g. near a hyperbolic fixed point the system is locally topologically equivalent to its linearization).

Definition A.1: Bifurcation: The appearance of a topologically nonequivalent phase portrait under variation of parameters is called a *bifurcation* [146].

Definition A.2: Bifurcation Diagram: The parametric portrait together with its characteristic phase portraits constitute a *bifurcation diagram*. [146].

Definition A1.3: Bifurcation Boundries: In the simplest cases, the parametric portrait is composed by a finite number of regions in R^m. Inside each region the phase portrait is topologically equivalent. These regions are separated by *bifurcation boundaries*, which are smooth submanifolds in R^m (i.e. curves, surfaces). A bifurcation boundary is defined by

specifying a phase object (equilibrium, cycle, etc.) and some *bifurcation conditions* determining the type of its bifurcation (Hopf, fold, etc., e.g. the Andronov-Hopf bifurcation of an equilibrium, which is discussed later, is characterized by one bifurcation condition, namely, the presence of a purely imaginary pair of eigenvalues of the Jacobian matrix evaluated at this equilibrium). When a boundary is crossed, the bifurcation occurs [146].

In the present work, we concentrate on three types of local bifurcation: *Fold Bifurcation*, *Pitchfork bifurcation*, and *Hopf bifurcation*.

A.1 Fold Bifurcation [146]

Consider a continuous-time system depending on a parameter

$$\dot{x} = f(x, \mu) \quad , \quad x \in R^n, \quad \mu \in R \qquad (A.1)$$

where f is smooth with respect to both x and μ. Let $x = x_0$ be a hyperbolic equilibrium (i.e. all eigenvalues have non-zero real parts) in the system for $\mu = \mu_0$. Under a parameter variation, we can monitor the movement of the equilibrium. There are, generically, only two ways in which the hyperbolicity condition can be violated. Either a simple real eigenvalue approaches zero and we have $\lambda_1 = 0$, or a pair of simple complex eigenvalues reaches the imaginary axis and we have $\lambda_{1,2} = j\omega_0$, $\omega_0 > 0$ for some value of the parameter. The bifurcation associated with the appearance of $\lambda_1 = 0$ is called a *fold bifurcation* (Figure A.1). This bifurcation has a lot of other names, including tangent, *limit point*, saddle-node bifurcation, and turning point. A fold bifurcation is reported in the bifurcation diagram of MG3 under the variation of γ_T which is pointed out as *LP*.

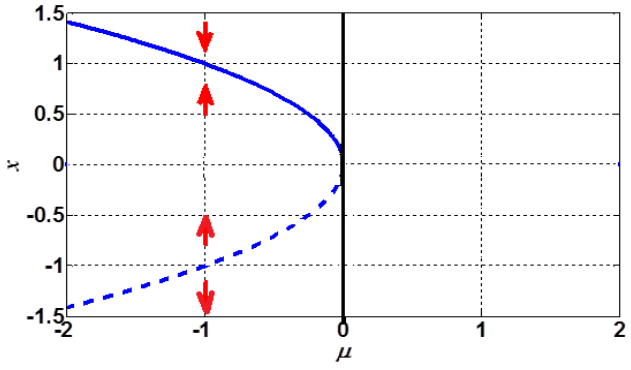

Figure A.1: Fold bifurcation

A.2 Pitchfork Bifurcation

In this bifurcation, from the loss of stability by a symmetric equilibrium, two new, less symmetric, equilibria branch out. In this process the symmetric equilibrium position continues to exist, but it loses its stability [176]. The name pitchfork bifurcation comes from the form of the branches of equilibria in the bifurcation diagram.

In many physical situations the problem possesses some symmetry. The simplest one that occurs in one dimension is the reflection or symmetry: $x \to -x$. In this section we discuss this situation and the corresponding generic bifurcation, which is the *pitchfork bifurcation*.

We consider a scalar differential equation $(A.2)$

$$\dot{x} = f(x, \mu) \qquad (A.2)$$

and now make the following assumptions.

Hypothesis A.1: Assume that the vector field in (A.2) is of class $C^k, k \geq 3$, in a neighborhood of $(0,0)$, that it satisfies $(A.3)$, and that it is odd with respect to x i.e., $f(-x, \mu) = -f(x, \mu)$.

$$f(0,0) = 0, \quad \frac{\partial f}{\partial x}(0,0) = 0 \qquad (A.3)$$

Further assume that

$$\frac{\partial^2 f}{\partial \mu \partial x}(0,0) := a \neq 0 \quad , \frac{\partial^3 f}{\partial x^3}(0,0) := 6b \neq 0 \qquad (A.4)$$

An immediate consequence of the oddness property of f is that $f(0, \mu) = 0$ for all μ, so that $x = 0$ is an equilibrium of $(A.2)$ for all μ. We continue by studying the truncated equation expansion of f (i.e. the higher order terms are ignored):

$$\frac{dx}{dt} = f(x, \mu) = a\mu x + bx^3 \qquad (A.5)$$

As for the full equation, $x = 0$ is equilibrium of this equation for all values of μ (i.e. recall that for an odd function, only, the odd degree terms of Taylor series has nonzero coefficients, because the derivative of an even function is odd and the derivative of an odd function is even. Also, the value of the odd function at 0 is 0).

Upon solving the equation $a\mu x + bx^3 = 0$, we find that $x = 0$ is the only equilibrium of $(A.5)$ if $ab\mu \geq 0$. For $ab\mu < 0$ there is an additional pair of nontrivial equilibria $x = \pm\sqrt{a\mu/b}$. As for the dynamics, the nonequilibrium solutions are monotone, with monotonicity determined by the sign of the function $a\mu x + bx^3$. This function changes sign precisely at the equilibrium points, and a direct calculation leads to the diagram in Figure (A.2).

The qualitative behavior of the solutions changes when μ crosses 0, so that $\mu = 0$ is a bifurcation point. At this value, the trivial equilibrium $x = 0$ changes its stability, and a pair of equilibria having the same stability, but opposite to that of the trivial equilibrium, emerges for $\mu > 0$ when $ab < 0$, and $\mu < 0$ when $ab > 0$. Here we are in the presence of a *pitchfork bifurcation*. The cases in which the emerging nontrivial equilibria are stable are called *supercritical*, whereas the cases in which these equilibria are unstable are called *subcritical.*[177].

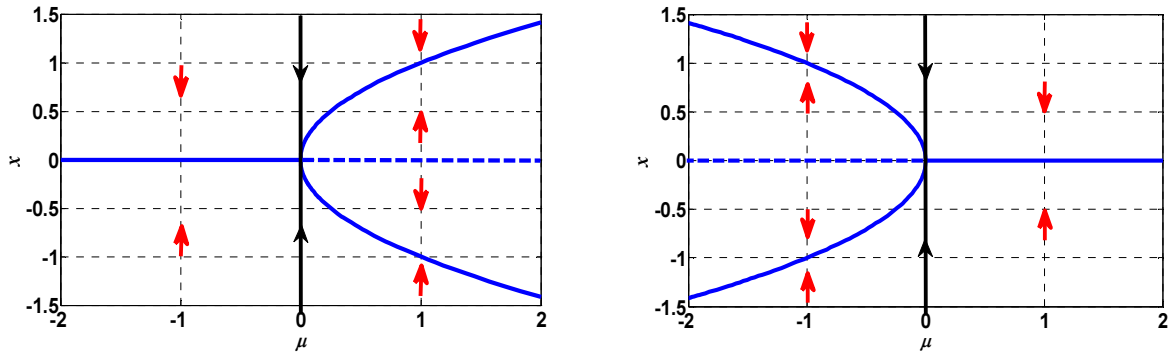

Figure A.2-a: Supercritical Pitchfork Bifurcation (b<0): left $a > 0$ and right $a < 0$

Solid lines represent stable manifolds, while dotted line represents unstable one

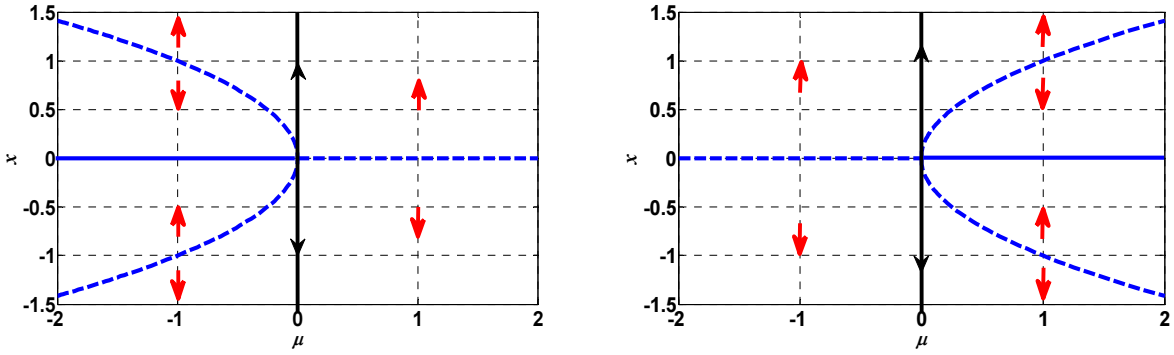

Figure A.2-b: Subcritical Pitchfork Bifurcation (b>0): left $a > 0$ and right $a < 0$

Solid line represents stable point, while dotted lines represent unstable ones

MG3 reports a subcritical pitchfork bifurcation at the top of the compressor map where $\Phi = 2W$ which is pointed out as BP in Chapter 3 (similar to Figure A.1-b right).

A.3 Andronov-Hopf Bifurcation

Historically, this kind of local bifurcation was known to Poincaré but first published in 1939 by Andropov and later published independently in 1941 by Hopf. It is usually referred to as the Hopf bifurcation theorem or better as the Andropov-Hopf bifurcation theorem [178].

A Hopf bifurcation point connects stationary solutions with periodic solutions. In fact, the preceding bifurcation where a stable fixed point continuously changed into a stable periodic orbit was a so-called supercritical Hopf bifurcation. In contrast to this, in a subcritical Hopf bifurcation, an unstable periodic orbit coalesces into a stable fixed point so that the latter becomes repelling and no stable orbit is present anymore in its vicinity when the relevant parameter passes the bifurcation value. Thus, the dynamic behavior undergoes a discontinuous transition [179].

In this section we consider differential equations in R^2,

$$\dot{x} = \boldsymbol{F}(x, \mu) \qquad (A.6)$$

Now the unknown x takes values in R^2, just as the vector field $\boldsymbol{F}$, which depends again besides depending on x, upon a real parameter μ. We assume that the vector field $\boldsymbol{F}$ is of class C^k, $k \geq 3$, in a neighborhood of $(0,0)$, satisfying

$$\boldsymbol{F}(0,0) = 0 \qquad (A.7)$$

Again, this condition shows that $x = 0$ is an equilibrium of $(A.6)$ at $\mu = 0$.We are interested in (local) bifurcations which occur in the neighborhood of this equilibrium when varying the parameter μ. Hopf bifurcation is a generic bifurcation in two dimensions. The appearance, or the absence of bifurcations is determined by the linearization of the vector field at $(0,0)$ and bifurcation occurs when the Jacobian matrix $\boldsymbol{J}$ possesses a pair of purely imaginary complex conjugated eigenvalues. In this case the generated limit cycle is orbitally stable if a certain quantity called the first Lyapunov coefficient is negative, and the bifurcation is supercritical. Otherwise it is unstable and the bifurcation is subcritical.

Example:

$$\begin{cases}\dot{x}_1 = -x_2 + x_1(\mu - x_1^2 - x_2^2) \\ \dot{x}_2 = x_1 + x_2(\mu - x_1^2 - x_2^2)\end{cases} \quad (A.8)$$

A straightforward investigation shows that $x_1 = x_2 = 0$ is the only equilibrium for all μ and there is no stationary bifurcation. The Jacobian matrix is:

$$J = \begin{bmatrix}\mu & -1 \\ 1 & \mu\end{bmatrix}$$

has eigenvalues $\mu \pm j$. We conclude that the equilibrium is stable for $\mu < 0$ and unstable for $\mu > 0$ that is, there is a loss of stability at $\mu = 0$.

A limit cycle can be constructed for equations $(A.8)$. Using polar coordinates ρ, ϑ with

$x_1 = \rho cos\vartheta, x_2 = \rho sin\vartheta$

$\dot{\rho} cos\vartheta - \rho\dot{\vartheta} sin\vartheta = -\rho sin\vartheta + \rho cos\vartheta(\mu - \rho^2)$

$\dot{\rho} sin\vartheta - \rho\dot{\vartheta} cos\vartheta = \rho cos\vartheta + \rho sin\vartheta(\mu - \rho^2)$

Multiplying the first equation by $cos\,\vartheta$ and the second equation by $sin\,\vartheta$ and adding yields the following differential equations:

$$\begin{cases}\dot{\rho} = \rho(\mu - \rho^2) \\ \dot{\vartheta} = 1\end{cases}$$

For $\rho = \sqrt{\mu}$, we have $\dot{\rho} = 0$. Hence, there is a periodic orbit $\rho(t) \equiv \sqrt{\mu}$, $\vartheta(t) = t$ for $\mu > 0$, and the amplitude of the orbit grows with $\sqrt{\mu}$. Because $\dot{\rho} < 0$ for $\rho > \sqrt{\mu}$ and $\dot{\rho} > 0$ for $0 < \rho < \sqrt{\mu}$ the orbit is stable. For varying μ, the orbits form a branch, which merges at $\mu_0 = 0$ with the branch of equilibria [150]. Figure (A.3) summarizes the results.

Bifurcation analysis of MG3 reports a Hopf bifurcation in the case of high B-parameters (see Chapter 3).

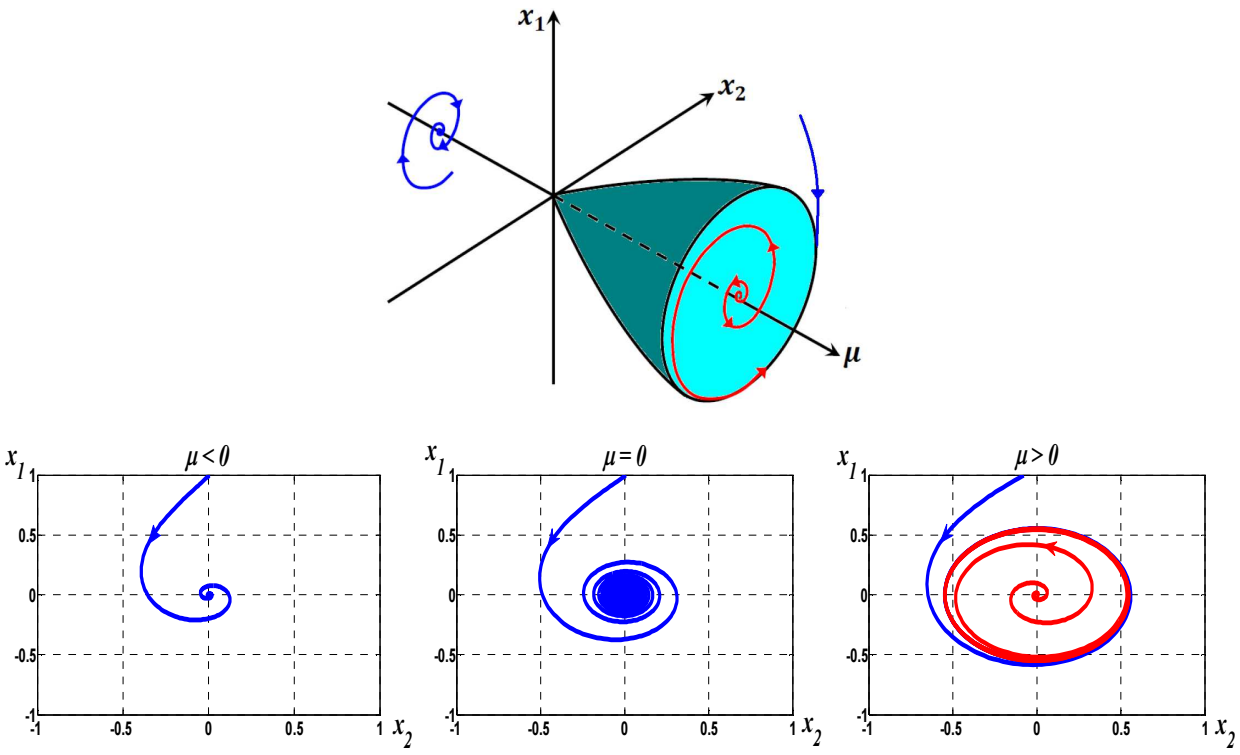

Figure A.3: Generation of stable limit cycles at $\mu > 0$ (parameter-dependent phase plane)

Supercritical Hopf bifurcation at $\mu = 0$

APPENDIX B

Continuation Method and Numerical Bifurcation Analysis

Bifurcation analysis as a standard, accepted and efficient approach for studying nonlinear dynamical system is being used. This analysis not only can validate the time-domain simulation outcomes but also can reveal significant aspects of dynamical systems' qualitative behaviors which are hard to be predicted by time-domain simulations. By this method and by comparing bifurcation analysis outcomes and time-domain results, one can refine his approaches, enhance model's simulations, and bring the developments into new alignment to achieves targeted results. Here, to study the qualitative behavior of compression systems and to verify the simulation outcomes, Matcont [180] and AUTO [181] packages are applied.

Matcont provides a continuation and numerical bifurcation Matlab toolbox. This graphical package is also developed in a command line version "Cl_Matcont" under the supervision of W. Govaerts and Yu.A. Kuznetsov (see [182]). In this research, the results of Matcont are verified by time-domain simulations and by AUTO. The graphical interface of Matcont is compatible with the standard Matlab ODE representation of differential equations. Figure B.1 shows the MG3 model in the editor of Matcont. Coordinates of the system are respectively pressure rise (Psi), mass flow (Phi) and the squared amplitude of rotating stall (J). There are only two varying parameters: B (B-parameter) and gt (γ_T throttle gain).

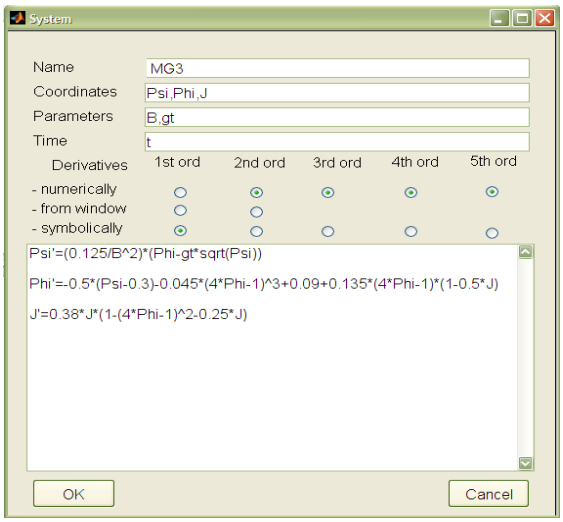

Figure B.1: Specifying MG3 model in Matcont [183]

Numerical bifurcation analysis packages are based on the application of *Implicit Function Theorem* to investigate the topological behavior of dynamic systems. In what follows, *Implicit Function Theorem* and the basic principles of *Continuation Method* are briefly reviewed.

B.1 Theorem: IFT (Implicit Function Theorem)

Let $G : R^n \times R \to R^n$ (including n state and one parameter) satisfies:

(i) $G(x_0, \lambda_0) = 0$, $x_0 \in R^n$, $\lambda_0 \in R$ is the parameter.

(ii) $G_x(x_0, \lambda_0)$ is nonsingular (i.e. x_0 is an isolated solution).

(iii) G and G_x are smooth near x_0 .

Then there exists a unique, smooth solution family $x(\lambda)$ such that (see Figure B.2):

$G(x(\lambda), \lambda) = 0$, for all λ near λ_0 , $x(\lambda_0) = x_0$.

In other words, IFT states that a given solution persists, at least locally, when a problem parameter is changed.

Problems arise when the family of the solution meets a *fold* where *IFT condition (ii)* is not satisfied. Consider the equation:

$G(x, \lambda) = 0 : x, G(\,.\,,\,.\,) \in R^n$, $\lambda \in R$

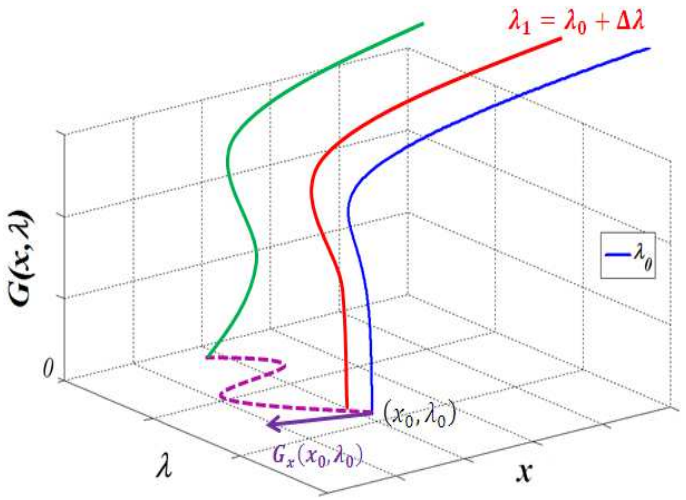

Figure B.2: IFT

Let $u \equiv (x, \lambda)$, then the equation can be written as:

$G(u) = 0$, $G: R^{n+1} \to R^n$

A solution u_0 of $G(u) = 0$ is regular if matrix $G_u^0 \equiv G_u(u_0)$ with n rows and n+1columns has maximal rank $Rank\ (G_u^0) = n$. We have then:

$$Rank(G_u^0 = Rank\left(G_x^0 \middle| G_\lambda^0\right) = n \Leftrightarrow \begin{cases} (i)\ G_x^0 \text{ is nonsingular} \\ \quad or \\ (ii) \begin{cases} dim\, \aleph(G_x^0) = 1 \\ G_\lambda^0 \notin \mathcal{R}(G_x^0) \end{cases} \end{cases}$$

where $\aleph(G_x^0)$ denotes the null space of G_x^0 and $\mathcal{R}(G_x^0)$ denotes the range of G_x^0.

The case above is that of a simple fold. Thus even near a simple fold, there is a unique solution family. However, near such a fold, the family cannot be parameterized by λ .

B.2 Numerical Continuation [149]:

Here we discuss algorithms for computing families of solutions to nonlinear equations. *IFT* is important in the design of such continuation methods.

Parameter Continuation

The continuation parameter is λ. Suppose we have a solution (x_0, λ_0) of $G(x, \lambda) = 0$ as well as the direction vector $\dot{x}_0$.

where $\dot{x} \equiv {}^{dx}/_{d\lambda}$ and we want to compute the solution x_1 at $\lambda_1 \equiv \lambda_0 + \Delta\lambda$.

To solve the equation $G(x_1, \lambda_1) = 0$, for x_1 (with $\lambda = \lambda_1$ fixed) we use $Newton's\ method$:

$G_x(x_1^\nu, \lambda_1)\Delta x_1^\nu = -G(x_1^\nu, \lambda_1), \qquad \nu :$ the itteration $= 0,1,2, \ldots$

$x_1^{\nu+1} = x_1^\nu + \Delta x_1^\nu$

As initial approximation, one can use $x_1^0 = x_0 + \Delta\lambda\, \dot{x}_0$. If $G_x(x_1, \lambda_1)$ is nonsingular and $\Delta\lambda$ is sufficiently small, then the Newton's convergence theory guarantees that this iteration will converge. After convergence, the new direction vector $\dot{x}_1$ can be computed by solving:

$G_x(x_1, \lambda_1)\, \dot{x}_1 = -G(x_1, \lambda_1)$

This equation follows from differentiating $G(x(\lambda), \lambda) = 0$ with respect to $\lambda = \lambda_1$ **.** In practice, in order to compute the continuation of a solution family past a fold *Keller's pseudo-arclength continuation method* is used in the literature. The *Jacobian* of the pseudo-arclength system is nonsingular at a fold point.

Following Folds

When a parameter passes a fold, then the behavior of a system can change drastically. Thus it is useful to determine how the location of a fold changes when a second parameter changes, i.e., we want the compute a critical stability curve, or a locus of fold points, in two-parameter space. Similar studies can be carried out to investigate the behavior of the system in other local and global bifurcation points. This leads to analyze the qualitative behavior of the system in the range of parameters variations.

REFERENCES

[1] C. G. Curtis, "Apparatus for generating mechanical power," USA Patent US635,919, 1899.

[2] ASME. (2013). *Neuchâtel Gas Turbine*. Available: https://www.asme.org/about-asme/who-we-are/engineering-history/landmarks/135-neuchatel-gas-turbine

[3] T. Giampaolo, *Compressor Handbook: Principles and Practice*. Lilburn: The Fairmont Press, Inc, 2010.

[4] P. C. Hanlon, *Compressor Handbook*: McGRAW-HILL, 2001.

[5] N. A. Cumpsty, *Compressor Aerodynamics*. London: Longman Scientific & Technical, 1989.

[6] H. W. Emmons, C. E. Pearson, and H. P. Grant, "Compressor Surge and Stall Propagation," in *American Society of Mechanical Engineers -- Meeting A-65, Nov 29-Dec 3 1953*, New York, NY, United States, 1953, p. 13.

[7] R. L. Behnken. (1997). *Nonlinear Control and Modeling of Rotating Stall in an Axial Flow Compressor* [Thesis].

[8] D. L. Gysling, J. Dugundji, E. M. Greitzer, and A. H. Epstein, "Dynamic Control of Centrifugal Compressor Surge Using Tailored Structures," in *International Gas Turbine and Aeroengine Congress and Exposition, June 11, 1990 - June 14, 1990*, Brussels, Belg, 1990, pp. GT122 13p-GT122 13p.

[9] I. J. Day, "Axial Compressor Performance during Surge," *Journal of Propulsion and Power,* vol. 10, 1994.

[10] G. Sari, O. Akhrif, and L. Satydy, "Qualitative Analysis of an Axial Compressor Model with Non-constant Speed," in *ASME 2011 Power Conference*, Denver, Colorado, USA, 2011.

[11] Tsai C. and Wu H., "Robust passivity-based control of weakly minimum phase nonlinear uncertain systems: An application to manipulator," in *2009 7th Asian Control Conference, ASCC 2009, August 27, 2009 - August 29, 2009*, Hong Kong, China, 2009, pp. 919-924.

[12] Zhong-Ping Jiang and Hill D. J., "Passivity and disturbance attenuation via output feedback for uncertain nonlinear systems," *Automatic Control, IEEE Transactions on,* vol. 43, pp. 992-997, 1998.

[13] T. B. Ferguson, *The Centrifugal Compressor Stage*. London: Butterworths, 1963.

[14] R. G. F. C. Cohen H., Saravanamuttoo H.I.H *Gas Turbine Theory*, 4th ed. Essex: Longman, 1996.

[15] R. H. Aungier, *Axial-flow Compressors: a Strategy for Aerodynamic Design and Analysis*: ASME Press, 2003.

[16] R. A. Izmailov, "Unsteady Processes in Centrifugal Compressors and Methods of Investigating Them," *Trudy LPI,* pp. 91-96, 1982.

[17] R. A. Izmajlov and K. P. Seleznev, "Unsteady Processes in Centrifugal Compressors," *Khimicheskoe I Neftegazovoe Mashinostroenie,* pp. 21-24, 1995.

[18] E. M. Greitzer, "Surge and Rotating Stall in Axial Flow Compressors - 1. Theoretical Compression System Model," *Journal of Engineering for Power, Transactions ASME,* vol. 98 Ser A, pp. 190-198, 1976.

[19] E. M. Greitzer, "Surge and Rotating Stall in Axial Flow Compressors - 2. Experimental Reasults and Comparison with Theory," *Journal of Engineering for Power, Transactions ASME,* vol. 98 Ser A, pp. 199-217, 1976.

[20] S. Mizuki, Y. Kawashima, and I. Ariga, "Investigation Concerning Rotating Stall and Surge Phenomena within Centrifugal Compressor Channels," *American Society of Mechanical Engineers (Paper),* 1978.

[21] U. Schlamann, I. Teipel, and W. Riess, "Experimental Study of the Flow Phenomena of Rotating Stall and Surge in Multistage Highly Loaded Axial-Flow Compressor," 03411753, 1985.

[22] S. H. Stenning, "Rotating Stall and Surge," *Journal of Fluids Engineering, Transactions of the ASME,* vol. 102, pp. 14-20, 1980.

[23] I. J. Day, "Stall Inception in Axial Flow Compressors," in *International Gas Turbine and Aeroengine Congress and Exposition, June 3, 1991 - June 6, 1991*, Orlando, FL, USA, 1991.

[24] D. Tang, J. Guo, L. Li, and W. Qiao, "Rotating Stall and Surge in Axial Flow Compressor," *Hangkong Dongli Xuebao/Journal of Aerospace Power,* vol. 5, pp. 245-250, 1990.

[25] H. Ishii and Y. Kashiwabara, "Study on Surge and Rotating Stall in Axial Compressors (1st Report, a Summary of the Measurement and Fundamental Analysis Method)," *Nippon Kikai Gakkai Ronbunshu, B Hen/Transactions of the Japan Society of Mechanical Engineers, Part B,* vol. 54, pp. 1669-1676, 1988.

[26] H. Ishii and Y. Kashiwabara, "Study on Surge and Rotating Stall in Axial Compressors (3rd Report, Numerical Model for Multiblade-row Compressors)," *Nippon Kikai Gakkai Ronbunshu, B Hen/Transactions of the Japan Society of Mechanical Engineers, Part B,* vol. 59, pp. 1127-1133, 1993.

[27] C. Holloway and D. Pavlov, "Anti-Surge Control of Large Compressors," *Chemsa,* vol. 1, pp. 190-192, 1975.

[28] W. S. Buzzard, "Centrifugal Compressor Anti-Surge and Recycle Control," *Acta Metallurgica,* vol. 28, 1973.

[29] W. Blotenberg, "Digital Anti-Surge Controls - Advantages and Limits," *South African mechanical engineer,* vol. 35, pp. 336-342, 1985.

[30] W. Jansen, A. F. Carter, and M. C. Swarden, "Improvements in Surge Margin for Centrifugal Compressors, Flow Phenamena and Performance," *AGARD Conference Proceedings* vol. 282, 1980.

[31] I. J. Day, "The Fundamnetals of Stall and Surge in Axial Compressors " *ASME Transactions,* vol. 6, pp. 455-469, 1996.

[32] C. J. Freitas and A. J. Smalley, "Simulation of the Onset of Rotating Stall," in *2001 ASME International Mechanical Engineering Congress and Exposition, November 11, 2001 - November 16, 2001*, New York, NY, United states, 2001, pp. 119-124.

[33] H. M. Saxer-Felici, A. P. Saxer, A. Inderbitzin, and G. Gyarmathy, "Prediction and Measurement of Rotating Stall Cells in an Axial Compressor," *Journal of Turbomachinery,* vol. 121, pp. 365-375, 1999.

[34] N. Hagino, K. Uda, and Y. Kashiwabara, "Prediction of Surge Inception of a Centrifugal Compressor with Attractor Behaviors in Phase Portraits," *Nippon Kikai Gakkai Ronbunshu, B Hen/Transactions of the Japan Society of Mechanical Engineers, Part B,* vol. 68, pp. 1159-1165, 2002.

[35] H. Wu, X. Lian, and J. Cui, "New Method for Predicting Surge Line in Multistage Axial Compressors," *Tuijin Jishu/Journal of Propulsion Technology,* vol. 18, pp. 75-77, 116, 1997.

[36] F. K. Moore and E. M. Greitzer, "Theory of post-stall transients in axial compression systems: part I - development of equations," *Journal of Engineering for Gas Turbines and Power,* vol. 108, pp. 68-76, 1986.

[37] G. Gu, A. Sparks, and S. S. Banda, "An overview of rotating stall and surge control for axial flow compressors," *IEEE Transactions on Control Systems Technology,* vol. 7, pp. 639-47, 1999.

[38] J. D. Paduano, A. H. Epstein, L. Valavani, J. P. Longley, E. M. Greitzer, and G. R. Guenette, "Active Control of Rotating Stall in a Low-speed Axial Compressor," *Journal of Turbomachinery,* vol. 115, pp. 48-56, 1993.

[39] J. D. Paduano, L. Valavani, A. H. Epstein, E. M. Greitzer, and G. R. Guenette, "Modeling for Control of Rotating Stall," *Automatica,* vol. 30, pp. 1357-1373, 1994.

[40] Mansoux C. A., Gysling D. L., Setiawan J. D., and Paduano J. D., "Distributed nonlinear modeling and stability analysis of axial compressor stall and surge," *American Control Conference,* vol. Volume: 2, pp. 2305- 2316, 1994.

[41] J. D. Paduano, "Analysis of Compression System Dynamics," 2001.

[42] Adomaitis R. and Abed E. H., "Local nonlinear control of stall inception in axial flow compressors," *29th Joint Propulsion Conference and Exhibit. AIAA,* pp. 93--2230, 1993.

[43] A. Leonessa, V.-S. Chellaboina, and W. M. Haddad, "Globally stabilizing controllers for multi-mode axial flow compressor models via equilibria-dependent Lyapunov functions," in *Proceedings of the 1997 IEEE International Conference on Control Applications, October 5, 1997 - October 7, 1997*, Hartford, CT, USA, 1997, pp. 63-68.

[44] D. A. Fink, N. A. Cumpsty, and E. M. Greitzer, "Surge Dynamics in a Free-spool Centrifugal Compressor System," *Journal of Turbomachinery,* vol. 114, pp. 321-332, 1992.

[45] J. T. Gravdahl and O. Egeland, "Speed and Surge Control for a Low Order Centrifugal Compressor Model," in *Proceedings of the 1997 IEEE International Conference on Control Applications, October 5, 1997 - October 7, 1997*, Hartford, CT, USA, 1997, pp. 344-349.

[46] J. T. Gravdahl and O. Egeland, "Moore-Greitzer Axial Compressor Model with Spool Dynamics," in *Proceedings of the 1997 36th IEEE Conference on Decision and Control. Part 1 (of 5), December 10, 1997 - December 12, 1997*, San Diego, CA, USA, 1997, pp. 4714-4719.

[47] J. T. Gravdahl, "Modeling and control of surge and rotating stall in compressors " Dr.ing., Department of Engineering Cybernetics, Norwegian University of Science and Technology, Trondheim, 1998.

[48] E. S. Hendrickson and A. G. Sparks, "On the Suitability of Bifurcation Stabilization Control Laws for High Order Moore-Greitzer Compressor Models," in *Proceedings of the 1997 American Control Conference. Part 3 (of 6), June 4, 1997 - June 6, 1997*, Albuquerque, NM, USA, 1997, pp. 801-805.

[49] D.-C. Liawa and E. H. Abed, "Active control of compressor stall inception: a bifurcation-theoretic approach," *Automatica,* vol. 32, pp. 109-115, 1996.

[50] M. Krstic, D. Fontaine, P. V. Kokotovic, and J. D. Paduano, "Useful nonlinearities and global stabilization of bifurcations in a model of jet engine surge and stall," *IEEE Transactions on Automatic Control,* vol. 43, pp. 1739-1745, 1998.

[51] G. Gu, X. Chen, A. G. Sparks, and S. S. Banda, "Bifurcation Stabilization with Local Output Feedback," *SIAM Journal on Control and Optimization,* vol. 37, pp. 934-956, 1999.

[52] B. D. Coller, "Hopf-Hopf Interactions of Surge and Rotating Stall," *ASME,* 2006.

[53] M. Xiao, "Quantitative characteristic of rotating stall and surge for Moore-Greitzer PDE model of an axial flow compressor," *SIAM Journal on Applied Dynamical Systems,* vol. 7, pp. 39-62, 2008.

[54] K. E. Hansen, P. Jørgensen, and P. S. Larsen, "Experimental and Theoretical Study of Surge in a Small Centrifugal Compressor," *Fluids Engineering,* vol. 103, p. 391, 1981.

[55] K. M. Eveker and C. N. Nett, "Model Development for Active Surge Control/Rotating Stall Avoidance in Aircraft Gas Turbine Engines," in *American Control Conference, 1991*, 1991, pp. 3166-3172.

[56] R. A. Adomaitis, "Spatially Resolved Compressor Characteristics for Modeling and Control of Blade-scale Flow Instabilities," in *Sensing, Actuation, and Control in Aeropropulsion, April 17, 1995 - April 18, 1995*, Orlando, FL, USA, 1995, pp. 36-46.

[57] T. P. Hynes and E. M. Greitzer, "Method for Assessing Effects of Circumferential Flow Distortion on Compressor Stability," *Journal of Turbomachinery,* vol. 109, pp. 371-379, 1987.

[58] H. O. Wang, R. A. Adomaitis, and E. H. Abed, "Nonlinear Analysis and Control of Rotating Stall in Axial Flow Compressors," in *Proceedings of the 1994 American Control Conference. Part 1 (of 3), June 29, 1994 - July 1, 1994*, Baltimore, MD, USA, 1994, pp. 2317-2321.

[59] J. S. Humbert and A. J. Krener, "Analysis of Higher Order Moore-Greitzer Compressor Models," in *Proceedings of the 1997 IEEE International Conference on Control Applications, October 5, 1997 - October 7, 1997*, Hartford, CT, USA, 1997, pp. 651-656.

[60] G. J. Hendricks, J. S. Sabnis, and M. R. Feulner, "Analysis of Instability Inception in High-speed Multi-stage Axial-flow Compressors," in *Proceedings of the 1996 International Gas Turbine and Aeroengine Congress & Exhibition, June 10, 1996 - June 13, 1996*, Burmingham, UK, 1996, pp. 6pp-6pp.

[61] M. R. Feulner, G. J. Hendricks, and J. D. Paduano, "Modeling for Control of Rotating Stall in High Speed Multi-stage Axial Compressors," in *Proceedings of the International Gas Turbine and Aeroengine Congress and Exposition, June 13, 1994 - June 16, 1994*, Hague, Neth, 1994, pp. 1-12.

[62] Y. Gong, C. S. Tan, K. A. Gordon, and E. M. Greitzer, "Computational Model for Short Wavelength Stall Inception and Development in Multi-stage Compressors," in *Proceedings of the 1998 International Gas Turbine & Aeroengine Congress & Exhibition, June 2, 1998 - June 5, 1998*, Stockholm, Sweden, 1998.

[63] H. J. Weigl, J. D. Paduano, L. G. Frechette, A. H. Epstein, E. M. Greitzer, M. M. Bright, and A. J. Strazisar, "Active Stabilization of Rotating Stall and Surge in a Transonic Single-Stage Axial Compressor," *Journal of Turbomachinery,* vol. 120, pp. 625-636, 1998.

[64] O. O. Badmus, S. Chowdhury, K. M. Eveker, C. N. Nett, and C. J. Rivera, "Simplified Approach for Control of Rotating Stall Part 2: Experimental Results," *JOURNAL OF PROPULSION AND POWER,* vol. 11, pp. 1210-1223, 1995.

[65] Willems F., "Modeling and control of compressor flow instabilities," Eindhoven University of Technology (TUE),Faculty of Mechanical Engineering Control Engineering Section, Eindhoven WFW 96.151, 1997.

[66] R. L. Behnken, R. D'Andrea, and R. M. Murray, "Control of Rotating Stall in a Low-speed Axial Flow Compressor Using Pulsed Air Injection: Modeling, Simulations, and Experimental Validation," in *Proceedings of the 1995 34th IEEE Conference on Decision and Control. Part 1 (of 4), December 13, 1995 - December 15, 1995*, New Orleans, LA, USA, 1995, pp. 3056-3061.

[67] J. E. F. Williams, M. F. L. Harper, and D. J. Allwright, "Active Stabilization of Compressor Instability and Surge in a Working Engine," *Journal of Turbomachinery,* vol. 115, pp. 68-75, 1993.

[68] I. J. Day, "Active Suppression of Rotating Stall and Surge in Axial Compressors," *Journal of Turbomachinery,* vol. 115, pp. 40-47, 1993.

[69] M. Van de Wal, F. Willems, and B. De Jager, "Selection of Actuators and Sensors for Surge Control," *JOURNAL OF PROPULSION AND POWER,* vol. 18, pp. 84-92, 2002.

[70] R. L. Behnken and R. M. Murray, "Combined Air Injection Control of Rotating Stall and Bleed Valve Control of Surge," in *Proceedings of the 1997 American Control Conference. Part 3 (of 6), June 4, 1997 - June 6, 1997*, Albuquerque, NM, USA, 1997, pp. 987-992.

[71] J. T. Gravdahl and O. Egeland, "Compressor Surge Control Using a Close-coupled Valve and Backstepping," in *Proceedings of the 1997 American Control Conference. Part 3 (of 6), June 4, 1997 - June 6, 1997*, Albuquerque, NM, USA, 1997, pp. 982-986.

[72] D. Fontaine, L. Shengfang, J. Paduano, and P. V. Kokotovic, "Nonlinear Control Experiments on an Axial Flow Compressor," *Control Systems Technology, IEEE Transactions on,* vol. 12, pp. 683-693, 2004.

[73] F. Willems, W. P. M. H. Heemels, B. De Jager, and A. A. Stoorvogel, "Positive Feedback Stabilization of Centrifugal Compressor Surge," *Automatica,* vol. 38, pp. 311-318, 2002.

[74] T. R. Camp and I. J. Day, "A Study of Spike and Modal Stall Phenomena in a Low-speed Axial Compressor," *Journal of Turbomachinery,* vol. 120, pp. 393-401, 1998.

[75] J. E. Ffowcs Williams and X. Y. Huang, "Active Stabilization of Compressor Surge," *Journal of Fluid Mechanics,* vol. 204, pp. 245-262, 1989.

[76] J. G. Balchen and K. I. Mumme, *Process Control: Structures and Applications*. New York: VanNostrandReinhold, 1988.

[77] A. H. Epstein, J. E. F. Williams, and E. M. Greitzer, "Active Suppression of Aerodynamic Instabilities in Turbomachines," *JOURNAL OF PROPULSION AND POWER,* vol. 5, pp. 204-211, 1989.

[78] K. Breuer, M. Schmidt, and A. H. Epstein, "Active Control of Air-breathing Propulsion Using MEMS," MIT, MIT Year-end Report1998.

[79] D. Sanadgol and E. Maslen, "Effects of Actuator Dynamics in Active Control of Surge with Magnetic Thrust Bearing Actuation," in *Proceedings of the 2005 IEEE/ASME International Conference on Advanced Intelligent Mechatronics, AIM 2005, July 24, 2005 - July 28, 2005*, Monterey, CA, United states, 2005, pp. 1091-1096.

[80] H. D. Vo, "Control of Rotating Stall in Axial Compressors Using Plasma Actuators," in *37th AIAA Fluid Dynamics Conference, June 25, 2007 - June 28, 2007*, Miami, FL, United states, 2007, pp. 1-15.

[81] R. M. M. Yong Wang, "Bifurcation Control of Rotating Stall with Actuator Magnitude and Rate Limits," *Automatica,* 1999.

[82] H.-H. Wang, M. Krstic, and M. Larsen, "Control of Deep-hysteresis Aeroengine Compressors - Part I: A Moore-Greitzer Type Model," in *Proceedings of the 1997 American Control Conference. Part 3 (of 6), June 4, 1997 - June 6, 1997*, Albuquerque, NM, USA, 1997, pp. 998-1002.

[83] O. O. Badmus, S. Chowdhury, K. M. Eveker, and C. N. Nett, "Control-oriented High-frequency Turbomachinery Modeling Single-stage Compression System 1D Model," in *International Gas Turbine and Aeroengine Congress and Exposition, May 24, 1993 - May 27, 1993*, Cincinnati, OH, USA, 1993, pp. 1-16.

[84] O. O. Badmus, S. Chowdhury, and C. N. Nett, "Nonlinear Control of Surge in Axial Compression Systems," *Automatica,* vol. 32, pp. 59-70, 1996.

[85] W. M. Jungowski, M. H. Weiss, and G. R. Price, "Pressure Oscillations Occurring in a Centrifugal Compressor System with and Without Passive and Active Surge Control," in *Proceedings of the International Gas Turbine and Aeroengine Congress and Exposition, June 13, 1994 - June 16, 1994*, Hague, Neth, 1994, pp. 1-11.

[86] K. Nakagawa, M. Fujiwara, T. Nishioka, S. Tanaka, and Y. Kashiwabara, "Experimental and Numerical Analysis of Active Suppression of Centrifugal Compressor Surge by

Suction-side Valve Control," *JSME International Journal, Series B: Fluids and Thermal Engineering,* vol. 37, pp. 878-885, 1994.

[87] J. E. Pinsley, G. R. Guenette, A. H. Epstein, and E. M. Greitzer, "Active Stabilization of Centrifugal Compressor Surge," in *International Gas Turbine and Aeroengine Congress and Exposition, June 11, 1990 - June 14, 1990*, Brussels, Belg, 1990, pp. GT123 11p-GT123 11p.

[88] D. L. Gysling and E. M. Greitzer, "Dynamic Control of Rotating Stall in Axial Flow Compressors Using Aeromechanical Feedback," in *Proceedings of the International Gas Turbine and Aeroengine Congress and Exposition, June 13, 1994 - June 16, 1994*, Hague, Neth, 1994, pp. 1-18.

[89] J. M. Haynes, G. J. Hendricks, and A. H. Epstein, "Active Stabilization of Rotating Stall in a Three-Stage Axial Compressor," *Journal of Turbomachinery,* vol. 116, 1994.

[90] Y. W. Simon Yeung, "Evaluation of Bleed Valve Rate Requirements in Nonlinear Control of Rotating Stall on Axial Compreesors," *Propulsion and Power,* 1999.

[91] J. T. Gravdahl and O. Egeland, "Centrifugal Compressor Surge and Speed Control," *IEEE Transactions on Control Systems Technology,* vol. 7, pp. 567-579, 1999.

[92] Song C., Chen S., and Liaw D., "Sliding Mode Stabilization of a Centrifugal Compressor with Spool Dynamics," in *ICCAS-SICE 2009 - ICROS-SICE International Joint Conference 2009, August 18, 2009 - August 21, 2009*, Fukuoka, Japan, 2009, pp. 5139-5144.

[93] L. Der-Cherng, S. Chau-Chung, and H. Jeng-Tze, "Robust Stabilization of a Centrifugal Compressor with Spool Dynamics," *IEEE Transactions on Control Systems Technology,* vol. 12, pp. 966-72, 2004.

[94] G. Bartolini, A. Muntoni, A. Pisano, and E. Usai, "Compressor surge active control via throttle and CCV actuators. A second-order sliding-mode approach," in *IEEE 10th International Workshop on Variable Structure Systems, VSS'08, June 8, 2008 - June 10, 2008*, Antalya, Turkey, 2008, pp. 274-279.

[95] D. Liaw and J. Huang, "Robust Stabilization of Axial Flow Compressor Dynamics Via Sliding Mode Design," *Journal of Dynamic Systems, Measurement, and Control,* vol. 123, pp. 488-495, 2001.

[96] M. R. Feulner, "Modeling and Control of Rotating Stall in High Speed Multi-Stage Axial Compressors," *thesis,* 1994.

[97] R. G. Berndt, H. J. Weigl, J. D. Paduano, and A. H. Epstein, "Experimental Techniques for Actuation, Sensing, and Measurement of Rotating Stall Dynamics in High-speed Compressors," in *Sensing, Actuation, and Control in Aeropropulsion, April 17, 1995 - April 18, 1995*, Orlando, FL, USA, 1995, pp. 166-185.

[98] N. Staroselsky and L. Ladin, "Improved Surge Control for Centrifugal Compressors," *Chemical Engineering (New York),* vol. 86, pp. 175-184, 1979.

[99] N. Staroselsky and L. Ladin, "Compressors Simultaniously Approach Surge," *Oil and Gas Journal,* vol. 84, pp. 94, 96, 98, 100-94, 96, 98, 100, 1986.

[100] J. Hampel, "What Control Engineers Need to Know about Antisurge Protection," in *Proceedings of the Third Annual Control Engineering Conference. Held as part of the Control Engineering Conference & Exposition.*, Rosemont, IL, USA, 1984, pp. 373-380.

[101] J. T. Golla, "Centrifugal Compressor Variable Surge Line Computation and Control," in *Proceedings of the ISA/87 International Conference and Exhibit.*, Anaheim, CA, USA, 1987, pp. 567-571.

[102] H. Bozenhardt, "Integrated Aproach to Microprocessor-based Control," *Chemical Engineering Progress,* vol. 84, pp. 23-28, 1988.

[103] R. Vepa, "Modelling and Quasilinear Control of Compressor Surge and Rotating Stall Vibrations," *Mathematical Problems in Engineering,* vol. 2010, 2010.

[104] B. de Jager, "Rotating stall and surge control: a survey," *34th IEEE Conference on Decision and Control* vol. Volume 2, , pp. Page(s):1857 - 1862 1995.

[105] A. Leonessa, W. M. Haddad, and L. Hua, "Globally Stabilizing Switching Controllers for a Centrifugal Compressor Model with Spool Dynamics," *IEEE Transactions on Control Systems Technology,* vol. 8, pp. 474-82, 2000.

[106] M. Krstic, J. M. Protz, J. D. Paduano, and P. V. Kokotovic, "Backstepping designs for jet engine stall and surge control," in *Proceedings of the 1995 34th IEEE Conference on Decision and Control. Part 1 (of 4), December 13, 1995 - December 15, 1995*, New Orleans, LA, USA, 1995, pp. 3049-3055.

[107] J. T. E. Gravdahl, O., "Compressor surge control using a close-coupled valve and backstepping," *American Control Conference,* vol. Volume 2, , pp. Page(s):982 - 986, 1997.

[108] J. T. Gravdahl and O. Egeland, "Control of the Three State Moore-Greitzer Compressor Model Using a Close-coupled Valve," *Proceedings of the 36th IEEE Conference on,* vol. Volume 5, , pp. Page(s):4714 - 4719, 1997.

[109] P. Chen and H. Qin, "Bifurcation control of rotating stall in axial flow compressors via dynamic output feedback," in *2010 8th World Congress on Intelligent Control and Automation, WCICA 2010, July 7, 2010 - July 9, 2010*, Jinan, China, 2010, pp. 2919-2924.

[110] D. Fontaine, "Nonlinear Control Enlarges the Stability Region of an Axial Flow Compressor," 2004.

[111] D.-C. Liaw and E. H. Abed, "Active Control of Compressor Stall Inception: a Bifurcation-theoretic Approach," *Automatica,* vol. 32, pp. 109-115, 1996.

[112] A. Rajaeesani, "Robust Output Feedback Stabilization,Compressors Surge and Stall Example," *thesis,* 2003.

[113] Krstic M., Fontaine D., Kokotovic P., and Paduano J. D., "Useful nonlinearities and global stabilization of bifurcations in a model of jet engine surge and stall," *IEEE Transactions on Automatic Control,* vol. 43, pp. 1739-1745, 1998.

[114] Krstic M., "Lyapunov Feedback Design for Stabilization of Stall and Surge in Axial Compressors," in *Proceedings of the 1996 ASME International Mechanical Engineering*

Congress and Exposition, November 17, 1996 - November 22, 1996, Atlanta, GA, USA, 1996, pp. 73-78.

[115] J. T. Gravdahl and O. Egeland, "Two results on compressor surge control with disturbance rejection," in *Decision and Control, 1998. Proceedings of the 37th IEEE Conference on*, 1998, pp. 2563-2568 vol.3.

[116] Eveker K. M., Gysling D. L., Nett C. N., and Sharma O. P., "Integrated control of rotating stall and surge in aeroengines," in *Sensing, Actuation, and Control in Aeropropulsion, April 17, 1995 - April 18, 1995*, Orlando, FL, USA, 1995, pp. 21-35.

[117] Bohagen B. and Gravdahl J. T., "On active surge control of compressors using a mass flow observer," in *41st IEEE Conference on Decision and Control, December 10, 2002 - December 13, 2002*, Las Vegas, NV, United states, 2002, pp. 3684-3689.

[118] Maggiore M. and Passino K., "Output Feddback Control of Jet Engine Stall and Surge Using Pressure measurement," *IEEE Transactions on Automatic Control,* 2003.

[119] K. M. P. Manfredi Maggiore, "Output Feddback Control of Jet Engine Stall and Surge Using Pressure Measurement," *IEEE Transactions on Automatic Control,* 2003.

[120] K. M. P. Manfredi Maggiore, "Output Feedback Control for Stabilizable and Incompletely Observable Nonlinear Systems: Theory," *American Control Conference,* vol. 5, pp. 3641 - 3645, 2000.

[121] N. A. Chaturvedi and S. P. Bhat, "Output-feedback Semiglobal Stabilization of Stall Dynamics for Preventing Hysteresis and Surge in Axial-flow Compressors," *IEEE Transactions on Control Systems Technology,* vol. 14, pp. 301-307, 2006.

[122] J. Davila, L. Fridman, A. Pisano, and E. Usai, "Finite-time State Observation for Nonlinear Systems with Application to Compressor Surge Detection: A High Order Sliding-mode Approach," in *IEEE 10th International Workshop on Variable Structure Systems, VSS'08, June 8, 2008 - June 10, 2008*, Antalya, Turkey, 2008, pp. 197-202.

[123] D. Liaw, S. M. Ren, and S. Chang, "A feedback linearization design for compressor's surge control," in *Industrial Technology, 2008. ICIT 2008. IEEE International Conference on*, 2008, pp. 1-6.

[124] Simon J. S. and Valavani L., "A Lyapunov based nonlinear control scheme for stabilizing a basic compression system using a close-coupled control valve," in *Proceedings of the 1991 American Control Conference, June 26, 1991 - June 28, 1991*, Boston, MA, USA, 1991, pp. 2398-2406.

[125] A. Leonessa, V. Chellaboina, and W. M. Haddad, "Robust Stabilization of Axial Flow Compressors with Uncertain Pressure-Flow Maps," *IEEE Transactions on Control Systems Technology,* vol. 8, pp. 466-473, 2000.

[126] Z. Chen and J. Xu, "Nonlinear feedback control for rotating stall and surge of an axial flow compressor," *Zhendong yu Chongji/Journal of Vibration and Shock,* vol. 32, pp. 106-110+120, 2013.

[127] S. Lin, C. Yang, P. Wu, and Z. Song, "Fuzzy logic surge control in variable speed axial compressors," in *2013 10th IEEE International Conference on Control and Automation, ICCA 2013, June 12, 2013 - June 14, 2013*, Hangzhou, China, 2013, pp. 1178-1183.

[128] S. Ananth and A. Kushari, "A simple feedback control strategy for controlling the axial compressor surge," *International Journal of Flow Control,* vol. 4, pp. 109-124, 2012.

[129] L. Xiao and Y. Zhu, "Compressor active surge controller design based on uncertainty and disturbance estimator," in *10th World Congress on Intelligent Control and Automation, WCICA 2012, July 6, 2012 - July 8, 2012*, Beijing, China, 2012, pp. 2908-2912.

[130] J. Javadi Moghaddam and M. Madani, "A decoupled adaptive neuro-fuzzy sliding mode control system to control rotating stall and surge in axial compressors," *Expert Systems with Applications,* vol. 38, pp. 4490-4496, 2011.

[131] R. S. Shehata, H. A. Abdullah, and F. Areed, "Variable structure surge control for constant speed centrifugal compressors," *Control Engineering Practice,* vol. 17, pp. 815-833, 2009.

[132] H.-J. Ahn, M.-S. Park, D. Sanadgol, I.-H. Park, D.-C. Han, and E. H. Maslen, "A Pressure Output Feedback Control of Turbo Compressor Surge with a Thrust Magnetic Bearing Actuator," *Journal of Mechanical Science and Technology,* vol. 23, pp. 1406-1414, 2009.

[133] A. Pisano, G. Bartolini, A. Muntoni, and E. Usai, "Compressor surge suppression by second-order sliding mode control technique," *IFAC Proceedings Volumes (IFAC-PapersOnline),* vol. 17, 2008.

[134] Y. W. a. R. M. Murray, "Feedback stabilization of bifurcations in multivariable nonlinear systems}Part II: Hopf bifurcations," *ROBUST AND NONLINEAR CONTROL,* 2007.

[135] D. Sanadgol and E. Maslen, "Backstepping for Active Control of Surge in Unshrouded Centrifugal Compressors with Magnetic Thrust Bearing Actuation," in *ASME Turbo Expo 2005 - Gas Turbie Technology: Focus for the Future, June 6, 2005 - June 9, 2005*, Reno-Tahoe, NV, United states, 2005, pp. 883-889.

[136] B. Bohagen, J. T. Gravdahl, and Ieee, "Active Control of Compression Systems Using Drive Torque; a Backstepping Approach," in *2005 44th IEEE Conference on Decision and Control & European Control Conference, Vols 1-8*, ed New York: Ieee, 2005, pp. 2493-2498.

[137] D. Sanadgol, "Sliding Mode Controller for Active Control of Surge in Centrifugal Compressors with Magnetic Thrust Bearing Actuation," in *WEPAN National Conference*, ed. ST. Louis, MI, USA, 2004.

[138] D.-C. Liaw, C.-C. Song, and J.-T. Huang, "Robust stabilization of a centrifugal compressor with spool dynamics," *IEEE Transactions on Control Systems Technology,* vol. 12, pp. 966-972, 2004.

[139] N. Ananthkrishnan, U. G. Vaidya, and V. W. Walimbe, "Global Stability and Control Analysis of Axial Compressor Stall and Surge Phenomena Using Bifurcation Methods," *Proceedings of the Institution of Mechanical Engineers, Part A: Journal of Power and Energy,* vol. 217, pp. 279-286, 2003.

[140] D.-C. Liaw, S.-M. Ren, W.-C. Chung, and E. H. Abed, "Control of axial flow compression systems via linear and nonlinear designs," in *2002 American Control COnference, May 8, 2002 - May 10, 2002*, Anchorage, AK, United states, 2002, pp. 4347-4352.

[141] D.-C. Liaw and J.-T. Huang, "Robust Stabilization of Axial Flow Compressor Dynamics Via Sliding Mode Design," *Journal of Dynamic Systems, Measurement, and Control,* vol. 123, pp. 488-495, 2001.

[142] Hős C., Champneys A., and Kullmann L., "Bifurcation analysis of surge and rotating stall in the Moore-Greitzer compression system," 2002.

[143] Leonessa A., Chellaboina V., and Haddad W., "Globally stabilizing controllers for multi-mode axial flow compressor models via equilibria-dependent Lyapunov functions," in *Proceedings of the 1997 IEEE International Conference on Control Applications, October 5, 1997 - October 7, 1997*, Hartford, CT, USA, 1997, pp. 63-68.

[144] A. Dhooge, W. Govaerts, and Y. A. Kuznetsov, "MATCONT: A Matlab Package for Numerical Bifurcation Analysis of ODEs," *ACM Transactions on Mathematical Software,* vol. 29, p. 24, 2003.

[145] E. J. Doedel and B. E. Oldeman, "AUTO-07P : Continuation and Bifurcation Software for Ordinary Differential Equations," Concordia University, Montreal2009.

[146] Y. A. Kuznetsov, *Elements of Applied Bifurcation Theory, Second Edition*: Springer, 1998.

[147] G. Guoxiang, S. Banda, and A. Sparks, "An overview of rotating stall and surge control for axial flow compressors," in *Proceedings of 35th IEEE Conference on Decision and Control, 11-13 Dec. 1996*, New York, NY, USA, 1996, pp. 2786-91.

[148] R. A. Adomaitis and E. H. Abed, "Bifurcation Analysis of Nonuniform Flow Patterns in Axial-flow Gas Compressors," presented at the Proceedings of the first world congress on World congress of nonlinear analysts '92, volume II, Tampa, Florida, United States, 1995.

[149] E. J. Doedel "Lecture Notes on Numerical Analysis of Nonlinear Equations," Montreal2009.

[150] R. Seydel, *Practical Bifurcation and Stability Analysis*: Springer, 2010.

[151] J. S. Humbert and A. J. Krener, "Dynamics and Control of Entrained Solutions in Multi-mode Moore-Greitzer Compressor Models," *International Journal of Control,* vol. 71, pp. 807-821, 1998.

[152] Sepulchre R., Jankovic M., and Kokotovic P. V., *Constructive nonlinear control*. New York: Springer-Verlag, 1997.

[153] Willems J. C., "Dissipative dynamical systems," 14 rue de Provigny, Cachan Cedex, F-94236, France, 2007, pp. 134-151.

[154] C. I. Byrnes, A. Isidori, and J. C. Willems, "Passivity, feedback equivalence, and the global stabilization of minimum phase nonlinear systems," *IEEE Transactions on Automatic Control,* vol. 36, pp. 1228-1240, 1991.

[155] Bao J. and Lee P. L., *Process control*, 1st Edition. ed.: Springer, 2007.

[156] Krstic M. and Wang H., "Control of deep-hysteresis aeroengine compressors - Part II: design of control laws," in *Proceedings of the 1997 American Control Conference. Part 3 (of 6), June 4, 1997 - June 6, 1997*, Albuquerque, NM, USA, 1997, pp. 1003-1007.

[157] Dussourd J.L., Pfannebecker G.W. , and S. S.K., "An experimental investigation of the control of surge in radial compressors using close coupled resistances," *Journal of Fuids Engineering : Trans. ASME* vol. 99, pp. 64-76, 1977.

[158] Gravdahl J. T. and Egeland O., "Two results on compressor surge control with disturbance rejection," in *Decision and Control, 1998. Proceedings of the 37th IEEE Conference on*, 1998, pp. 2563-2568 vol.3.

[159] Lin W. and S. T., "Robust passivity and feedback design for minimum-phase nonlinear systems with structural uncertainty," *Automatica,* vol. 35, pp. 35-47, 1999.

[160] M. Krstic, K. Ioannis, and K. Petar, *Nonlinear and adaptive control design*. New York: John Wiley & Sons, Inc., 1995.

[161] Gravdahl J. T. and Egeland O., "Moore-Greitzer axial compressor model with spool dynamics," in *Proceedings of the 1997 36th IEEE Conference on Decision and Control. Part 1 (of 5), December 10, 1997 - December 12, 1997*, San Diego, CA, USA, 1997, pp. 4714-4719.

[162] Van de Wal M., Willems F., and De Jager B., "Selection of actuators and sensors for surge control," *JOURNAL OF PROPULSION AND POWER,* vol. 18, pp. 84-92, 2002.

[163] Simon J.S., Valavani L., Epstein A.H., and Greitzer E.M., "Evaluation of approaches to active compressor surge stabilization," *Journal Name: Journal of Turbomachinery; (United States); Journal Volume: 115:1,* pp. Medium: X; Size: Pages: 57-67, 1993.

[164] Defoort M., Floquet T., Kokosy A., and Perruquetti W., "A novel higher order sliding mode control scheme," *Systems and Control Letters,* vol. 58, pp. 102-108, 2009.

[165] M. Defoort, T. Floquet, A. Kokosy, and W. Perruquetti, "A novel higher order sliding mode control scheme," *Systems and Control Letters,* vol. 58, pp. 102-108, 2009.

[166] S. P. Bhat and D. S. Bernstein, "Geometric homogeneity with applications to finite-time stability," *Mathematics of Control, Signals, and Systems,* vol. 17, pp. 101-127, 2005.

[167] Boiko I., Fridman L., Pisano A., and Usai E., "Performance analysis of second-order sliding-mode control systems with fast actuators," *IEEE Transactions on Automatic Control,* vol. 52, pp. 1053-1059, 2007.

[168] C. Zaiet, O. Akhrif, and L. Saydy, "Modeling and Non Linear Control of a Gas Turbine," in *International Symposium on Industrial Electronics 2006, ISIE 2006, July 9, 2006 - July 13, 2006*, Montreal, QC, Canada, 2006, pp. 2688-2694.

[169] J. T. Gravdahl and O. Egeland, "Speed and surge control for a low order centrifugal compressor model," *Modeling, Identification and Control,* vol. 19, pp. 13-29, 1998.

[170] L. Der-Cherng, S. M. Ren, and C. Shih-Tse, "A Feedback Linearization Design for Compressor's Surge Control," in *Industrial Technology, 2008. ICIT 2008. IEEE International Conference on*, 2008, pp. 1-6.

[171] T. Ważewski, "Systèmes des équations et des inégalités différentielles ordinaires aux deuxième members monotones et leurs applications," *Ann. Soc. Polon. Math. ,* pp. pp. 112–166, 1950.

[172] H. Khalil, *Nonlinear Systems*, Third ed.: PRENTICE HALL, 2002.

[173] G. Sari, O. Akhrif, and L. Saydy, "The Impact of Speed Variation on the Stability of Variable Speed Axial Compressors at Efficient Operating Points," presented at the 2012 American Control Conference, 2012.

[174] S. N. Chow and J. K. Hale, *Methods of Bifurcation Theory* New York: Springer-Verlag, 1982.

[175] K. Shiraiwa, "Bibliography of Dynamical Systems," 1985.

[176] A. V. S. Arnol'd V.I. , *Dynamical Systems V Bifurcation Theory and Catastrophe Theory*: Springer-Verlag, 1993.

[177] Haragus M. and I. G., *Local Bifurcations, Center Manifolds, and Normal Forms in Infinite-Dimensional Dynamical Systems*: Springer, 2010.

[178] W. O. Bray, "Lecture 5: Local Bifurcation of Vector Fields," 2002.

[179] J. Jost, *Dynamical Systems: Examples of Complex Behaviour*: Springer, 2005.

[180] matcont. (2010). *matcont*. Available: http://www.matcont.ugent.be/

[181] E. J. Doedel. (2002). *AUTO 2000*. Available: http://www.enm.bris.ac.uk/staff/hinke/dss/continuation/auto.html

[182] W. G. A. Dhooge, "MATCONT and CL MATCONT: Continuation toolboxes in matlab," 2006.

[183] Y. A. Kuznetsov, "Computer Session I: Using Matcont for Numerical Integration of ODEs," Department of Mathematics, Utrecht University, Budapestlaan 62009.